ANALYTICAL AND EXPERIMENTAL STUDY OF SOUND TRANSMISSION LOSS OF ACOUSTIC ENCLOSURES

Ph.D. Thesis

By

PAVAN GUPTA

DEPARTMENT OF MECHANICAL ENGINEERING

INDIAN INSTITUTE OF TECHNOLOGY INDORE

JULY 2022

ANALYTICAL AND EXPERIMENTAL STUDY OF SOUND TRANSMISSION LOSS OF ACOUSTIC ENCLOSURES

A THESIS

Submitted in partial fulfillment of the

requirements for the award of the degree

of

DOCTOR OF PHILOSOPHY

by

PAVAN GUPTA

DEPARTMENT OF MECHANICAL ENGINEERING

INDIAN INSTITUTE OF TECHNOLOGY INDORE

JULY 2022

INDIAN INSTITUTE OF TECHNOLOGY INDORE

CANDIDATE'S DECLARATION

I hereby certify that the work which is being presented in the thesis entitled **"ANALYTICAL AND EXPERIMENTAL STUDY OF SOUND TRANSMISSION LOSS OF ACOUSTIC ENCLOSURES"** in the partial fulfillment of the requirements for the award of the degree of **DOCTOR OF PHILOSOPHY** and submitted in the **DEPARTMENT OF MECHANICAL ENGINEERING, INDIAN INSTITUTE OF TECHNOLOGY INDORE**, is an authentic record of my own work carried out during the time period from **December 2017** to **July 2022** under the supervision of **Prof. Anand Parey,** Professor, Department of Mechanical Engineering, IIT Indore.

The matter presented in this thesis has not been submitted by me for the award of any other degree of this or any other institute.

25/07/2022

Signature of the student with date

(PAVAN GUPTA)

This is to certify that the above statement made by the candidate is correct to the best of my knowledge.

25/07/2022

Signature of the Thesis Supervisor with date

(Prof. ANAND PAREY)

PAVAN GUPTA has successfully given his Ph.D. Oral Examination held on **November 30, 2022.**

30/11/2022

Signature of the Thesis Supervisor with date

(Prof. ANAND PAREY)

Dedicated

to my parents

ACKNOWLEDGEMENT

My deep gratitude goes first to my supervisor **Prof. Anand Parey**, who expertly guided me through my Ph.D. work. I am grateful for his dedicated supervision, and without him, the work reported in this thesis would not have been possible.

I sincerely thank **Prof. Suhas S. Joshi,** Director, IIT Indore, and **Deans** of Academic Affairs, Research and Development, and Student Affairs for their kind support and for providing appropriate facilities.

I would like to thank my Ph.D. progress committee members, **Prof. Bhupesh Kumar Lad** and **Prof. Santosh Kumar Vishvakarma**, for their valuable suggestions right from the beginning of my research work.

I express my sincere thanks to **Prof. Santosh K. Sahu,** Head of the Department of Mechanical Engineering, for providing me the opportunity and necessary infrastructure to carry out my research work.

I am indebted to the Noise and Vibration Control Laboratory and Solid Mechanics Laboratory of IIT Indore for their valuable support in conducting the experiments.

I extend my hearty thanks to all the staff members of the Department of Mechanical Engineering, Central library, Academic section, Accounts section, Purchase section, and all departments of IIT Indore for their kind cooperation.

I would like to thank the technical staff of the Central Workshop of IIT Indore for their valuable work supporting my experimental set-ups. I would like to give a special thank to **Mr. Sandeep Patil,** Deputy Manager of Solid Mechanics Lab for every stage of my experiments.

I would also like to express my sincere thanks to **Prof. Ram Bilas Pachori**, **Dr. Pavan Kumar Kankar,** and **Dr. Girish Chandra Verma** for their guidance during my research.

I would like to extend my sincere thanks to my brother like friend **Mr. Vipin Goyal** for helping me during my Ph.D. journey.

I acknowledge with a deep sense of thankfulness my current and previous laboratory colleagues **Mr. Dada Saheb Ramteke, Mr. Palash Dewangan, Mr. Anupam Kumar, Ms. Pallavi Gautam, Mr. Yogesh Andhale, Dr. Ankur Saxena, Dr. Naresh Kumar Raghuwanshi, Dr. Vikas Sharma, Dr. Amandeep Singh Ahuja, Dr. Yogesh Pandya** for always standing there through my trough and crest during my Ph.D. journey. I would like to acknowledge the support of the late **Dr. Ram Bihari Sharma.**

I would like to thank all of the seniors, colleague researchers friends who have been highly supportive, especially Dr. Tameshwar Nath Tiwari, Mr. Vivek Rana, Mr. Pradyumn Kumar Arya, Mr. Vinod Singh Thakur, Mr. Nagendra Singh Ranawat, late Dr. Ankit Rathi, Mr. Subhash Nehwal, Mr. Rajnish Modanwal, Mr. Bhavesh Chaudhary, Ms. Shruti Baghel, Mr. Manish Carpenter, Mr. Vishal Jagdale, Mr. Devashish Chorey, Mr. Pravin Kumar for their endless support and encouragement during the course of my research.

I am also highly thankful to my fellow Ph.D. student, Mr. Jatin Prakash and Mr. Pankaj Kumar, for their continuous help in every problem I faced in manuscript and thesis writing.

I take this opportunity to express my special thanks and gratitude to my dear friend Prashant Bharadwaj**.** Without his moral support, I could not have been able to cross over the ocean of Ph.D. tasks.

I will be failing in my duties if I do not extend my thanks to my mother **Mrs. Sharda Gupta,** and my father, **Mr. Om Prakash Gupta,** for their enormous support, sincere advice, and guidance. They sacrificed many things and always stood by to support me at every moment of my life. I could not imagine the success of my Ph.D. journey without them. I would like to thank them for their constant support and love.

A very special thanks and love to my beloved wife Vaishali for her unconditional love and care. I extend my love and gratitude to my sweetheart son **Ayansh**, my elder brother **Mr. Amit Gupta**, my lovely sisters **Sangeeta Gupta, Vinita Gupta, Rashmi Gupta**, and other family members **Mr. Vedprakash Gupta**, **Mr. Jitendra kumar Jain**, **Mr. Vinit Gupta, Mayur, Tanish, Divyansh, Kriti, Pranay, Prashu**, Shubham for their love and moral support, which made this journey successful.

I am also grateful to my in-laws, Mr. Pramod Kumar Gupta and Mrs. Kamlesh Gupta, for their endless love and blessings. A special thanks and gratitude to Mr. Manish Gupta and his family, who always motivated, supported and helped me unconditionally in every situation of my life. I am also thankful to all those who helped and supported me directly or indirectly during this journey.

In the end, I would like to thank the Almighty for everything he has done for me.

Pavan Gupta

IIT Indore

ABSTRACT

Acoustic enclosures made of thin elastic structural panels are broadly employed in many industries and applications such as aerospace, submarines, tanks, and architectural structures and safeguarding human hearing in a noisy environment. The applications of the acoustic enclosure are significant because it reduces the sound transmission from noise sources such as operating machines or noisy engines. There is a need to evaluate the acoustic performance of enclosures due to the commercial demand for quieter systems. Sound transmission loss is identified as an effective physical measure for quantifying the capability of acoustical enclosures for attenuating noise. Noise control is of primary importance to design the acoustic enclosure. Hence, an accurate prediction model of transmission loss is usually required during the design and development phases of the acoustic enclosures.

Numerous innovative methods have been developed by researchers for the analysis of sound transmission through acoustic enclosures and panels. However, the analytical methods based on the wave approach does not produce satisfactory results in the low-frequency region. Moreover, Numerical methods based on finite element and boundary element methods are not well suited to high-frequencies transmission loss calculation of complicated structures due to extensive computing resources and high computation time. A technique which is employed for predicting the transmission loss of finite structural panels is the Statistical energy analysis method (SEA). SEA method can be applied to a wide frequency range in order to predict the transmission loss of structural panels. Modeling the transmission loss of flat panels, shells and rectangular acoustic enclosures using the SEA technique is well documented in the literature. Significantly less work based on the SEA method has been reported for the prediction of sound transmission loss of cylindrical acoustic enclosure, conical acoustic enclosure, and hemispherical acoustic enclosure.

Additionally, there is a need to study the influence of different shapes of sound-absorbing materials on the noise reduction of the acoustic enclosure. In this thesis, the sound transmission loss evaluation methodologies based on the SEA method and experimental technique are presented for different shapes of acoustic enclosures namely, cylindrical enclosure, conical enclosure, and hemispherical enclosure. It is found that the analytical predictions show fairly a good agreement with the measured results. The parametric study is performed using the SEA method to study the influence of design parameters such as the internal absorption coefficient, thickness, radius, and different panel materials on the transmission loss of different shapes of acoustic enclosures. It is found that the greater transmission loss of acoustic enclosure can be achieved using a higher absorption coefficient inside the cavity. Further, it is shown that the sound insulation performance of the acoustic enclosure increases with the increase of shell thickness. Moreover, it is demonstrated that the larger radius reduces transmission loss of acoustic enclosure. It is found that the enclosure made of high-density material effectively provides superior transmission loss in a wide frequency range compared to an enclosure made of low-density material. Furthermore, the experimental study is performed to investigate the transmission loss of four different shape enclosures, viz. rectangular, cylindrical, conical, and hemispherical. The volume of all the shapes has been kept the same. It is demonstrated that the acoustic enclosure of the hemispherical shape is efficient in improving the acoustic performance of the enclosure. Additionally, an experimental study is performed to investigate the influence of different shapes of sound-absorbing materials on the noise reduction of the acoustic enclosure. The commercially available sound-absorbing materials (polyurethane foam) of three different surface shapes are chosen for the analysis viz. plane, wedge, and pyramid. The experimental result shows that the pyramid shape sound-absorbing material is very efficient compared to plane and wedge shape sound-absorbing material for noise reduction of the acoustic enclosure. The experimental

study demonstrates that the implementation of sound-absorbing material of different surface shapes would be an appropriate method for improving the acoustic performance of the enclosure.

Keywords: Transmission loss; statistical energy analysis; acoustic enclosure; noise reduction; radiation efficiency; critical frequency; ring frequencies; dissipation loss factor.

TABLE OF CONTENTS

LIST OF FIGURES

LIST OF TABLES

NOMENCLATURE

c_o	Speed of sound in air
C_L	Panel longitudinal wave speed
d	Diameter of cylindrical shell
E	Elastic Young's modulus
E_1	Average acoustic energy stored in the internal sound field
E_i	Average acoustic energy of i^{th} resonant subsystem
E_j	Average acoustic energy of j^{th} resonant subsystem
E_k	Average acoustic energy of k^{th} non- resonant subsystem
f	Frequency of the analysis
f_c	Critical frequency
f_r	Ring frequency
f_L	Lower ring frequency
f_U	Upper ring frequency
h	Thickness
I_{in}	Incident sound intensity
I_t	Transmitted sound intensity
L	Length of conical shell
L_s	Cone slant length
L_T	Length of cone truncation
m_i	Mass of i^{th} resonant panel
m_k	Mass of k^{th} non-resonant panel

P_{in}	External power input to subsystem 1
p_i	Acoustic pressure
P_3	Total edge length
r	Radius of hemispherical shell
R_1	Smaller radius of cone
R_2	Larger radius of cone
S_i	Surface area of i^{th} resonant subsystem
S_k	Surface area of k^{th} non-resonant subsystem
$T_{1/2}$	Time-averaged decay time
T_{60}	Reverberation time of receiving room
V_1	Volume of the internal sound field
v_i	Vibration velocity of i^{th} resonant subsystem
v_k	Vibration velocity of k^{th} non-resonant subsystem
W_{1-nr}	Non-resonant sound power input to internal sound field
W_{i-r}	Resonant power input to i^{th} resonant subsystem
W_{2-r}	Resonant sound power input to cylindrical shell
W_{3-r}	Resonant sound power input to flat panel
W_O	Measured sound power of internal sound field
W_R	Radiated sound power level by enclosure panels
W_r	Sound power level radiated by hemispherical enclosure

Greek Symbols

η_i	Modal density of i^{th} subsystem
η_i^d , η_k^d	Dissipation loss factor of i^{th} resonant and k^{th} non- resonant subsystem
η_1^d	Dissipation loss factor of internal sound field
η_{ij}	Coupling loss factor between subsystems ***i*** and ***j***
η_{1k} , η_{k1}	Coupling loss factor between internal sound field to k^{th} non-resonant subsystem or vice-versa
ω	Radial frequency of the band
ρ , ρ_o	Material density and density of air
υ	Poisson's ratio of material
σ	Panel radiation efficiency of the force response
$\sigma(\theta_c)$	Panel radiation efficiency for the forced wave response at the point of coincidence angle
σ_i	Radiation efficiency of i^{th} resonant subsystem
σ_k	Radiation efficiency of k^{th} non- resonant subsystem
τ_4	Transmission coefficient of non-resonant cylindrical shell
τ_5	Sound transmission coefficient of non- resonant flat panel
τ_o	Overall transmission coefficient of cylindrical acoustic enclosure
τ	Mass law transmission coefficient
α	Truncation ratio $= \frac{L_T}{L_s}$

γ	Internal absorption coefficient
ψ	One-half cone angle at apex

ABBREVIATION

BEM	Boundary element method
DAQ	Data acquisition system
dB	Decibels
FEM	Finite element method
LMS	Leuven measurement systems
NR	Noise reduction
SEA	Statistical energy analysis
SI	Sound intensity
SPL	Sound pressure level
TL	Transmission loss
TMM	Transfer matrix method

Chapter 1

Introduction and Literature Review

This chapter presents the application and usefulness of acoustic enclosure to study sound transmission loss in automotive vehicles. A comprehensive review of the previously reported works by various authors in the domain of sound transmission of acoustic enclosures is also discussed. This chapter also describes the scope and objectives of the presented thesis in the later section. Towards the end, the organization of the thesis is presented.

1.1 Introduction

In the past few years, issues regarding structural vibration and airborne noise transmission control in the automotive passenger compartment have received great attention due to growing customer demands for improved comfort environments. Internal noise control is becoming of primary concern for such structures. Therefore, abating internal noise and excessive vibration levels are a major concern in the design of engineering structures from an acoustic point of view.

A thin-walled acoustic enclosure made of flexible panels is a significant kind of engineering structure. It is of interest because acoustic enclosures are the most adopted technique for decreasing the transmission of sound from noisy engines, equipments, and protecting drivers and occupants suffering from deteriorated voice communication, impaired efficiency, higher fatigue, and hearing damage at the workplace. Acoustic enclosures consisting of thin structural panels have a wide range of industrial applications. They are used in the cabinet of automotive vehicles, aircraft nacelles, tanks, undersea vehicles, machine parts, and architectural structures. Acoustic enclosures can be employed when the encapsulation of the noise source is a feasible and cost-efficient solution for noise control. Acoustic enclosures alter the sound transmission path by keeping the sound energy inside the enclosure and dissipating it through the mechanism of sound absorption.

Acoustic enclosures are classified into different categories: (1) large size loose-fitting type enclosures for containing the machine, (2) small size enclosures for enclosing smaller machine subsystems or components, (3) close-fitting type enclosures to enclose the machine part, (4) lagging or wrapping materials for the application of wrapping pipes, ducting and other systems, (5) large size enclosures to contain the passenger of the vehicle.

To predict cabin interior noise levels effectively, a clear understanding of the vibro-acoustic characteristics and the parameters which govern the response is imperative. There is a need to determine the acoustic performance of enclosures due to the commercial demand for quieter systems. The performance of an acoustic enclosure is strongly influenced by many variables such as geometry, panel material, thickness, the position of a source interior of the enclosure, noise control treatments, and occurrence of small apertures, etc.

Sound transmission loss is identified as an effective physical measure for quantifying the capability of acoustical enclosures for attenuating noise. Transmission loss has been defined as the most significant indicator to evaluate the performance of an acoustic enclosure which is described as the sound power level difference corresponding to internal and external acoustic fields of the enclosure, expressed in decibels. A study of sound transmission loss is imperative in the development and assessment steps of such systems.

1.2 Literature review

In this section, a state of the art literature review on the sound transmission loss of the acoustic enclosure is presented.

The literature on different techniques of transmission loss evaluations is reviewed for different shapes of acoustic enclosures. The applications of the acoustic enclosure are so broad that the sound transmission loss evaluation has become the most focusing research topic during the design and development phases of noise control engineering.

A significant number of approaches and methodologies have been defined in the past dealing with the noise control of acoustic enclosures and panels. For the determination of the transmission loss of an acoustic enclosure, four different methods are being employed by the researchers. These methods are the analytical method, numerical method based on finite element method and boundary element method, analytical-numerical method, and experimental method [1,2]

1.2.1 Analytical method

Some research on sound transmission loss for structural panels and acoustic enclosures using the analytical method is discussed here. Trochidis and Kalaroutis [3] computed the sound transmission loss through a double panel containing porous absorbing material between them. Chonan and Kugo [4] presented an exact analytical solution of the sound transmission loss of double-wall panels based on the two-dimensional elasticity principle. Osipov et al. [5] studied the transmission loss of a single plate of room partition in the low-frequency region from 20 Hz to 250 Hz. Pellicier and Trompette [6] documented a review work about the analytical methods based on the wave techniques to predict the transmission loss for infinite panels.

Besides the analytical methods, other analytical techniques such as transfer matrix methods [7–10] have also been used in order to study the transmission loss through panels. Campolina et al. [11] proposed the transfer matrix method and determined the transmission loss of a single-walled plate lined with sound-absorbing material. They investigated the influence of sound-absorbing material on the transmission loss of plate. Zhou et al. [12] presented the wave approach in order to calculate the transmission loss of a double-walled panel. They optimized the transmission loss of plates by its weight reduction and enhancing the sound transmission loss. Koval [13–15] developed an analytical model for predicting the transmission loss of a cylindrical shell for investigating the airborne sound transmission of an aerospace vehicle. Blaise et al. [16] advanced Koval's formulation to study the sound transmission of the orthotropic cylindrical shell. Lee and Kim [17–19] predicted the transmission loss of cylindrical structures subjected to acoustic excitations and examined the effect of different design variables on the acoustic performance of shells. Zhou et al. [12,20] presented the analytical model based on Love's theory [21–23] to predict the transmission loss of infinite plates and shells with sound-absorbing materials and incorporated the influence of the external mean flow in the formulation. Liu and He [24] developed the analytical model of double-walled sandwich cylindrical shells with poroelastic materials to calculate the transmission loss. They demonstrated that the sound transmission loss can be improved effectively using a poroelastic core in the mass-controlled range. Oliazadeh and Farshidianfar [25] developed an exact analytical model based on Donnell's theory [26] for the triple-walled shells lined with poroelastic materials to predict transmission loss. They showed that Donnell's theory is more precise than Love's theory and demonstrated that the triple-walled panels have better sound insulation performance than double-walled shells.

In order to study the sound transmission loss of conical shape structures, some analytical models are presented. Golzari and Jafari [27] proposed an analytical model to study the acoustic behavior of the truncated conical shell. Recently, Golzari and Jafari [28] studied an analytical model of a truncated conical shell to investigate the influence of poroelastic material on the sound transmission characteristics of the structure. Additionally, few analytical models are developed to study the acoustic performance of spherical and hemispherical structures.

Hasheminejad and Mehdizadeh [29] developed an analytical formulation using Biot theory along with Havriliak-Negami model to compute the noise reduction of the multi-layer hemispherical enclosure.

The literature work introduced so far in the analytical method used the wave propagation technique for the infinite plates and shells to investigate the sound transmission loss. The analytical method based on the wave approach has many benefits, in general, it offers relatively simple calculations, further reducing the computational cost [6]. The wave approach considers the physical mechanism such as critical frequency and mass law phenomenon. The approach can be applied to a broad frequency region.

The approach, however, has a number of drawbacks for predicting the transmission loss through infinite plates and shells. The wave approach does not include the influence of boundary conditions and damping of the system in the analytical formulation [30,31]. Therefore, the results are often reliable. Moreover, the wave approach is not capable to predict the transmission loss of nonhomogeneous panels.

A technique which is suitable for predicting the transmission loss of finite models of panels with specified boundary conditions is the statistical energy analysis (SEA) approach. The prediction of acoustic performance using the SEA approach has also received significant attention.

The SEA technique was introduced by Maidanik [32], Lyon [33], and Crocker and Price [34]. SEA is a modeling method to predict the transmission loss and acoustic response levels of structures in resonant motion using the energy flow relationships [33]. The SEA technique must therefore be considered as an alternative to the other analytical approach because it provides reliable estimates of sound transmission problems and allows computation over a broad frequency range. Cole et al. [35] predicted the in-cab noise reduction of a commercial vehicle or equipment enclosure by the SEA method by modeling the cabin enclosure as a rectangular box made of steel, incorporating the presence of sound-absorbing material inside the box and a small aperture in one side of the panel.

Oldham and Hillarby [36,37] described the two models for estimating the performance of an enclosure that is close-fitted and validated experimentally. The first model was related to the low-frequency excitation, and the latter was related to the higher frequency excitation based on the SEA technique. The experimental results suggested that the high-frequency excitation model provides a reliable and accurate prediction of insertion loss and depends on the sizes of panels and the dimension of the cavity volume. Renji et al. [38,39] studied theoretically and experimentally the phenomenon of the non-resonant response of structural panels and evaluated the non-resonant sound transmission of the thin structural panel. They demonstrated that consideration of non-resonant wave response in the analytical model is expected to improve the response estimation. Craik [40] and several other researchers [30,41,42] investigated the acoustic response and sound transmission through structural panels using the SEA approach. They considered the mechanism of non-resonant transmission for predicting the noise reduction of acoustic panels based on the limp plate mass law theory. Many studies were performed to examine the influence of resonant and non-resonant wave responses on the sound radiation characteristics and noise mitigation of rectangular acoustic enclosures using the SEA method [43–45]. The theoretical and experimental investigation presented that the analytical model considering the non-resonant response produces more accurate results than limp plate mass law.

Ming and Pan [44] presented the SEA model to predict the insertion loss of a rectangular acoustic enclosure at different frequency regions and investigated it experimentally using the sound intensity method. They showed that the acoustic performance of an enclosure is primarily controlled by the non-resonant modes in the mid-frequency region, while in the higher frequency region, it can be enhanced by maintaining the higher sound absorption internally of the enclosure. Lei et al. [45] employed the improved SEA model for predicting the noise reduction of rectangular acoustic enclosures in broad frequency ranges. They considered the non-resonant response and more precise transmission coefficient in the analytical formulation. Oliazadeh et al. [30,31] used the SEA theory to examine the sound transmission characteristics of flat panel and cylindrical structures with absorbing material. They adopted the mass law sound transmission coefficient in the developed SEA model to predict the transmission loss of cylindrical shells. They compared the theoretical results with the sound intensity and transmission suite experimental techniques. Numerous researchers [46–51] employed SEA theory to study the sound transmission behavior of automotive structures. Zhou and Crocker [52] performed the experimental and analytical study of sound transmission through foam-filled honeycomb sandwich structures using the SEA model. Recently, Oliazadeh et al. [53] developed a SEA model to investigate the acoustic behavior of honeycomb sandwich panels. They used a sound intensity experimental approach to measure the transmission loss and compared it with the analytical results.

Chronopoulos et al. [54] developed a SEA model to predict the transmission loss of composite cylindrical shells of various geometries for the design study of the aircraft fuselage. They computed the essential SEA parameters such as modal density and the sound radiation efficiency using the analytical formulas. Xie et al. [55] investigated the vibroacoustic response of a complex structure subjected to broadband excitations by an identification technique of high-frequency loads based on the SEA technique. Chronopoulos et al. [56] presented the work based on the SEA technique to predict the structural response of an aerospace structure subjected to broadband excitations. They estimated the energy parameter of each subsystem and validated the model with experimental measurements.

1.2.2 Numerical method

Numerical methods based on the finite element method and boundary element method are effectively used for predicting the transmission loss of structures and are generally employed for comparing the transmission loss results obtained by other methods.

Many theoretical models based on finite elements (FE) and boundary elements (BE) numerical methods were developed to investigate the acoustic response and sound transmission through structural panels [57–61]. Shi et al. [62] and many other researchers [63,64] used numerical approaches and focused on vibration behaviors and transmission loss of rectangular acoustic enclosures. Several other researchers [65–71] focused on vibration behaviors, interior acoustic responses, and sound radiation characteristics of three-dimensional, thin-walled elastic or box-type structures. Cheng and Nicolas [72], and many other researchers [73–77], conducted numerical examinations to assess the sound transmission behavior of aircraft cabins. Numerous research studies are performed to examine the sound radiation of conical shape panels. Vipperman et al. [78] employed the finite element approach to explore the acoustic behavior of a conical shape structure. Wang et al. [79] demonstrated a numerical technique to evaluate the acoustic performance of a conical panel. Eslaminejad et al. [80] presented the experimental and numerical modal analysis to study the modes of a fluid-filled aluminum hemispherical shell.

1.2.3 Analytical -numerical method

The transmission loss prediction requires complex mathematical formulations and takes higher computational time. Researchers are trying to solve these problems using an analytical method and the numerical approach to analyze sound transmission.

The approaches based on numerical models are not well suited to high-frequencies transmission calculation of complicated structures due to extensive computing resources and high computation cost. However, some

FE-based strategies employ periodic structure theory, which significantly improves the numerical efficiency of the model [81–84]. Parrinello et al. [85] proposed an approach for predicting the transmission loss of multilayered cylinders using the dynamic stiffness matrix of the FE model in a framework of the transfer matrix method (TMM). These techniques are represented as an efficient acoustic tools and are numerically efficient in modeling complex structures. Tebyanian and Ghazavi [86] devised a combination technique employing the analytical approach with boundary and finite element approaches. Few theoretical and mathematical methods are developed to study the acoustic performance of spherical and hemispherical structures using an analytical-numerical approach [87,88].

1.2.4 Experimental method

Experimental methodologies have also been established to measure the transmission loss and other useful parameters of the structures.

Crocker and Price [34] measured transmission loss of partition through the transmission suite technique based on sound pressure measurement to validate the analytical model. Zhou and Crocker [52] employed the transmission suite method to measure the sound transmission loss of honeycomb sandwich panels and verify the SEA model of transmission loss. Cole et al. [35] and other researchers [31,37,89] employed the transmission suite method to evaluate the sound transmission loss of acoustic enclosures. Wang et al. [90] and numerous researchers [30,44,45] used the sound intensity technique to measure the sound transmission loss of structural panels and enclosures. Oliazadeh et al. [53] measured the transmission loss of honeycomb sandwich panels using sound intensity experimental technique to validate the analytical model. Lai and Burgess [91] and other researchers [92] proposed a sound intensity experimental technique to measure the damping of plates. Additionally, many studies investigated the coupling loss factor parameters used in the SEA analysis. Mace [93] and other researchers [94–101] estimated the coupling loss factor of complex vibroacoustic systems.

Many experimental techniques have also been developed to measure the dissipation loss factor of the structures. These are: the half-power bandwidth technique, decay rate technique, and power injection method. Bies and Hamid [102] and many other researchers [103–105] used experimental techniques to measure the frequency average loss factors of the structures.

1.2.5 Conclusions of the literature

It is found from the above literature survey that four different methods evaluate the sound transmission loss of structures. These methods are the Analytical method, numerical method, analytical, numerical method, and experimental method. These methods are also used for the analysis of structure acoustic interaction.

The literature review has revealed that the performance of an acoustic enclosure and panels is strongly influenced by many variables such as geometry, panel material, thickness, the position of a source interior of the enclosure, noise control treatments, and occurrence of small apertures, etc. It has been shown in the theoretical and experimental investigation that the presence of sound-absorbing material inside the enclosure improves the transmission loss effectively. Commonly applied analytical methods in the literature are based on the wave approach for predicting the transmission loss of single and multilayer plates and shells. The analytical models based on the transfer matrix method consider the influence of sound-absorbing material between multilayer partitions. Further, the transfer matrix method is adequate for predicting the transmission loss of infinite multilayer panels lined with sound-absorbing materials. However, the analytical method based on the wave approach does not produce satisfactory results in the low-frequency region. Several studies based on finite element and boundary element methods have demonstrated the usefulness and application of numerical methods to evaluate the transmission loss of panels. However, the numerical methods are not well suited to high-frequencies transmission loss calculation of complicated structures due to extensive computing resources and high computation time. However, some FE-based strategies based on the combination of numerical and analytical methods employ periodic structure theory, which significantly improves the numerical efficiency of the model.

A technique which is suggested based on the literature review for the finite dimensions of the structural panels is the Statistical energy analysis method. The SEA includes the influence of boundary conditions and damping considerations of the system. From the literature review, it is clear that the SEA method can be applied to a wide frequency range to predict transmission loss.

1.3 Motivation of the research

From the introduction and literature review, it is found that transmission loss evaluation is the current topic for research. The researchers are trying to improve the existing methods in order to predict the transmission loss of structural panels.

Apart from the Analytical methods based on the wave approach and numerical methods, the analytical method based on the SEA technique is also used for predicting the transmission loss. It has shown that the transmission loss evaluation of structural panels using the SEA method has gained notable consideration. SEA method considers the effect of boundary condition and dissipation mechanism of the panels in the analytical formulation. It produces reliable results compared to the analytical method based on the wave approach. The approaches based on numerical methods are not well suited to high-frequencies transmission calculation of complicated structures due to extensive computing resources and high computation cost. Therefore, the SEA technique must be used as an alternative approach to the wave-based and numerical methods to evaluate the transmission loss of the structural panels because it enables the computation in a broad frequency range and provides accurate results. The

SEA method contributes a good basis for evaluating the structural response and transmission loss of panels due to acoustic excitation, consisting of the contributions through a physical mechanism of resonant and non-resonant modes. With regards to evaluate the transmission loss of cylindrical acoustic enclosures, modeling the transmission loss of flat panels and rectangular acoustic enclosures by considering non-resonant response using the SEA technique is well documented in the literature. To the best of the knowledge based on the literature survey, there is no published work for computing the transmission loss of cylindrical acoustic enclosure using SEA when there is a consideration of non-resonant wave response and using the more precise and accurate sound transmission coefficients of structural panels in the analytical model. It is pertinent to emphasize that non-resonant wave response is significant for structural panels such as aircraft fuselage, and hence it becomes essential to compute it.

With regards to model the acoustic behavior and predicting the transmission loss of conical and hemispherical shape structures, most of the research focused on the sound transmission and acoustic behavior of single and multilayer plates and shells and rectangular shape enclosures. There is only a little work in a SEA context to study the sound transmission characteristic of conical and hemispherical shape structures. Hence sound transmission loss of the conical and hemispherical shape enclosure is required to evaluate using the SEA method. The effect of significant acoustic parameters such as radiation efficiency, ring, and critical frequencies on the transmission loss performance of conical and hemispherical shape enclosures is needed to study.

With regards to investigate the acoustic performance of different shapes of acoustic enclosures, there is a need to measure the transmission loss of different shapes of acoustic enclosures by keeping the same volume.

Additionally, there is a need to study the influence of different shapes of sound-absorbing materials on the noise reduction of the acoustic enclosure.

1.4 Objectives of the research

The objective of this research is to develop an analytical model for predicting the transmission loss and verifying it using the experimental study. The objectives are as following:

- To predict the sound transmission loss of cylindrical shape acoustic enclosure using SEA method and verifying the analytical model using sound intensity technique.
- To predict the sound transmission loss of conical shape acoustic enclosure using SEA method and validating the analytical model using sound intensity technique.
- To predict the sound transmission loss of hemispherical shape acoustic enclosure using SEA method and verifying the analytical model using sound intensity technique.
- To study the sound transmission loss of different shapes of acoustic enclosures using the sound intensity technique.
- To experimentally investigate the effect of sound absorbing material of different surface shapes on the noise reduction of an acoustic enclosure.

1.5 Outline of the thesis

The chapter-wise breakup of the presented thesis is as follows:

Chapter 1 deals with the introduction and enlists a review of the previously carried out works in the evaluation of the sound transmission loss of acoustic enclosure and structural panels. A brief introduction of the different methods: analytical methods, numerical methods, analytical-numerical methods, and experimental methods are discussed. After that motivation of the research and the objectives of the thesis are presented.

Chapter 2 demonstrates the SEA methodology for predicting the sound transmission loss of a cylindrical acoustic enclosure. The description of the experimental setup to measure the sound transmission loss is presented. The analytical predictions are compared with the measured results to validate the analytical model. The parametric study is also performed to investigate the influence of different design parameters on the sound transmission loss of cylindrical acoustic enclosure. In the last, the summary of the chapter is presented.

Chapter 3 presents the SEA procedure for predicting the sound transmission loss of a conical acoustic enclosure. The experimental setup to evaluate the sound transmission loss is described in detail. A comparison of the analytical predictions with the measured results is presented to verify the analytical model. The parametric study is also conducted to examine the influence of various design variables on the sound transmission loss of conical acoustic enclosure. In the last, the summary of the chapter is discussed.

Chapter 4 describes the SEA methodology for predicting the sound transmission loss of a hemispherical acoustic enclosure. The experimental setup to measure the sound transmission loss is explained in detail. A comparison of the analytical predictions with the measured results is demonstrated for validating the analytical model. The parametric study is also carried out to investigate the influence of various design variables on the sound transmission loss of hemispherical acoustic enclosure. In the last, the summary of the chapter is presented.

Chapter 5 presents the experimental study to investigate the sound transmission loss of different shapes of acoustic enclosures. The description of the experimental setup to measure the sound transmission loss is presented in detail. After that, the experimental results are compared for the different shapes of acoustic enclosures. In the last, the summary of the chapter is presented.

Chapter 6 demonstrates the experimental investigation of sound-absorbing material of different surface shapes on the noise reduction of an acoustic enclosure. The experimental setup to measure noise reduction is described. The experimentally obtained noise reduction is compared for the different shapes of sound-absorbing materials. In the last, the summary of the chapter is discussed.

Chapter 7 enlists the overall conclusion of the thesis. In the last, the future scope of the study is discussed.

Chapter 2

Prediction of sound transmission loss of cylindrical acoustic enclosure

In this chapter, sound transmission through a cylindrical shape acoustic enclosure is predicted analytically and verified experimentally. An analytical model is developed based upon the statistical energy analysis (SEA) approach to examine the transmission loss of a cylindrical acoustic enclosure in different frequency regions, including low, intermediate, and high-frequency ranges. In the developed model, the non-resonant wave response is included in addition to the consideration of resonant response for obtaining more accurate results. To validate the analytical model, an experimental setup was developed, and sound transmission loss of a cylindrical acoustic enclosure was measured using the sound intensity experimental technique. It was found that the analytical results are in good agreement with the measured transmission loss. The results obtained indicate that the proposed analytical model is efficient to predict the sound transmission loss of cylindrical acoustic enclosures.

2.1 Introduction

Cylindrical acoustic enclosures made of thin elastic structural panels are broadly employed in the applications of many transport vehicles, mainly in the aerospace industry. Internal noise control is becoming of primary concern for aerospace structures. To predict cabin interior noise levels effectively, a clear understanding of the vibro-acoustic characteristics and the parameters which govern the response is imperative.

Transmission loss has been identified as the most significant indicator to evaluate the performance of an acoustic enclosure which is described as the sound power level difference corresponding to the interior and exterior acoustic fields of the enclosure, expressed in decibels [30,106].

The transmission loss of a structural component because of acoustic excitation is the result of contributions through the resonant and non-resonant wave responses [38,107]. The resonant component of the response is also called free-response due to resonant structural modes as a result of the interaction between free bending sound waves and the structural boundaries and causing resonant wave sound radiation. Moreover, the non-resonant component of the wave response is termed as the forced response which contributes significantly to the occurrence of non-resonant sound transmission because of matching of the trace wavelength of the incident sound with the wavelength of the propagating waves in the structure. As a result of a similar wavelength, the non-resonant wave response radiates more effectively, and greater sound energy is transmitted through the structure. However, the response of resonant wave components is considerably small at frequencies lower than the critical frequencies of structural panels due to a shorter wavelength of resonant wave response than the wavelength of incident sound waves in the air [39]. Therefore, the resonant wave response is an insufficient radiator compared to the non-resonant wave response lower than the critical frequencies of the structural panels. The resonant wave response has the same wavelength as that of the non-resonant wave response, at a frequency around the critical frequencies of panels. Thus, the radiating property of free response is similar to that of forced response about these frequencies.

The non-resonant wave response is normally estimated through the sound transmission characteristics of panels based on mass law. In general, a panel which does not have flexural rigidity (limp panel), exhibits mass law sound transmission behavior. In a practical situation, structural panels having a certain amount of stiffness and sound radiation and transmission behavior of such panels can not be given by mass law. In such a situation, sound transmission behavior also depends on the bending stiffness.

Although the non-resonant wave response is dependent directly on the panel's sound power transmission coefficient, it becomes significant around the critical frequencies of structural panels. Therefore, it is significant to include the non-resonant wave response contribution of structure to investigate their sound transmission behavior when excited acoustically.

Renji et al. [38,39] studied theoretically and experimentally the phenomenon of the non-resonant response of structural panels and evaluated the non-resonant sound transmission of the thin structural panel. They demonstrated that consideration of non-resonant wave response in the analytical model is expected to improve the response estimation. Many studies were performed to examine the influence of resonant and non-resonant wave responses on the sound radiation characteristics and noise mitigation of rectangular acoustic enclosures using the SEA method. The theoretical and experimental investigation presented that the analytical model considering the non-resonant response produces more accurate results than limp plate mass law.

To this end, this chapter contributes a good basis for evaluating the transmission loss of cylindrical acoustic enclosure due to acoustic excitation, consisting of the contributions through a physical mechanism of resonant and non-resonant modes. To predict the resonant and non-resonant sound transmission, the resonant wave response and the non-resonant wave response are treated as two separate subsystems in the present SEA formulation. The presented SEA model can evaluate the resonant and non-resonant sound transmission of the cylindrical acoustic enclosure. Experimental measurements on acoustic cylindrical enclosure using sound intensity technique are exhibited to measure the sound transmission loss of a cylindrical acoustic enclosure to validate the accuracy and robustness of the developed analytical model.

2.2 Analytical model formulation

In the SEA technique, a system under investigation refers to the entire assembly of linked structures and acoustic spaces. The system is then distributed into a number of subsystems that are characterized by its modal energy. The total power supply to every subsystem is provided from an external acoustic source of excitation, which is equivalent to the power losses due to the internal damping of subsystems and transmitted between them. A model of an acoustic cylindrical enclosure consists of a cylindrical shell, and a flat circular top panel welded together, as shown in Fig. 2.1 and Fig. 2.2.

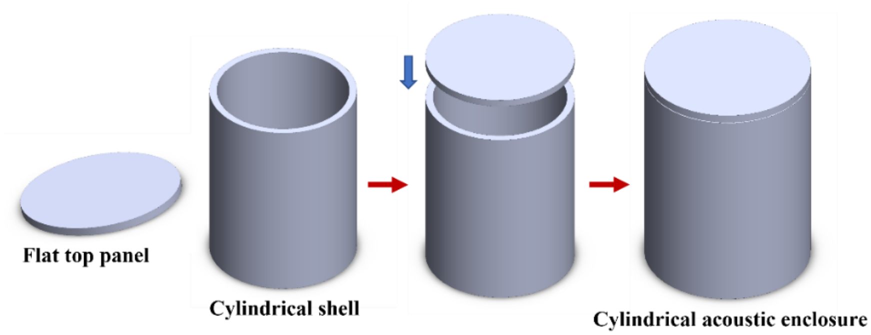

Figure 2.1 A schematic sketch showing the various components of a cylindrical acoustic enclosure

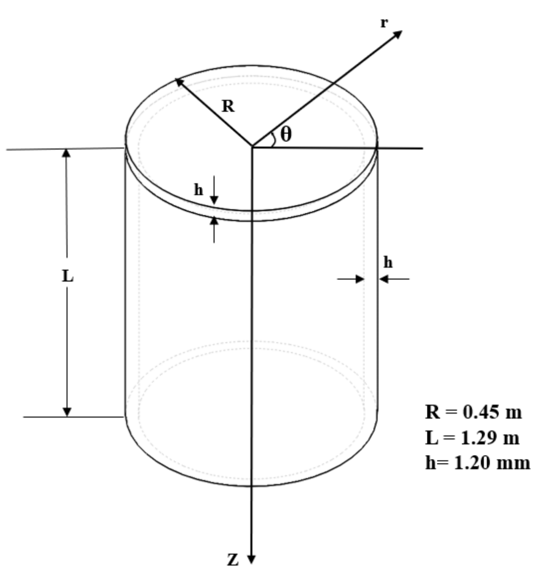

Figure 2.2 Schematic diagram of a cylindrical acoustic enclosure

Each panel is assumed to be thin, isotropic elastic, and of uniform thickness. The external source exciting the considered system is acoustic. The external sound source excites the enclosure cavity acoustically, placed inside the enclosure. Table 2.1 shows the material properties used in the transmission loss problem of the acoustic cylindrical enclosure.

Table 2.1 Material properties used in the transmission loss problem of a cylindrical acoustic enclosure

Symbol	System variable	Value
ρ	Density	7850 kg/m^3
E	Elastic Young's modulus	2×10^{11} Pa
υ	Poisson's ratio	0.3
R	Radius of cylindrical shell	0.45 m
L	Length of cylinder	1.29 m
h	Thickness	1.20 mm

In the present analytical formulation for the proposed SEA model, both the resonant as well as non-resonant wave responses are considered separately as two individual subsystems. The internal sound field in the enclosure cavity is not split through resonant and non-resonant subsystems, considering the losses due to coupling are signified with regard to the total acoustic power.

The SEA model for the low-frequency regions and the intermediate and high-frequency regions is shown in Fig. 2.3 and Fig. 2.4, in which subsystem 1 represents the internal sound field stored in the enclosure cavity. Subsystems 2 and 4 are represented by the resonant and non-resonant wave response of the shell (cylindrical panel), respectively. Similarly, subsystems 3 and 5 are represented by the resonant and non-resonant wave response of the enclosure flat panel, respectively.

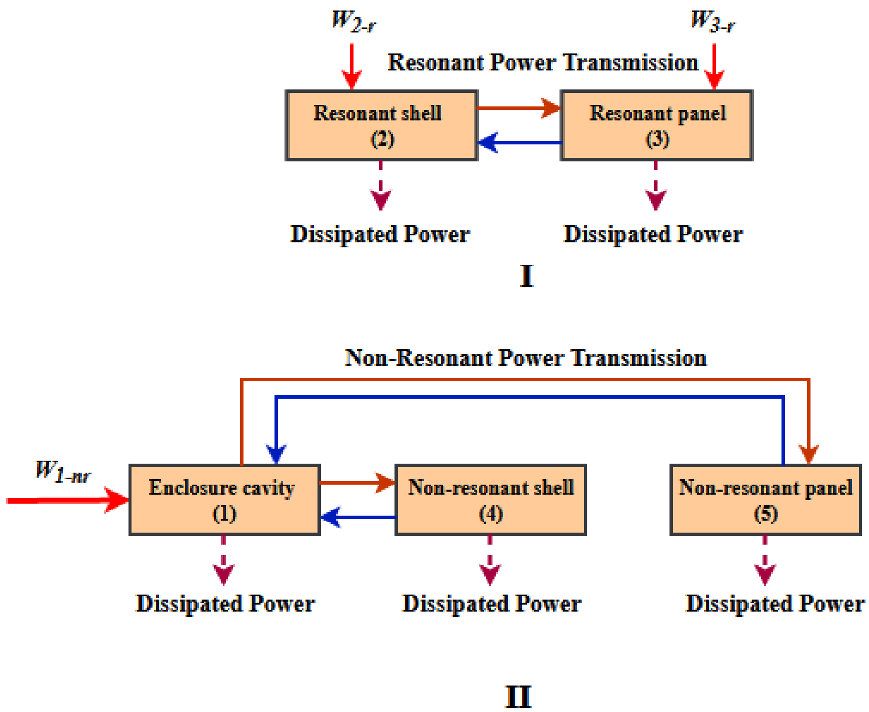

Figure 2.3 Schematic representation of energy flow paths I and II for low-frequency SEA model

Hence, five subsystems exist in the developed SEA model of an acoustic cylindrical enclosure. In the low-frequency region, the enclosed fluid volume is stiffness controlled and has insufficient resonant modes, though enclosure panels act resonantly. In this frequency range, the acoustic energy transmits from the enclosed air volume to the panels and follows two energy flow paths, as shown in Fig. 2.3.

The first energy flow path introduces the resonant power transmission between the subsystems, as shown in Fig. 2.3 (I). Path I does not consider the internal sound field as a separate individual subsystem in the low-frequency SEA model due to the absence of resonant modes inside the enclosure cavity. Hence, the enclosure cavity becomes non-resonant. However, the acoustic sound source excites the resonant response of the panels.

Thus, as a result of power balance for Path I, the equation can be written for the ***i***th resonant structural subsystem (***i***= 2,3,…..,N):

$$\omega\left[n_i^d E_i - \sum_{\substack{j=2 \\ j\neq i}}^{N} n_{ji} E_j\right] = W_{i\text{-}r} \tag{2.1}$$

where, $\omega = 2\pi f$, in which f is the frequency band of the analysis, E_i and E_j are the average stored acoustic energy in the ***i***th subsystem and ***j***th subsystem respectively, n_i^d is the dissipation loss factor of ***i***th subsystem, n_{ji} is the coupling loss factors from ***j***th subsystem to ***i***th subsystem, $W_{i\text{-}r}$ is the resonant power input at the ***i***th subsystem, and can be written as [17] :

$$W_{i\text{-}r} = \frac{n_i n_i^d \left(1-\tau_o\right) W_s}{\sum_{i=2}^{N} n_i n_i^d} \tag{2.2}$$

where, W_s is the measured sound power of the enclosed noise source, n_i is the modal density of ***i***th subsystem.

τ_o is the overall sound transmission coefficient of the cylindrical acoustic enclosure which is given as follows:

$$\tau_o = \tau_4 \tau_5 \tag{2.3}$$

where, τ_4 and τ_5 are the sound transmission coefficient of non-resonant component of enclosure cylindrical shell and flat panel, respectively.

In the present SEA formulation, in addition to the inclusion of non-resonant wave response, the more precise and accurate non-resonant sound transmission coefficient of structural panels is used in the whole frequency range, which considers the influence of bending stiffness and size of the panels. The expression of non-resonant sound transmission of the cylindrical shell is given by Szechenyi [108] based on statistical conception.

In the present formulation, the non-resonant sound transmission coefficient is obtained by rearranging and solving the expression of Szechenyi [108] and given as follows:

$$\tau_4 = \begin{cases} \dfrac{1.996}{x^{0.833} y^2}, & f \le f_r \\ \dfrac{1.996}{x^{0.833}} & f > f_r \end{cases} \tag{2.4}$$

where, f_r is the cylindrical shell ring frequency. The variables x and y can be given as follows:

$$x = \left[\upsilon_o^{\,2} \left(\frac{h}{R} \right)^2 \frac{E\rho}{4{\rho_o}^2 {c_o}^2} \right] \left[1 - \left(\frac{\upsilon_o f_r}{f_c} \right)^2 \right]^2 + 2.3 \tag{2.5}$$

$$y = \frac{\pi}{2} \sin^{-1} \left\{ \upsilon_o \left(1 - \left(\upsilon_o \frac{f_r}{f_c} \right)^2 \right)^{1/2} \right\}^{1/2} \tag{2.6}$$

where, $\upsilon_o = \dfrac{f}{f_r}$, ρ and E are the density and Young's modulus of the panel material, respectively.

The sound transmission coefficient of the enclosure non-resonant flat panel is expressed as [109]:

$$\tau_5 = \begin{cases} \dfrac{\sigma^2(\theta_c)}{2ar(\sigma(\theta_c) + a\eta_5^d)} \left\{ \arctan\left[\dfrac{2a}{\sigma(\theta_c) + a\eta_5^d} \right] - \arctan\left[\dfrac{2a(1-r)}{\sigma(\theta_c) + a\eta_5^d} \right] \right\} + \dfrac{2\langle\sigma\rangle}{a^2}, & f \le f_c \\ \dfrac{\sigma^2(\theta_c)}{2ar(\sigma(\theta_c) + a\eta_5^d)} \left\{ \arctan\left[\dfrac{2a}{\sigma(\theta_c) + a\eta_5^d} \right] - \arctan\left[\dfrac{2a(1-r)}{\sigma(\theta_c) + a\eta_5^d} \right] \right\}, & f > f_c \end{cases} \tag{2.7}$$

where, $a = \omega\rho h / 2\rho_o c_o$, in which, h is the thickness of the panel, ρ_o and c_o are the density and sound speed in the air, $\sigma(\theta_c)$ is the panel radiation efficiency for the forced wave response at the point of coincidence angle, f_c is referred to as panel critical frequency, $r = f / f_c$ is addressed as the ratio of frequency.

$\langle\sigma\rangle$ is the panel radiation efficiency of the forced structural response averaged for all the wave incidence angles.

The second energy flow path II describes the acoustic energy transmission non-resonantly through the interior acoustic field to the enclosure panels, as shown in Fig. 2.3 (II). Therefore, the enclosure cavity can be considered a separate subsystem in the developed analytical model.

The internal sound field of the enclosure cavity is denoted as subsystem 1, then, the power balance equations for Path II, can be written respectively for the subsystem 1 and ***k^th^*** non-resonant structural subsystem (***k***= 4, 5,…..,N) as follows:

$$\omega\left[n_1^d E_1 - \sum_{k=4}^{N} n_{k1} E_k\right] = W_{1\text{-}nr} \tag{2.8}$$

$$\omega\left[n_k^d E_k - n_{1k} E_1\right] = 0 \tag{2.9}$$

where, n_1^d and E_1 are the dissipation loss factor and average acoustic energy of the sound field stored in the enclosure cavity respectively, n_k^d and E_k are the dissipation loss factor and average acoustic energy of the $\boldsymbol{k^{th}}$ non-resonant subsystem respectively, n_{1k} and n_{k1} is the coupling loss factors from enclosure cavity to non-resonant subsystem and coupling loss factor from non-resonant subsystem to enclosure cavity respectively.

W_{1-nr} is the sound power that causes the non-resonant wave response, which is given by [44]:

$$W_{1\text{-}nr} = \tau_o W_s \tag{2.10}$$

In the intermediate and high-frequency ranges, both the internal sound field as well as enclosure panels exhibit resonant modes. Therefore, the internal sound field in the enclosure cavity can be considered as a separate individual subsystem in this case as shown in Fig. 2.4.

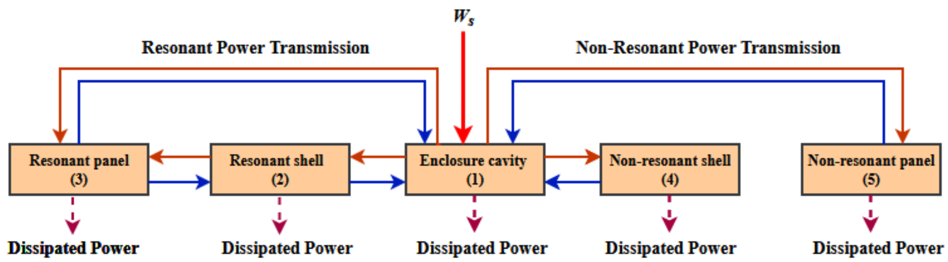

Figure 2.4 Schematic representation of energy flow paths for the developed SEA model at intermediate and high-frequency regions

Moreover, apart from resonant transmission between the enclosed acoustic field and the enclosure panels, the internal sound field is further coupled to the non-resonant wave response of structural panels.

Therefore, the power balance equations in this case, can be written respectively for the subsystem1, ***i**th* resonant subsystem (***i***= 2, 3,…..,N) and for the ***k**th* non-resonant structural subsystem (***k***= 4, 5,…..,N) as follows:

$$\omega\left[n_1^d E_1 - \sum_{i=2}^{N} n_{i1} E_i - \sum_{k=4}^{N} n_{k1} E_k \right] = W_s \tag{2.11}$$

$$\omega\left[n_i^d E_i - n_{1i} E_1 - n_{ji} E_j \right] = 0 \tag{2.12}$$

$$\omega\left[n_k^d E_k - \eta_{1k} E_1 \right] = 0 \tag{2.13}$$

where, n_{1i} and n_{i1} is the coupling loss factor from enclosure cavity to resonant subsystem and coupling loss factor from resonant subsystem to enclosure cavity, respectively.

The Eqs. (2.1), (2.8), (2.9) are rearranged in the form of matrix equations. Therefore, SEA matrix equation at the low frequencies can be written as:

$$\omega \begin{bmatrix} n_1^d & 0 & 0 & -n_{41} & -n_{51} \\ 0 & n_2^d & -n_{32} & 0 & 0 \\ 0 & -n_{23} & n_3^d & 0 & 0 \\ -n_{14} & 0 & 0 & n_4^d & 0 \\ -n_{15} & 0 & 0 & 0 & n_5^d \end{bmatrix} \begin{Bmatrix} E_1 \\ E_2 \\ E_3 \\ E_4 \\ E_5 \end{Bmatrix} = \begin{Bmatrix} W_{1\text{-}nr} \\ W_{2\text{-}r} \\ W_{3\text{-}r} \\ 0 \\ 0 \end{Bmatrix} \tag{2.14}$$

Similarly, Eqs. (2.11), (2.12) and (2.13) are rearranged in the form of matrix equations. Thus, the SEA matrix equation at the intermediate and high frequencies can be written as follows:

$$\omega\begin{bmatrix} n_1^d & -n_{21} & -n_{31} & -n_{41} & -n_{51} \\ -n_{12} & n_2^d & -n_{32} & 0 & 0 \\ -n_{13} & -n_{23} & n_3^d & 0 & 0 \\ -n_{14} & 0 & 0 & n_4^d & 0 \\ -n_{15} & 0 & 0 & 0 & n_5^d \end{bmatrix}\begin{Bmatrix} E_1 \\ E_2 \\ E_3 \\ E_4 \\ E_5 \end{Bmatrix} = \begin{Bmatrix} W_s \\ 0 \\ 0 \\ 0 \\ 0 \end{Bmatrix} \tag{2.15}$$

Therefore, the average acoustic energy of each subsystem at the low, intermediate, and high frequencies can be obtained through inverting the coefficient matrix of Eqs. (2.14) and (2.15).

It is noted that the expression of the important SEA parameters, modal density, coupling loss factor, and dissipation loss factor are given in Appendix A.

2.2.1 Transmission loss

The acoustic property of an enclosure is evaluated by the sound transmission loss, which is classified as the most important and appropriate performance indicator for such structures. The transmission loss is expressed in decibels (dB) and is defined as [44,110]:

$$TL = 10\log_{10}\left(W_s / W_R \right) \tag{2.16}$$

where, W_R is the radiated sound power level by the exciting enclosure panels.

Moreover, the total sound power which is radiated through all the resonant and non-resonant structural subsystems into the exterior receiving room is estimated by [45]:

$$W_R = \sum_{i=2}^{N} \rho_o S_i c_o \sigma_i v_i^{\,2} + \sum_{k=4}^{N} \rho_o S_k c_o \sigma_k v_k^{\,2} \tag{2.17}$$

where, σ_i , S_i ,and v_i are respectively the radiation efficiency, surface area, and vibration velocity of the ***ith*** resonant subsystem. Similarly, σ_k , S_k , and v_k are respectively the radiation efficiency, surface area, and vibration velocity of the ***k*** th non-resonant subsystem.

The mean square vibration velocity of each subsystem $v_i^{\ 2}$ and $v_k^{\ 2}$ is obtained as follows:

$$v_i^{\ 2} = E_i / m_i \ , \tag{2.18}$$

$$v_k^{\ 2} = E_k / m_k \ , \tag{2.19}$$

where, m_i and m_k are the mass of the i^{th} resonant subsystem and k^{th} non-resonant subsystem respectively. It should be noted that geometric parameters such as mass and surface area of resonant and non-resonant subsystems are identical.

The transmission loss of an acoustic cylindrical enclosure is computed by using Eqs. (2.16) and (2.17) for the developed SEA model.

2.2.2 Resonant mode number study

In order to apply the SEA model in the different frequency regions, the number of total resonant modes at each center frequencies of 1/3 octave band of the internal sound field, cylindrical shell, and the top panel is plotted in Fig. 2.5. Based on the data in Fig. 2.5, it can be evaluated that the internal sound field in the enclosed volume has very less resonant modes in the range of frequency from 100 Hz to 250 Hz while structural panels possess sufficient resonant modes in this region.

Cremer and Heckl [1,36] recommended that greater than six number of resonant modes are required in each frequency band of interest in each subsystem to represent the diffuse sound field. In the range of frequency from 315 Hz to 400 Hz, the internal sound field and structural panels have a sufficient number of resonant modes to have diffuse sound fields.

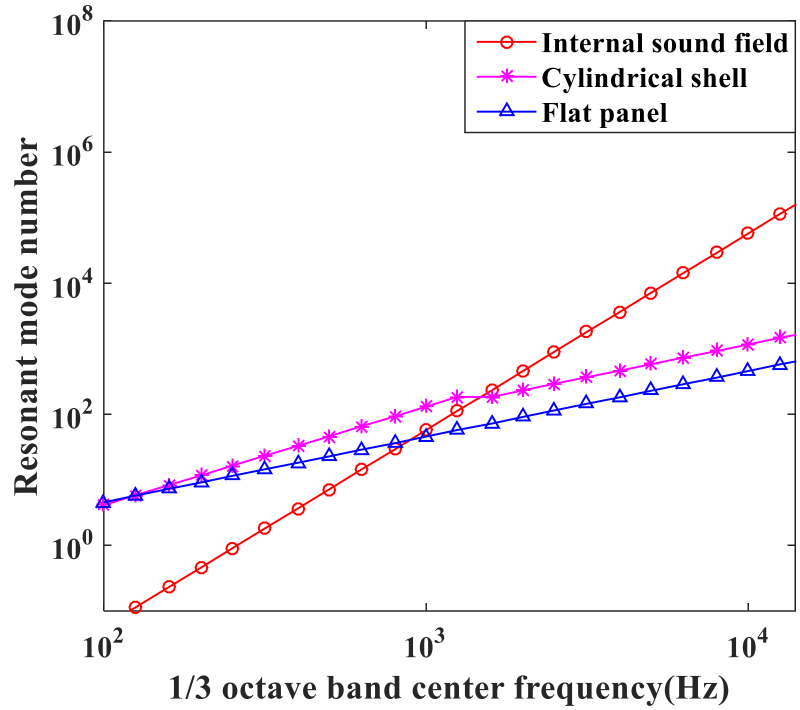

Figure 2.5 Resonant mode number of the internal sound field, shell, and the top panel at the center frequency of 1/3 octave band

Similarly, the resonant modes greatly increase for the higher frequencies, and internal sound field and structural panels represent diffuse sound fields. Thus, for the present analytical models, based on the number of resonant modes, it is evaluated that the low range of frequency begins with 100 Hz to 250 Hz, the medium range of frequency is between 315 Hz to 400 Hz, and the higher frequency region begins through 500 Hz.

2.3 Experimental studies

To validate the analytical model of the cylindrical acoustic enclosure, developed using the SEA method for evaluating the transmission loss, the experimental investigation was conducted in the soundproof chamber in the air medium, as shown in Fig. 2.6. The volume of the soundproof chamber is 16 m^3. The experiments were performed on a cylindrical shape acoustic enclosure made of galvanized steel, which has a diameter and length of 0.9 m and 1.29 m, respectively.

Figure 2.6 Soundproof chamber

The dimensions of the acoustic enclosure are the same as those considered in analytical modeling, which is listed in Table 1. The air density and speed of the sound in the air are taken as 1.21 kg/m^3 and 344 m/s, respectively.

2.3.1 Dissipation loss factor measurement

The dissipation loss factor of the structural panels is evaluated experimentally using the decay rate technique based on a resonant mode transient response [33]. The flat-top panel and the cylindrical shell were hung freely and excited separately using the impact hammer [Model: Dytran series 5800B4] of sensitivity 2.25 mV/N, which is shown in Fig. 2.7.

Figure 2.7 Impulse hammer: Dytran series model -5800B4

The schematic diagrams of the measurement of the dissipation loss factor of the flat top panel and the cylindrical shell are shown in Fig.2.8 and Fig. 2.9, respectively.

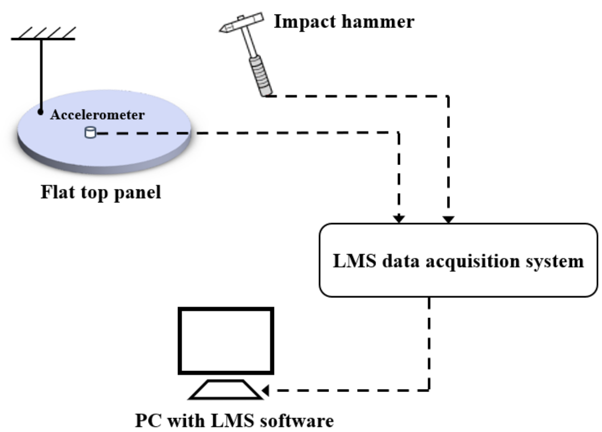

Figure 2.8 Schematic diagram of the experimental setup to measure the dissipation loss factor of the flat top panel

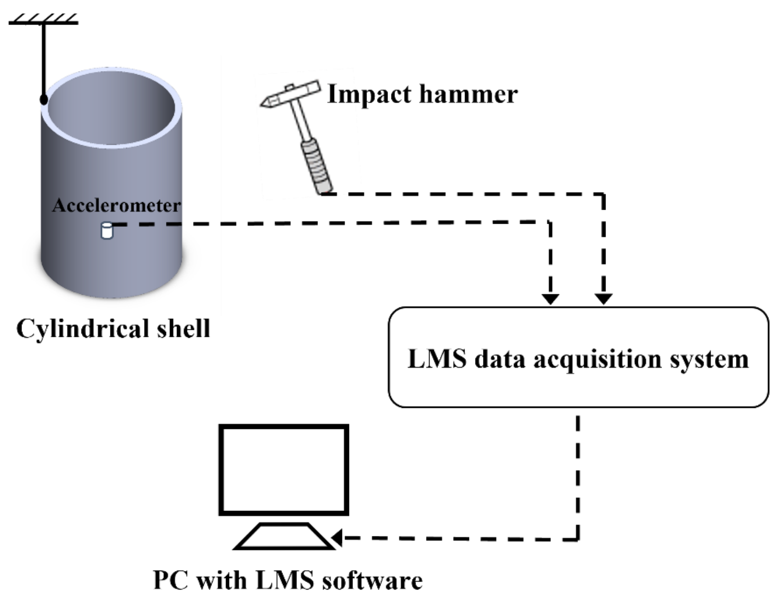

Figure 2.9 Schematic diagram of the experimental setup to measure the dissipation loss factor of the cylindrical shell

Fig. 2.10 and Fig. 2.11 show the experimental setup of the dissipation loss factor measurement for the flat top panel and the cylindrical shell, respectively.

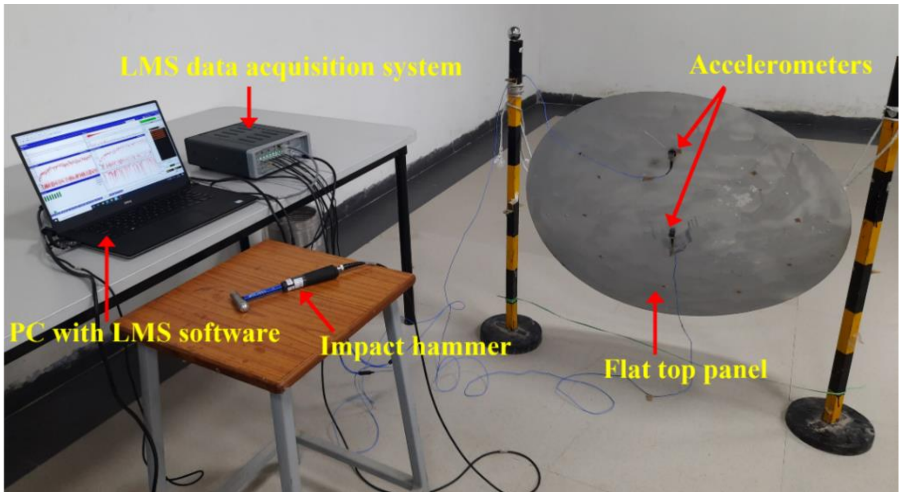

Figure 2.10 Experimental setup to measure the dissipation loss factor of the flat top panel

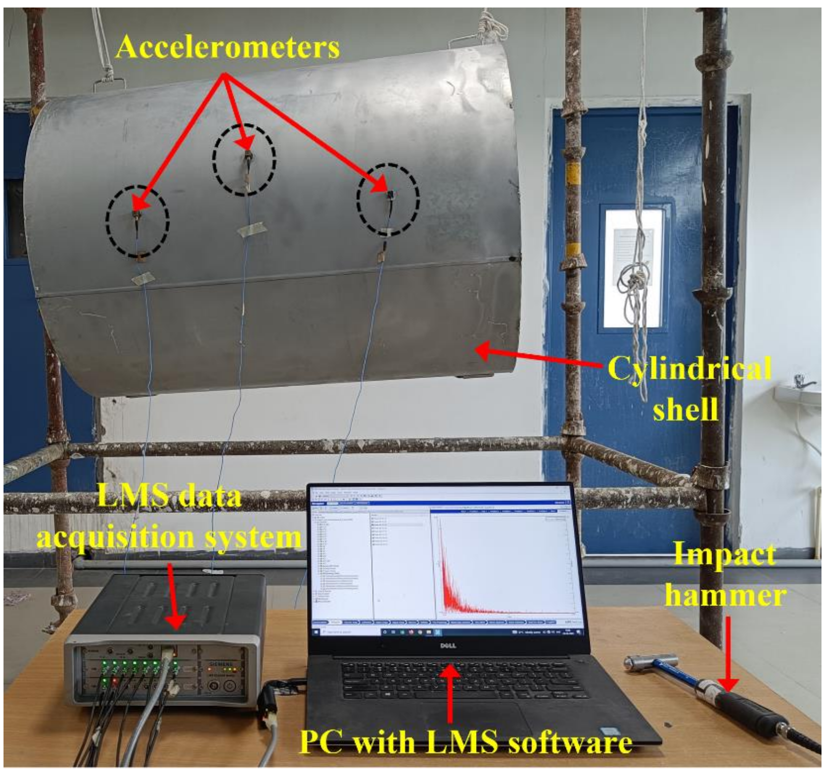

Figure 2.11 Experimental setup to measure the dissipation loss factor of the cylindrical shell

The decay characteristic of the top panel and cylindrical shell is tested at different positions of the piezoelectric accelerometer, as shown in Fig. 2.12.

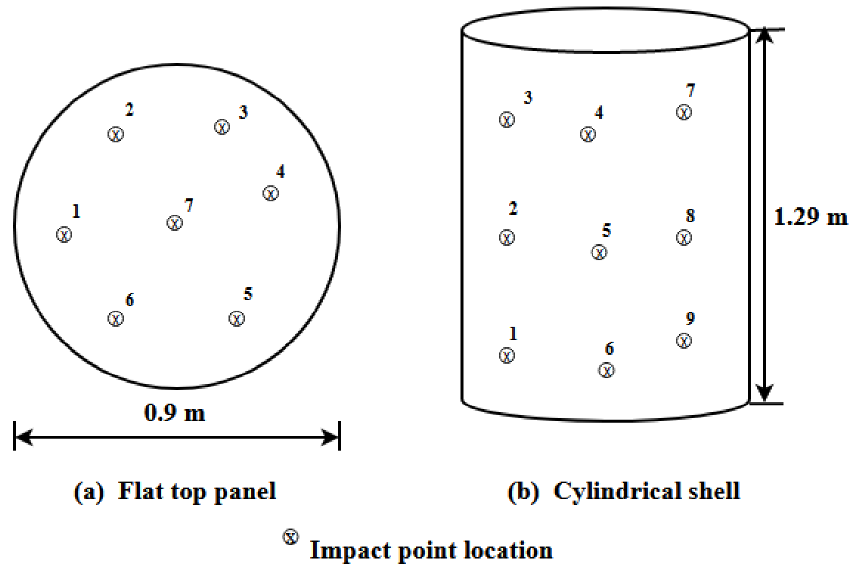

Figure 2.12 Hammer impact point positions on enclosure panels

The impulse hammer was connected to a 16-channel LMS data acquisition system, a PC (Dell-INTEL Core), and PCB356A16 series lightweight accelerometers of sensitivity 100 mV/g. For obtaining reliable results, the measurement was repeated two times, and a total of five impacts were made at each accelerometer location, and then the time-averaged decay time was measured.

The dissipation loss factor of the panels is correlated to time-averaged decay time $T_{1/2}$ by the following expression [33]:

$$\eta_i^d = {0.22}/{fT_{1/2}} \tag{2.20}$$

The time-averaged dissipation loss factor of the structural flat top panel and cylindrical shell at the center frequency of 1/3 octave band is shown in Fig. 2.13.

The results obtained from the impact hammer experiments are reliable up to 14kHz. The impact test experiment was performed using a hammer tip made of metal to cover the frequency range of interest. The measured dissipative loss factor was utilized to predict the sound transmission loss of the enclosure for more accurate results.

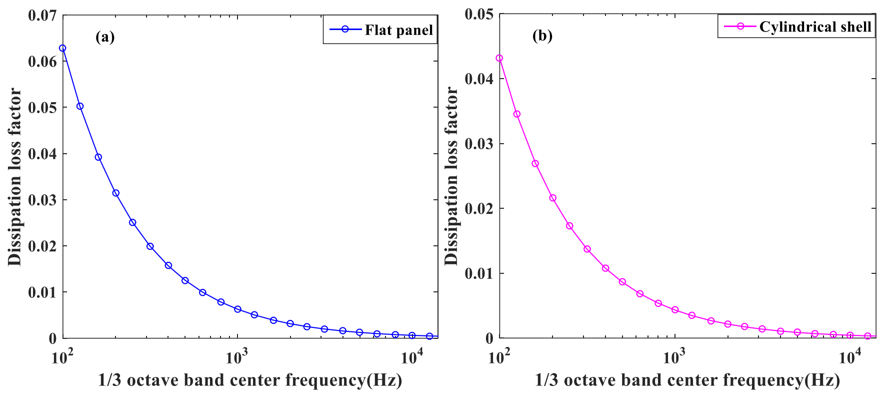

Figure 2.13 Measured dissipation loss factor: (a) top flat panel (b) cylindrical shell

2.3.2 Transmission loss measurement using sound intensity method

The sound intensity technique is based on the measurement of the sound intensity of the enclosed noise source and the transmitted sound intensity through the structure. Thus, the sound transmission loss can be evaluated through the expression given [30,106]:

$$TL = 10\log_{10}\left(\frac{I_{in}}{I_t}\right) \tag{2.21}$$

where, I_{in} and I_t are the incident sound intensity of the noise source and transmitted sound intensity, respectively.

To investigate the effectiveness of the acoustic enclosure and the accuracy of the analytical model, it was desirable to obtain transmission loss of the enclosure based on Eq. (2.21). The internal volume of the enclosure was excited acoustically using a sound source to measure transmission loss.

An omnidirectional sound Source type 4292-L (Brüel & Kjær system) (product operating frequency range 50 Hz -5000 Hz) was employed as an actual sound source with different acoustic excitations (pink noise and white noise). The sound source is controlled by LMS data acquisition system (Test lab 17.0) through source control option with high amplification rate (2.5 Volt) in order to generate acoustic power of high frequencies. Therefore, the omnidirectional sound source was placed centrally inside the enclosure and fed with pink noise and white-noise signals to generate the sound power at adequate low, intermediate, and higher frequencies. During the measurements, the opening of the enclosure was faced to the ground on the soundproofing mat to prevent any acoustic leakage. The measured transmission loss is obtained using the sound intensity method from the spatial average sound intensity measurement over the enclosure panels and the sound intensity determination of the noise source in the soundproof chamber.

The schematic sketch of the experimental test setup is shown in Fig. 2.14. The experimental setup of the sound transmission loss measurement of the cylindrical acoustic enclosure is presented in Fig. 2.15. The essential components of the test setup are shown in Fig. 2.16.

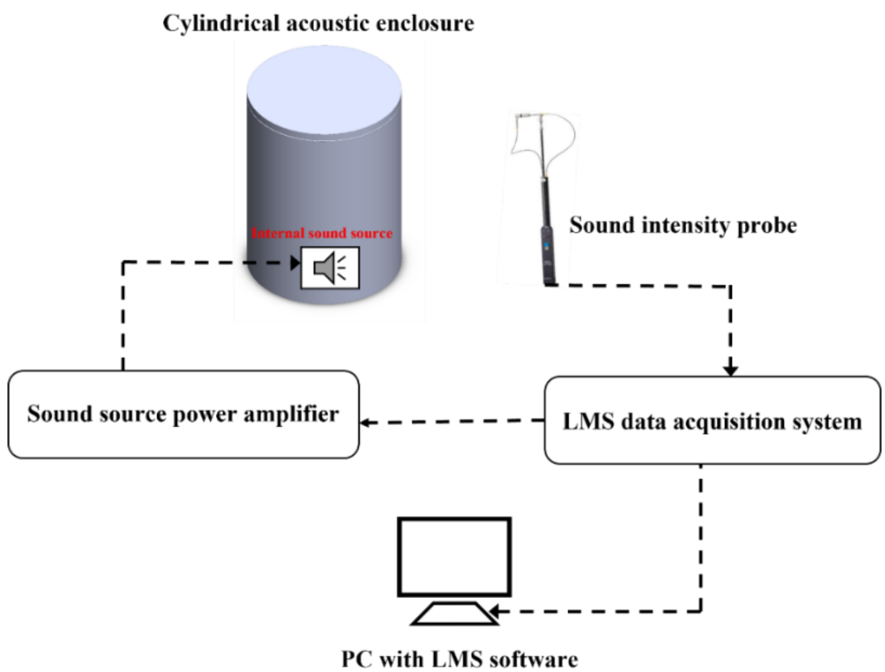

Figure 2.14 Schematic sketch of the experimental setup for measuring the transmission loss using the sound intensity method

The sound intensity was measured using the G.R.A.S intensity probe (type 50GI-R), connected with a 16-channel LMS data acquisition system and a PC (Dell-INTEL Core). The probe consisted of two 1/2-inch microphones, which were phase-matched together and separated through a spacer. To cover the whole frequency range during the measurements, four interchangeable solid spacers were used to maintain the spacing of microphones at 12 mm, 25 mm, 50 mm, 100mm.

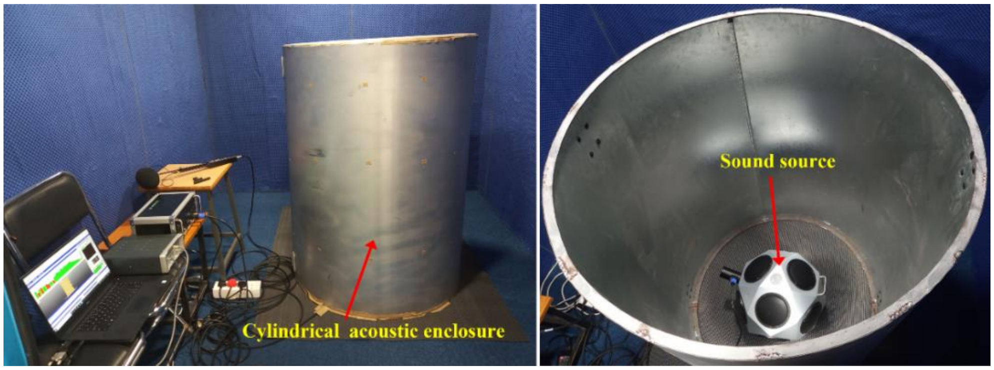

Figure 2.15 Experimental setup for measuring the transmission loss using the sound intensity method

Table 2.2 shows a list of measurable frequency range for different spacers.

Table 2.2 List of measurable frequency range for different spacers

Spacer size (mm)	Measurable frequency range (f) (Hz)
12	f>120 Hz
25	120-6000
50	60-2000
100	30 -1000

The sound intensity measurement was carried out following the international standard ISO 9614-1 discrete point technique [111] by dividing each enclosure panel surface into small segments and measuring the sound intensity in each segment.

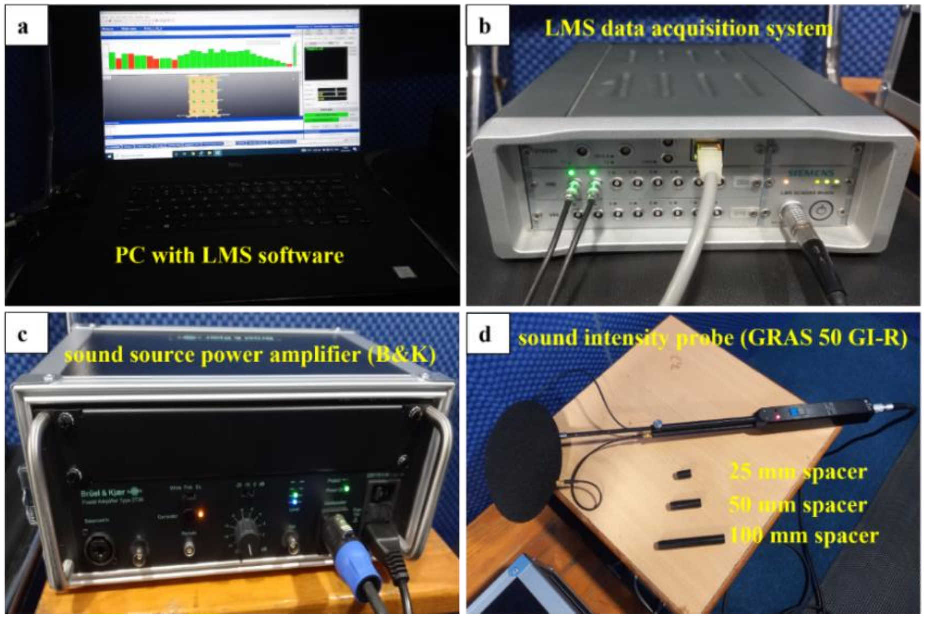

Figure 2.16 Essential components of an experimental setup for the measurement of the transmission loss

Each segment was measured three times using different spacers for obtaining more accurate and reliable results. The sound intensity was measured at a 0.05 m distance from the respective surface of the sound source and enclosure panels. The transmission losses were measured repetitively at different sections of the enclosure. The averaging time considered for sound intensity data acquisition was of 12 seconds.

Fig. 2.17 shows the measured sound power of the noise source at the center frequency of 1/3 octave band to produce the acoustic energy of different frequencies with respect to white noise and pink noise.

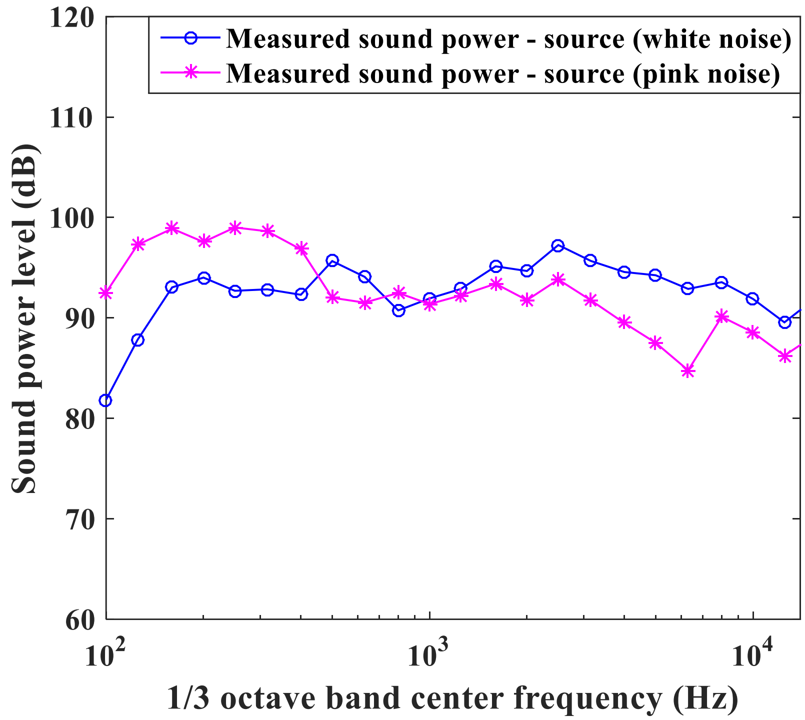

Figure 2.17 Comparison between measured sound power of noise source (white noise) with the measured sound power of source (pink noise)

White noise is a signal which contains equal energy per hertz and has a constant power spectral density, whereas pink noise is a signal that contains equal energy in each octave band and has the power spectral density that is inversely proportional to frequency. Moreover, the pink noise signal contains high acoustic energy at lower frequencies, whereas the white noise signal allocates more acoustic energy to the higher frequencies. Therefore, low frequencies are emphasized for the case of pink noise compared with that of white noise. The experiment was repeated two times to measure the reliable sound power of the noise source under different excitation conditions. Based on the experimental data, the measured sound power under pink noise excitation is reliable in the frequency range from 100 Hz to 250 Hz. Similarly, the measured sound power under white noise excitation is used in the frequency region starts through 315 Hz.

2.4 Results and Discussion

In this section, the results of the experimental measurements and analytical results of the SEA model are presented. The curves drawn in Fig. 2.18 show the sound power levels transmitted and radiated through the cylindrical acoustic enclosure and predicted analytically with different energy transmission mechanisms at the one-third octave frequency band.

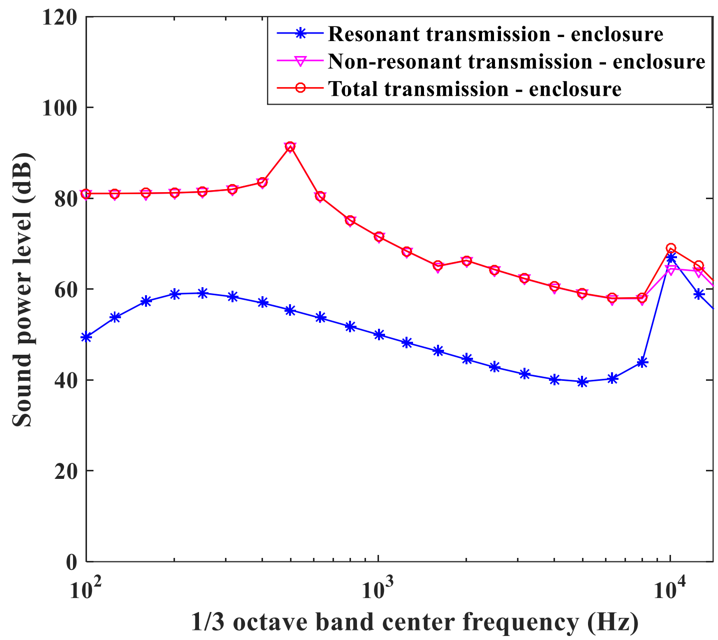

Figure 2.18 Radiated sound power from the acoustic cylindrical enclosure using different energy transmission mechanisms

A comparison is made between the radiated sound power levels of resonant subsystems (by considering the resonant response only) with that of non-resonant subsystems. The results indicate that non-resonant sound energy transmission is larger than resonant energy transmission at frequencies lower than the critical frequencies of panels, which is 10280 Hz. It is also observed that the acoustic sound energy transmission and radiation are dominated by resonant responses as well as by non-resonant components of the wave response around the critical frequencies. Moreover, the prediction of sound power levels through different sound transmission phenomena indicates that considering non-resonant response in the analytical model is very significant for evaluating acoustical energy transmission more precisely. Thus, the non-resonant response component is additionally considered with the resonant wave response in the present analytical formulation. Based upon the foregoing consideration, it is of interest to evaluate the sound power levels radiated through various sections of the enclosure surface area. The sound power radiated from the flat top panel of a cylindrical acoustic enclosure is predicted analytically and presented in Fig. 2.19 at the center frequency of one-third octave bands, comprising resonant, non-resonant, and total sound transmission. It is observed that the sound power transmitted through the top panel below the critical frequencies is mainly controlled by only non-resonant sound transmission but governed by both the resonant as well as non-resonant sound transmission around the critical frequencies of panels. The sound power levels radiated through the cylindrical section of the acoustic enclosure are predicted analytically and shown in Fig. 2.20 in the one-third octave frequency bands, comprising of resonant, non-resonant, and total sound transmission. The analytical calculations estimated the ring frequency of the cylindrical panel, which is about 1860 Hz. It is seen that the sound energy radiated and transmitted from the cylindrical section is governed by only non-resonant sound transmission below critical frequencies of the panel but regulated by both the resonant as well as for non-resonant sound transmission near and above the critical frequencies of panels. The sound transmission is principally governed by the non-resonant wave response below the critical frequency because the resonant wave response has a poor radiation efficiency in this range of frequency.

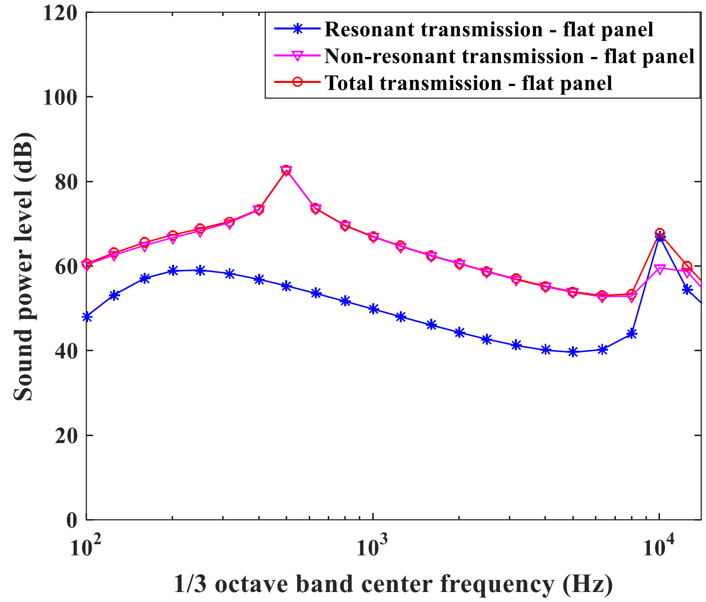

Figure 2.19 Flat-panel sound power transmission: analytical comparison between resonant transmission, non-resonant transmission, and total transmission

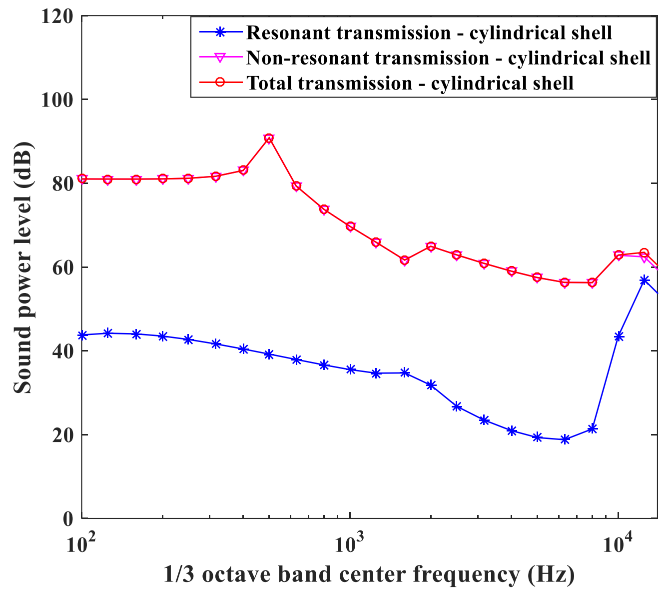

Figure 2.20 Cylindrical shell sound power transmission: analytical comparison between resonant transmission, non-resonant transmission, and total transmission

The resonant wave response is an insufficient radiator because the wavelength of the resonant wave response is smaller than that of sound in the air below the critical frequency of the structure. The resonant wave response and the corresponding radiation efficiency are large at frequencies near the critical frequency. Thus, the sound radiation from resonant wave response is significant only at frequencies near the critical frequency of the panel. Moreover, structural panels possess some amount of stiffness, and their sound power transmission characteristics depend on the bending stiffness as well. In this situation, the sound power transmission coefficient near the critical frequency of the panel is very large. Since the non-resonant response contribution is directly dependent on the sound power transmission coefficient, it becomes significant near about the critical frequency of the structure. Hence, above the ring frequency also, the non-resonant wave response is dominant, compared to the resonant wave response below the critical frequency. While near about the critical frequency, both the resonant and non-resonant wave responses are significant.

Fig. 2.21 predicted analytically the sound transmission loss of the cylindrical acoustic enclosure using different energy transmission mechanisms at the one-third octave frequency bands comprising of resonant, non-resonant, and total sound transmission loss. The analytical model predicts the ring frequency of the cylindrical panel, which is about 1860 Hz. Similarly, the critical frequency of enclosure panels is predicted to be about 10280 Hz. As expected, the sound transmission loss of a cylindrical acoustic enclosure is mainly controlled by non-resonant sound transmission below the critical frequencies but regulated by both the resonant and non-resonant sound transmission near and above the critical frequencies of panels. Therefore, it is observed that non-resonant transmission is equally significant as resonant transmission, particularly at frequencies near around the critical frequencies of the top panel and cylindrical shell, respectively. Meanwhile, it is noted from the above results that responses could be chiefly underestimated if the non-resonant wave responses are not considered in the analytical model.

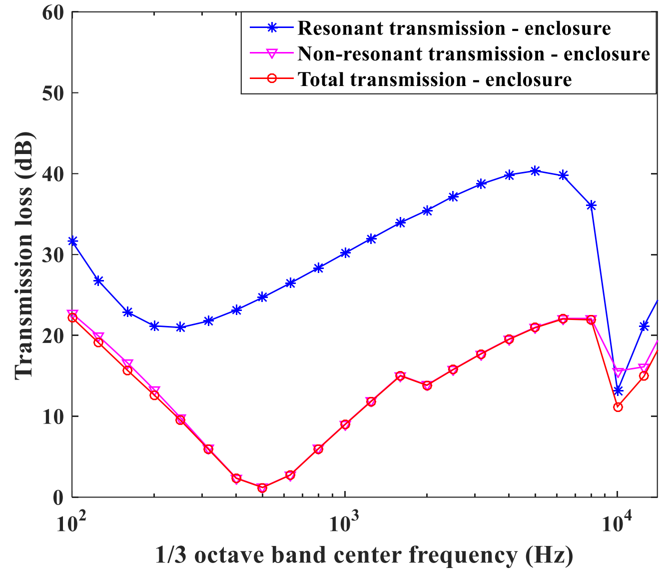

Figure 2.21 Sound transmission loss of cylindrical acoustic enclosure using different energy transmission mechanisms

Fig. 2.22 compares the results of the SEA model prediction and measured sound transmission loss of a cylindrical acoustic enclosure using the experimental sound intensity method in the 1/3 octave frequency band.

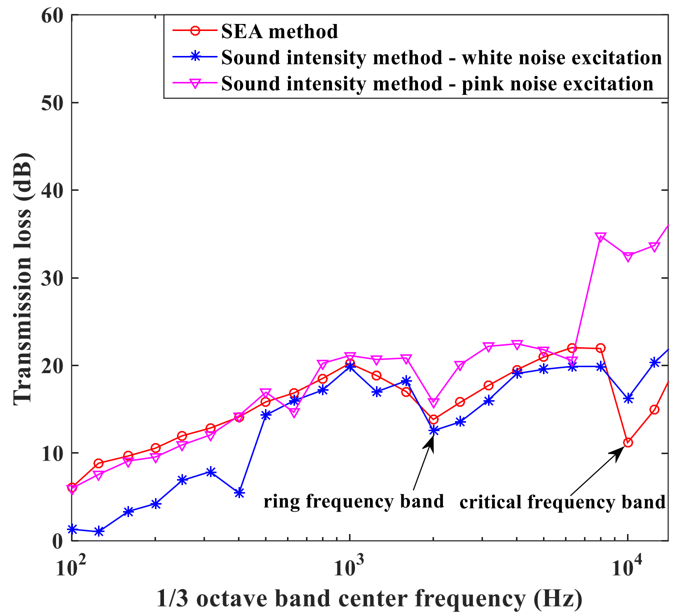

Figure 2.22 Analytical and experimental comparison of transmission loss of the acoustic cylindrical enclosure at the center frequency of 1/3 octave band

It is seen that the measured results of the transmission loss under pink noise excitation agree well with the analytical prediction from the frequency region of 100 Hz to 250 Hz. The transmission loss results under white noise excitation are compared with the analytical predictions that indicate reasonably good agreement at frequencies starts through 315 Hz. However, the discrepancy between the experimental results and analytical predictions above the critical frequency may be presumably due to a limited number of measurement points.

As expected, the developed SEA model estimated the two noticeable drops in the sound transmission loss graph presented in Fig. 2.22. The first drop appears at the frequency of 1860 Hz, the ring frequency of the cylindrical shell, strongly associated with the breathing mode of shell resonance nearest to the measured result, which is 1761 Hz. The second drop appears at the point of 10280 Hz, which is the critical frequency of the enclosure panels. The predicted critical frequency of the enclosure panels is found to be nearest to the measured results of critical frequency, which is about 9880 Hz. Comparing the analytical prediction and measured results, the percentage error of the ring frequency is 5.32 % and that for the critical frequency of the enclosure panels is 3.89 % which represents fairly a reasonable agreement between the analytical and experimental results. It can be observed from the analytical and experimental results, as shown in Fig. 2.22, that sound transmission loss increases through the low-frequency range up to the ring frequency at which sudden drop occurs because of the breathing mode of cylindrical panel resonance. Above the ring frequency, the transmission loss further increases up to the critical frequency of the enclosure panels. The trend of the sound transmission loss curve is to be anticipated, which rises through the lower frequency range to intermediate frequency range based on the non-resonant sound transmission, which is mainly regulated by non-resonant wave modes because of the low radiation efficiency of resonant modes below the critical frequencies. As the impinging sound waves frequencies get closer to the critical frequencies of the enclosure panels, an abrupt fall occurs due to the higher radiation efficiencies and a strong excitation of structural panels in a resonance condition. In this condition, flexural wave speed in the structural panels is equivalent to the sound wave speed in the air. Above the critical coincidence frequency of the enclosure panels, transmission loss further increases because, in this range of frequency, sound transmission strongly depends upon the impinging sound waves frequency and structural damping, which controls the vibration and sound radiation characteristics of enclosure panels.

It is found from the analytical and experimental results in Fig. 2.22 that sound transmission loss of the acoustic cylindrical enclosure increases about 8 dB and 12 dB, respectively, in the lower and intermediate range of frequency. At the high-frequency bands, transmission loss is enhanced by about 21 dB, which is a great achievement from an acoustic point of view.

2.5 Parametric studies

The analytical model formulated for the acoustic cylindrical enclosure can be used very efficiently at the fundamental design and assessment stages of cylindrical shape vibro-acoustic systems.

To investigate the efficacy of various design parameters to improve the effectiveness and transmission loss performance of a cylindrical acoustic enclosure, parametric studies are performed.

2.5.1 Effect of the internal absorption coefficient

The internal absorption coefficient of the enclosure acts significantly in transmission loss performance. Fig. 2.23 shows that the use of a larger internal absorption coefficient ($3.6\times10^{-4}\sqrt{f}$) inside the acoustic enclosure in comparison to a smaller internal absorption coefficient ($1.8\times10^{-4}\sqrt{f}$), improves the transmission loss performance effectively.

It is seen in Fig. 2.23 that transmission loss can be raised to 3 dB if the internal absorption coefficient is doubled.

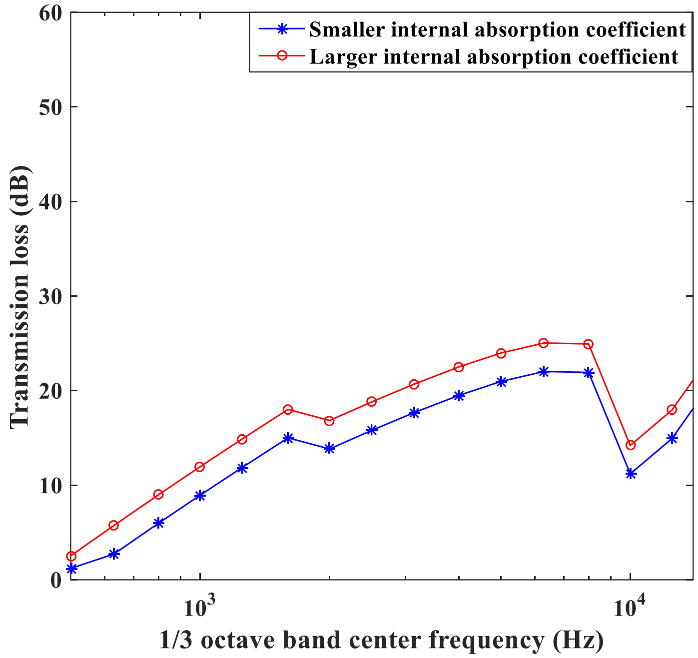

Figure 2.23 Comparison of transmission loss with respect to internal absorption coefficient of acoustic cylindrical enclosure

2.5.2 Effect of thickness

In a practical application, the enclosure panels are designed only as thick as required due to weight constraints.

It is seen in Fig. 2.24 that doubling the thickness caused about 5 dB enhancement of transmission loss up to the frequency band of 4000 Hz. There is no improvement of transmission loss by increasing the thickness in the frequency regions between 4000 Hz to 8000 Hz. Above the frequency of 8000 Hz, the transmission loss increases greatly, about 15 dB. Therefore, changing the thickness of panels significantly influences the transmission loss performance of the cylindrical acoustic enclosure. If the target transmission loss is known from the noise level consideration, an appropriate thickness of the enclosure panels can be easily estimated.

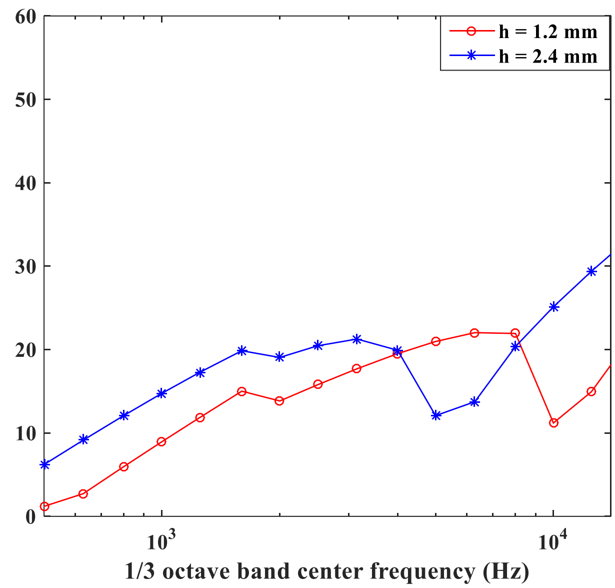

Figure 2.24 Comparison of transmission loss with respect to the thickness of acoustic cylindrical enclosure

2.5.3 Effect of length to diameter ratio

As shown in Fig. 2.25, a larger l/d ratio reduces transmission loss performance of an enclosure, mainly due to the curvature influence of the cylindrical shell on its stiffness and larger surface area.

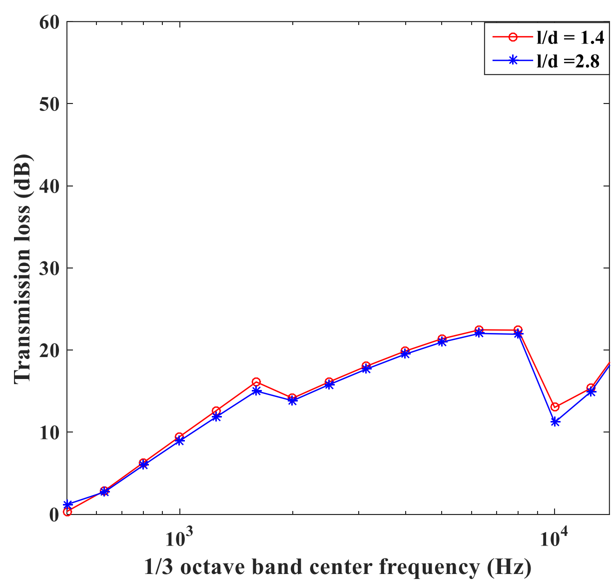

Figure 2.25 Comparison of transmission loss with respect to length to diameter ratio of the acoustic cylindrical enclosure

Because of this, enclosure panels radiate the acoustic energy more effectively. Therefore, this critical parameter should be considered more carefully while designing the cylindrical acoustic enclosure.

2.5.4 Effect of different materials

Fig. 2.26 shows the influence of the panel materials on the sound transmission efficiency of the acoustic cylindrical enclosure.

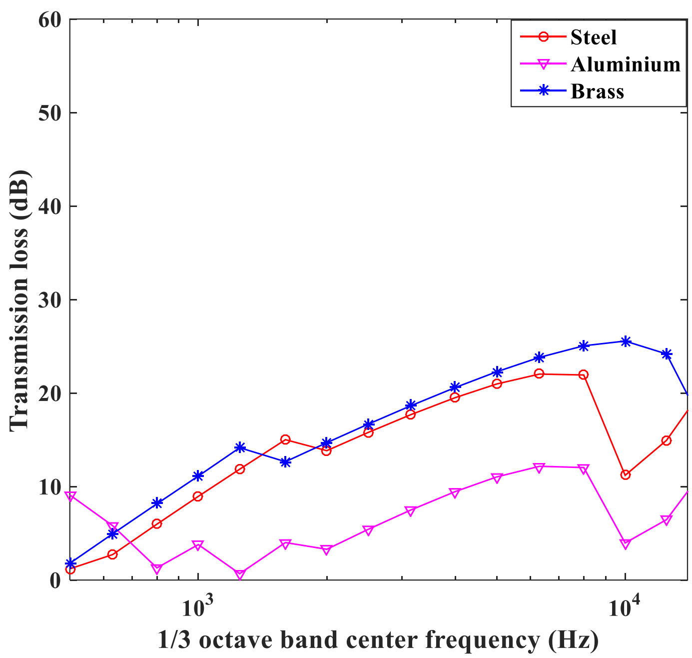

Figure 2.26 Comparison of transmission loss with respect to the material of acoustic cylindrical enclosure

The materials selected for the comparison are steel, aluminum, and brass, with the properties of materials given in Table 2.3.

Table 2.3 Material properties used for a cylindrical acoustic enclosure

Material	Density (kg/m^3)	Elastic Young's modulus (GPa)	Poisson's ratio
Steel	7850	200	0.3
Aluminum	2700	69	0.33
Brass	8500	104	0.36

Fig. 2.26 indicates that the transmission loss performance of a cylindrical acoustic aluminum enclosure is least effective in the entire frequency regions because of the lowest mass and stiffness, which is well anticipated. The result shows that the cylindrical acoustic enclosures made of steel and brass improve the sound transmission loss performance effectively in the broad frequency regions, which are well anticipated because both the steel and brass have higher stiffness and mass, respectively. Moreover, the transmission loss performance of the cylindrical acoustic enclosure made of brass is most effective because it has the largest density, enabling it to be more efficient in the mass-controlled high-frequency region.

2.6 Conclusions

In this work, the analytical models are presented based upon the SEA technique for predicting the transmission loss performance of cylindrical shape acoustic enclosures. The analytical formulation, models the cylindrical acoustic enclosure in different frequency regions, including low, intermediate, and high frequencies. In addition to resonant responses, the non-resonant responses are also considered in the model for predicting more accurate transmission loss of acoustic enclosure. The more precise sound transmission coefficient of enclosure panels that incorporate the influence of bending stiffness, structure size, and more accurate forced radiation efficiency, is utilized in the analytical formulations. It is found that resonant responses and non-resonant responses are very much significant at frequencies around the critical frequencies of panels. It is demonstrated that, below the critical frequency, transmission loss of cylindrical enclosure is principally regulated by the non-resonant wave modes only. The sound intensity experimental technique is employed for measuring the sound transmission loss of acoustic cylindrical enclosure. It is found that the analytical predictions show fairly a good agreement with the measured transmission loss and predict well the ring and critical frequencies of enclosure panels. The percentage error between analytical and measured ring frequencies is 5.32 %, and that for the critical frequency of enclosure panels is 3.89 % which is acceptable.

It was predicted analytically and experimentally that transmission loss of the cylindrical acoustic enclosure increases about 8 dB and 12 dB, respectively, in the lower and intermediate range of frequency. The sound transmission loss is enhanced by about 21 dB in the region of high frequencies which is a great achievement from an acoustic point of view.

Based on the proposed SEA technique, the influence of various design variables, the internal absorption coefficient, the thickness of the panels, length -diameter ratio, and different materials of the panels on the transmission loss was investigated.

Chapter 3

Prediction of sound transmission loss of conical acoustic enclosure

In this chapter, an analytical model is proposed using the statistical energy analysis (SEA) technique to predict the sound transmission loss of a conical shape acoustic enclosure in a broad frequency range. The proposed model is verified experimentally using the sound intensity experimental technique. It was found that the analytical predictions are in good agreement with the measured transmission loss. The results obtained indicate that the developed analytical model can be used as an efficient design tool to predict the acoustic performance of conical shape structures.

3.1 Introduction

The conical shape structures are widely employed in many practical applications such as aircraft, rockets, tanks, and submarines. In recent years, structural vibration and noise-related problems for such structures have drawn more attention due to the acoustic environment exposed to these structures. In order to study the sound transmission loss of conical shape structures, various analytical and numerical models are presented. Vipperman et al. [78] investigated the acoustic performance of an advanced grid-stiffened composite structure of conical shape using the finite element method (FEM). Wang et al. [79] presented a numerical model to examine the structural and acoustic responses of a conical structure. Tebyanian and Ghazavi [86] developed a combined method using the analytical method, boundary element method (BEM), and FEM to investigate the transmission loss of truncated conical shells. Golzari and Jafari [27] proposed an analytical model to study the acoustic behavior of the truncated conical shell. Golzari and Jafari [28] studied an analytical model of a truncated conical shell to investigate the influence of poroelastic material on the sound transmission characteristics of the structure. Besides the numerical methods, other approaches such as transfer matrix methods [7–10,85] have also been used to study sound transmission through structures.

The prediction of acoustic performance using the statistical energy analysis (SEA) approach has also received significant attention. The SEA technique can be used as an alternative approach to the numerical methods because it enables the computation in a broad frequency range and provides accurate results. Numerous researchers [46–51] employed SEA theory to study the sound transmission behavior of automotive structures. Recently, Oliazadeh et al. [53] developed a SEA model to investigate the acoustic behavior of honeycomb sandwich panels. Prediction of sound transmission loss is often required at the acoustic design and evaluation stages of complicated structures. However, the investigation on sound transmission performance of conical shape structures has received little consideration using SEA.

This chapter plugs this gap by developing an efficient analytical model to predict the transmission loss of the conical acoustic enclosure and investigate the effect of significant acoustic parameters such as radiation efficiency, ring, and critical frequencies on the transmission loss performance. The sound intensity experimental technique is exhibited to assess the transmission loss to validate the accuracy of the developed analytical model.

3.2 SEA model of a conical acoustic enclosure

In the SEA modeling approach, a system under investigation refers to the entire assembly of linked structures and acoustic spaces. The system is then distributed into a number of subsystems that are characterized by its model energy.

The total power supply to every subsystem is provided from an external source of excitation, which is equivalent to the power losses due to the internal damping of subsystems and transmitted between them. A model of conical acoustic enclosure consists of a truncated conical shell and a flat circular top panel welded together, as shown in Fig. 3.1. A cylindrical coordinate system (r, θ, z) is implemented as shown in Fig. 3.2 and represents the structure.

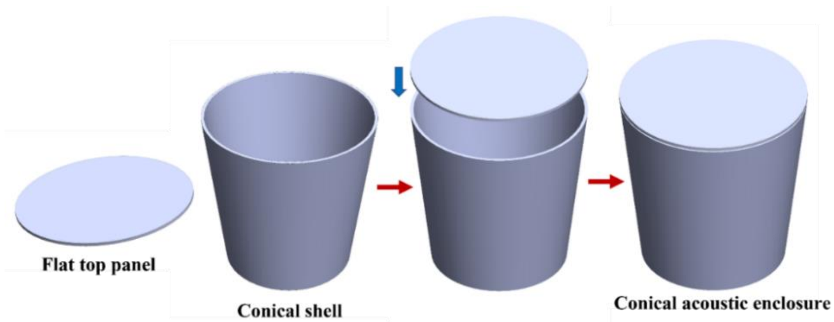

Figure 3.1 A schematic sketch showing the various components of a conical acoustic enclosure

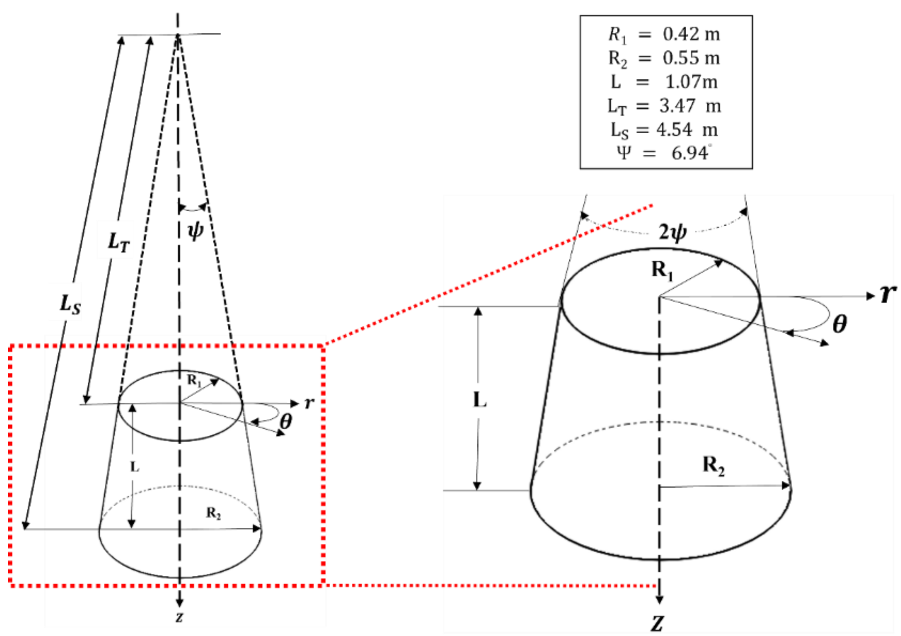

Figure 3.2 Schematic representation of a model of the conical acoustic enclosure

Each panel is considered to be elastic, isotropic, thin, and of uniform thickness. Table 3.1 shows the dimensions and the system variables used in the problem of transmission loss of the conical acoustic enclosure.

Table 3.1 Material properties and system variables used in the transmission loss problem of a conical acoustic enclosure

Symbol	System variable	Value
ρ	Mass density	7850 kg/m^3
E	Elastic Young's modulus	2×10^{11} Pa
υ	Poisson's ratio	0.3
R_1	Smaller radius of cone	0.42 m
R_2	Larger radius of cone	0.55 m
L	Length of conical shell	1.07 m
L_T	Length of cone truncation	3.47 m
L_s	Cone slant length	4.54 m
ψ	One-half cone angle at apex	6.94°
α	Truncation ratio = $\frac{L_T}{L_s}$	0.76
h	Thickness	1.20 mm

SEA model is presented here by considering only the resonant power transmission of acoustic noise source between all the subsystems. Lyon [112] reported that the relative roles of resonant and non-resonant transmission can be evaluated by considering the structural damping of the structure. Pope [113] stated the fact that large, thin, and heavily damped systems tend to transmit in a non-resonant manner. In the present analysis, the resonant transmission is considered significant compared to non-resonant transmission because of lightly damped enclosure panels.

Hence, to reduce the complexity of the model and based on the literature [36–38,112–116], non-resonant transmission is not considered in the current analytical model.

In the present analytical formulations, the system under analysis is separated into three individual subsystems and comprised of subsystems 2 to 3, these beings the truncated conical shell and a top flat panel of the enclosure, respectively, while the enclosure cavity is regarded as a subsystem 1 as displayed in Fig. 3.3. A sound source is placed inside the enclosure cavity producing an internal diffuse sound -field that vibrates the panels of the enclosure.

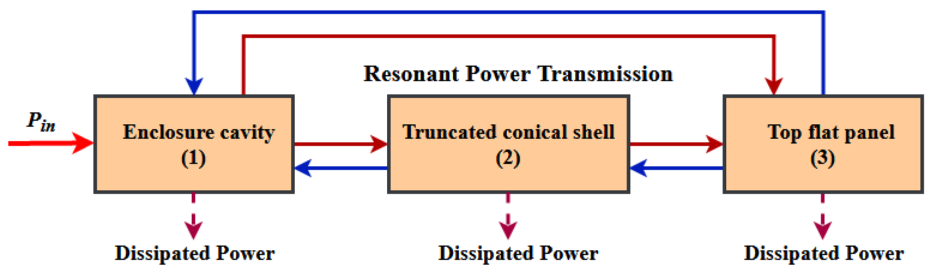

Figure 3.3 Schematic representation of energy flow paths for the developed SEA model of conical acoustic enclosure

The exciting panels thus transmit sound into space outside of the enclosure which is the receiving room. Only subsystem 1 obtains a power input because the noise source is only situated inside the enclosure cavity; therefore, the energy flow into the remaining subsystems is zero.

A three-element acoustic system requires a 3×3 matrix equation to model the power flow by assuming that the power supply between the subsystem is proportionate to the modal energy difference of the connected subsystem. The energy flow equations of subsystem 1, subsystem 2, and subsystem 3 can be written in the following manner:

$$\omega \left[n_1^d E_1 - n_{21} E_2 - n_{31} E_3 \right] = P_{in} \tag{3.1}$$

$$\omega \left[n_2^d E_2 - n_{12} E_1 - n_{32} E_3 \right] = 0 \tag{3.2}$$

$$\omega\left[n_3^d E_3 - n_{13}E_1 - n_{23}E_2\right] = 0 \tag{3.3}$$

where $\omega = 2\pi f$ is the radial frequency of the band, P_{in} is the external power input to subsystem 1, n_i^d and E_i are the dissipation loss factor and average acoustic energy of the subsystem ***i*** respectively, n_{ij} is the loss factor due to coupling from subsystem ***i*** to subsystem ***j***.

It is to be noted that the loss factor due to coupling between resonant subsystems in opposite direction is estimated using the reciprocity rule [31,33]:

$$n_{ij}n_i = n_{ji}n_j \tag{3.4}$$

where n_i and n_j are referred to as the modal density of the respective subsystem ***i*** and ***j,*** which is a frequency-dependent function that describes the expected number of total resonant modes per unit frequency available to obtain and store energy in the subsystem.

The Eqs. (3.1), (3.2), and (3.3) are rearranged in the form of matrix equations. Thus, the SEA matrix equation can be written as follows:

$$\omega\begin{bmatrix} n_1^d & -n_{21} & -n_{31} \\ -n_{12} & n_2^d & -n_{32} \\ -n_{13} & -n_{23} & n_3^d \end{bmatrix}\begin{Bmatrix} E_1 \\ E_2 \\ E_3 \end{Bmatrix} = \begin{Bmatrix} P_{in} \\ 0 \\ 0 \end{Bmatrix} \tag{3.5}$$

Therefore, the average acoustic energy of each subsystem can be obtained through inverting the coefficient matrix of Eq. (3.5).

3.2.1 SEA parameter estimation

To assess the acoustic performance of a conical acoustic enclosure theoretically, the important SEA parameters of the developed model, are essential to calculate which are mainly the modal density, loss factors, and radiation efficiency.

3.2.1.1 Modal density

The modal density of subsystem 1 is expressed by [33]:

$$n_1 = \frac{4\pi f^2 V_1}{c_o^3} \tag{3.6}$$

where, V_1 is the volume of the internal sound field.

The modal density of the resonant subsystem 2 is given as follows [117]:

$$n_2 = \begin{cases} \dfrac{1.31}{f_L}\left[\dfrac{\pi}{\sin\psi}\left(\dfrac{h(1-\alpha)^{3/4}}{L_s(\tan\psi)^{1/2}}\right)\right]\left(\dfrac{f}{f_L}\right)^{1/2} & f < f_L\ , \\ \dfrac{2}{f_U}\left[\dfrac{L_s\sin\psi(1-\alpha)^{4/5}}{\pi h}\right] & f > f_U \end{cases} \tag{3.7}$$

where, f_L and f_U are the lower and upper ring frequency of the truncated conical shell.

The modal density of the resonant subsystem 3 is given as follows [117]:

$$n_3 = \frac{8\sqrt{3}S_3}{\pi^2 h c_L}$$

(3.8)

where, S_3 is the area of the flat top panel, C_L is the longitudinal wave speed in the panel which is given as [118]:

$$C_L = \sqrt{\frac{E}{\rho(1-\upsilon^2)}}$$

(3.9)

where, E , ρ and υ are Young's modulus, density, and Poisson's ratio of the material respectively.

3.2.1.2 Dissipation loss factor

The dissipation loss factor of subsystem 1 is expressed by [44]:

$$n_1^d = \frac{S_1 c_o \gamma}{4\omega V_1} \tag{3.10}$$

where, γ is the internal absorption coefficient of the enclosure, $\gamma = 1.8\times10^{-4}\sqrt{f}$ (minimum value) for the ambient condition when no absorbing material was used for the enclosure.

The dissipation loss factors of the enclosure panels were measured experimentally using the decay rate technique since there is no exact analytical expression available for computing the loss factor due to dissipation.

3.2.1.3 Coupling loss factor

The loss factor due to coupling between resonant subsystem 2 to subsystem 1 is given as [31]:

$$n_{21} = \begin{cases} \dfrac{2\rho_o c_o \sigma_2}{2\pi f \rho h} & f < f_c, \\ \dfrac{\rho_o c_o \sigma_2}{2\pi f \rho h} & f \geq f_c \end{cases} \tag{3.11}$$

where, ρ_o and c_o are respectively, the density and speed of sound in air, σ_2 is the radiation efficiency for the truncated conical shell.

The loss factor due to coupling between resonant subsystem 3 to subsystem 1 is given as [30]:

$$n_{31} = \begin{cases} \dfrac{2\rho_o c_o \sigma_3}{2\pi f \rho h} & f < f_c, \\ \dfrac{\rho_o c_o \sigma_3}{2\pi f \rho h} & f \geq f_c \end{cases} \tag{3.12}$$

where, σ_3 is the radiation efficiency for the resonant flat top panel.

Subsystem 2 is connected to subsystem 3 with a line junction, and a wave approach adopted by [102], is used to compute the coupling loss factor.

The expression of coupling loss factor between resonant subsystem 2 and resonant subsystem 3, considering same material and thickness, is given as [44,102]:

$$n_{23} = \frac{0.2068 c_B L_{23}}{\omega S_i} \tag{3.13}$$

where, L_{23} is the junction length, c_B is bending wave speed on the panel which is given by [33,35]:

$$c_B = \left[\frac{\omega h c_L}{\sqrt{12}} \right]^{1/2} \tag{3.13}$$

3.2.1.4 Radiation efficiency

The sound radiation efficiency is an appropriate acoustic descriptor of a structure excited acoustically. It has a direct correlation between radiated sound power W_r, surface mean square velocity $\langle v^2 \rangle$, and radiating surface area S [30,106]:

$$\sigma = \frac{W_r}{\rho_o c_o S \langle v^2 \rangle} \tag{3.14}$$

The radiation efficiency of the flat top panel is computed with the approach given in the reference number, as in [30]. The truncated conical shell is approximated through a series of cylindrical segments of the structure to calculate the radiation efficiency of the truncated conical shell [119].

3.2.2 Ring and critical frequencies

Three significant frequencies play an influential role in the acoustic characteristics of a conical acoustic enclosure. These significant frequencies are the lower ring frequency, upper ring frequency, and critical frequency. The lower ring frequency f_L is explained as the frequency at which the longitudinal wavelength is equal to the circumference of the large end of the cone. The upper ring frequency f_U is the frequency at which the longitudinal wavelength is equal to the circumference of the small end of the cone. The third important frequency, the critical frequency, f_c is the frequency at which flexural waves speed in the panel is equivalent to the incident sound waves speed in the medium of air.

The lower and upper ring frequencies and the critical frequency are given by reference number, as in [30,110,119]:

$$f_L = \frac{c_L}{2\pi R_2}, \tag{3.15}$$

$$f_U = \frac{c_L}{2\pi R_1}, \tag{3.16}$$

$$f_c = \frac{\sqrt{12}c_o^2}{2\pi h c_L}, \tag{3.17}$$

where, R_1 is the small radius of the cone; R_2 is the large radius of the cone.

3.2.3 Transmission loss

The acoustic property of an enclosure is evaluated by the sound transmission loss, which is classified as the most important and appropriate performance indicator for such structures. The transmission loss is expressed in decibels (dB) is defined [44,118]:

$$TL = 10\log_{10}\left(W_O / W_R \right) \tag{3.18}$$

where, W_O is the measured sound power of the internal sound field and W_R is the radiated sound power level by the exciting enclosure panels. Moreover, the total sound power which is radiated through all the resonant structural subsystems into the exterior receiving room is estimated by [44]:

$$W_R = \sum_i \rho_o S_i c_o \sigma_i v_i^2 \tag{3.19}$$

where ρ_o and c_o denote the density and speed of sound in the air medium; σ_i , S_i , and v_i are respectively the radiation efficiency, surface area, and vibration velocity of the ***ith*** subsystem.

The mean square vibration velocity of each subsystem v_i^2 is obtained as follows:

$$v_i^2 = E_i / m_i \ , \tag{3.20}$$

where m_i is the mass of i^{th} panel.

The transmission loss of a conical acoustic enclosure is computed by using Eqs. (3.5), (3.18), (3.19), and (3.20) for the developed SEA model.

3.3 Experimental studies

The experiments were performed on a conical shape acoustic enclosure in a soundproof chamber to validate the analytical model. The volume of the soundproof chamber is 16 m^3. The conical shape acoustic enclosure was made of galvanized steel, with the exact dimensions considered in analytical modeling.

3.3.1 Dissipation loss factor measurement

The dissipation loss factor of the enclosure panels is evaluated experimentally using the decay rate technique, which is based on a resonant mode transient response [33]. The flat-top panel was hung freely and excited separately using the impulse hammer [Modal: Dytran 5800B4 series] of sensitivity 2.25 mV/N as displayed in Fig. 3.4.

The conical shell was hung freely and excited separately using the impulse hammer, as shown in Fig. 3.5. The impulse hammer was connected to a 16-channel LMS data acquisition analyzer, a PC (Dell-INTEL Core), and PCB356A16 series lightweight accelerometers of sensitivity 100 mV/g. The decay characteristic of the flat top panel and the conical shell is tested at different accelerometer positions.

The dissipation loss factor of the structural panels is correlated to time-averaged decay time $T_{1/2}$ by the given expression [33]:

$$n_i^d = 0.22 / fT_{1/2} \tag{3.21}$$

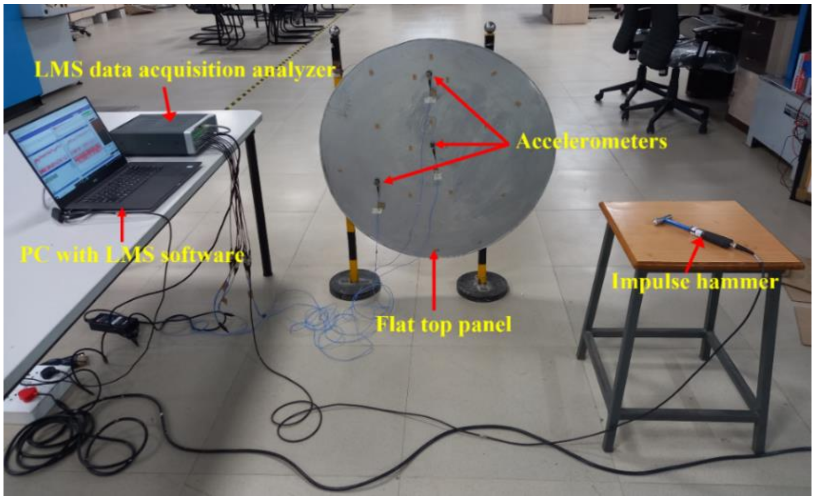

Figure 3.4 Experimental setup for measuring the dissipation loss factor of the flat top panel

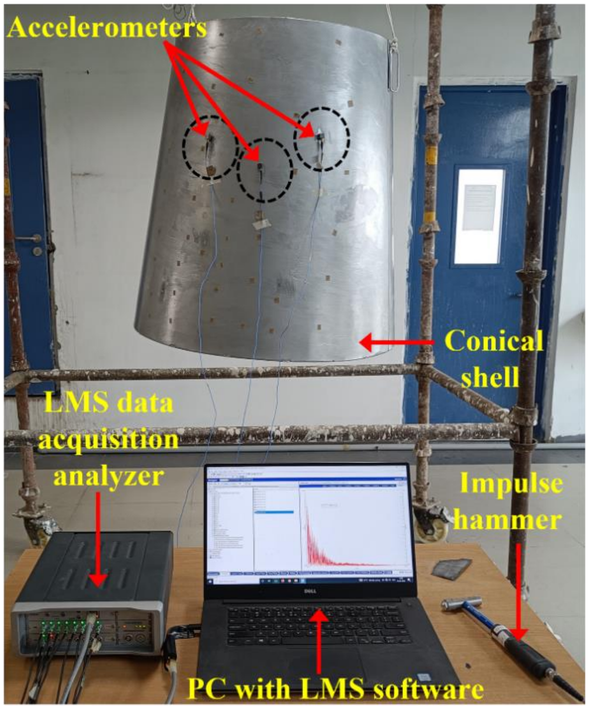

Figure 3.5 Experimental setup for measuring the dissipation loss factor of the truncated conical shell

For obtaining accurate and reliable results, the measurement was repeated two times, and a total of five impacts were made at each accelerometer location, and then the time-averaged decay time was measured.

Fig. 3.6 shows the time-averaged dissipation loss factor of the structural flat top panel and conical shell at the center frequency of 1/3 octave band.

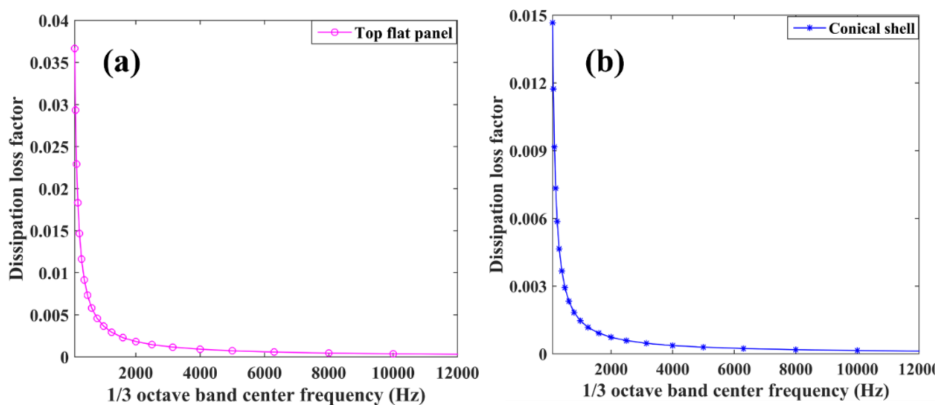

Figure 3.6 Measured dissipation loss factor: (a) top flat panel, (b) conical shell

The measured dissipative loss factors were utilized to predict the sound transmission loss of the conical acoustic enclosure for more accurate results.

3.3.2 Radiation efficiency measurement

To measure the radiation efficiency of the enclosure panels, it is essential to measure the mean square velocity and radiating sound power of the respective enclosure panel. The enclosure panels were excited acoustically using the omnidirectional sound source of the Brüel & Kjær system placed inside the enclosure. The radiation efficiencies of the enclosure panels were measured based on Eq. (3.14).

3.3.3 Sound transmission loss measurement using sound intensity technique

The sound intensity technique is based on the sound intensity measurement of the enclosed noise source and the transmitted sound intensity through the structure. Thus, the sound transmission loss can be evaluated through the expression given [30]:

$$TL = 10\log_{10}\left(\frac{I_{in}}{I_t}\right) \tag{3.22}$$

where, I_{in} and I_t are respectively the incident and transmitted intensity of sound.

To investigate the accuracy of the developed model, it was desirable to obtain transmission loss of the enclosure based on Eq. (3.22). The internal volume of the enclosure was excited acoustically using a sound source to measure the sound transmission loss. An omnidirectional sound source [Model: 4292-L, Brüel & Kjær system] was employed as an actual sound source. The sound source was placed centrally inside the enclosure and fed with white-noise signals to generate the acoustic sound power to excite the enclosure. The schematic diagram of the experimental test setup is shown in Fig. 3.7.

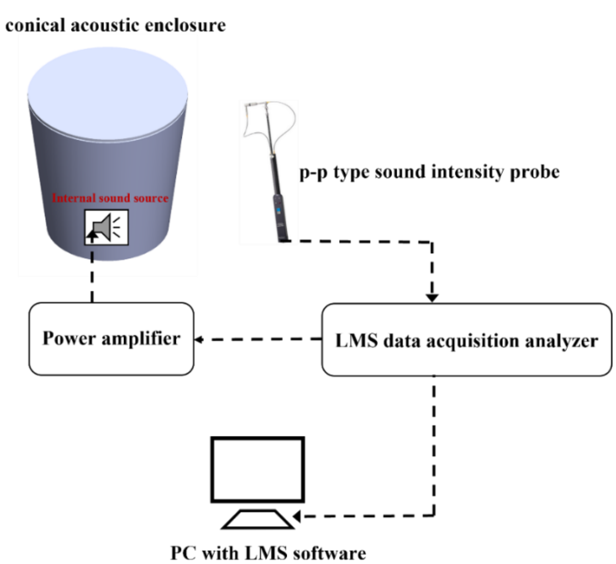

Figure 3.7 Schematic diagram of the experimental setup for measuring the transmission loss of conical acoustic enclosure

The photographic view of the experimental setup of the sound transmission loss measurement is presented in Fig. 3.8. The position of the sound source inside the enclosure is shown in Fig. 3.9. The sound intensity was measured using the G.R.A.S pp type sound intensity probe (type 50GI-R), connected with a 16-channel LMS data acquisition system and a PC (Dell-INTEL Core).

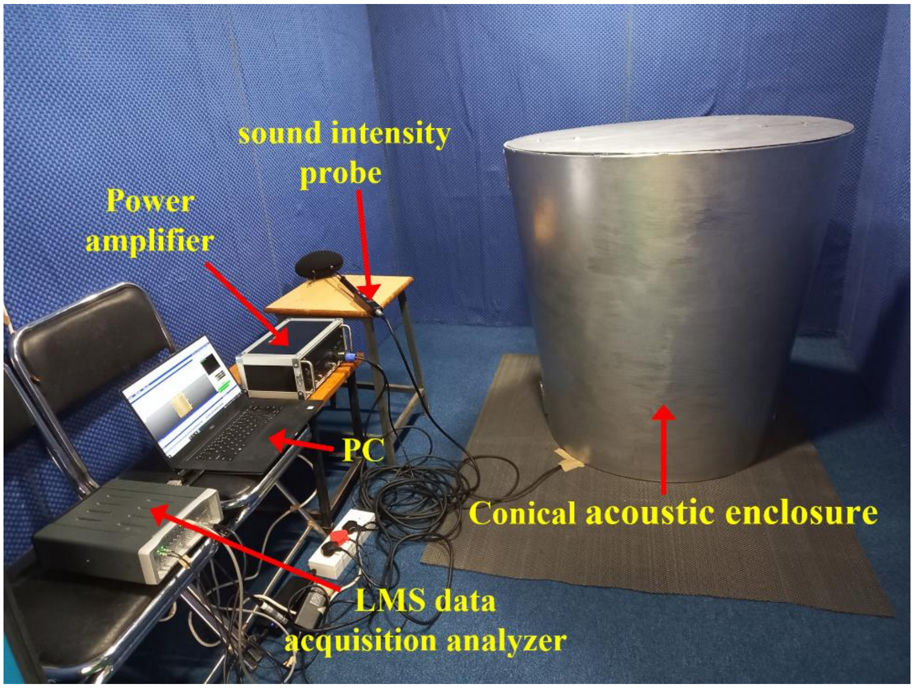

Figure 3.8 Experimental setup for measuring the transmission loss of conical acoustic enclosure

Figure 3.9 Position of the sound source inside the enclosure

The measured sound transmission loss is obtained from the spatial average sound intensity measurement over the enclosure panels, and the incident sound intensity determination of the noise source. The probe consisted of two 1/2-inch microphones, phase-matched together and separated through a spacer. To cover the whole frequency range during the measurements, four interchangeable solid spacers were used to maintain the spacing of microphones at 12 mm, 25 mm, 50 mm, 100mm. The averaging time considered for sound intensity data acquisition was of 12 seconds.

Fig. 3.10 shows the measured sound power of the internal sound field at the center frequency of 1/3 octave band.

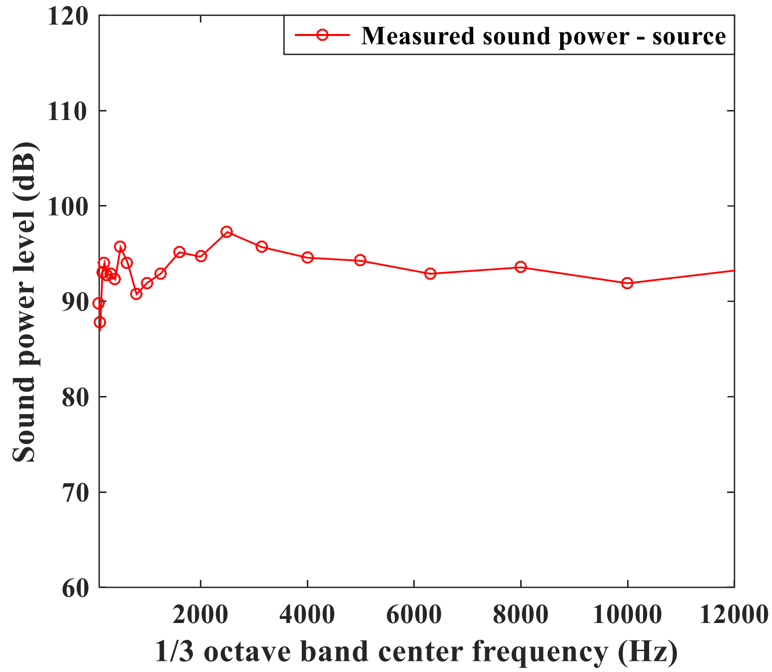

Figure 3.10 Measured sound power of the internal sound field

3.4 Results and Discussion

In this section, the developed model predictions are compared with the results of the experimental measurements to validate the analytical model. The curves drawn in Fig. 3.11 depict the comparison of measured radiation efficiency of enclosure top flat panel with the analytical predictions. Comparing the analytical predictions with the measured results shows fairly a good agreement. It can be seen in Fig. 3.11 that the radiation efficiency of the flat top panel has one peak tends to unity about the frequency of 10000 Hz, which is the critical frequency of the top panel that is nearest to the result computed by Eq. (3.17) which is 10280 Hz. In this condition, the flexural waves speed in the structural panel is equivalent to the speed of the sound waves in the air, and the structural top panel is associated with the strong excitation in a resonance condition due to the high radiation efficiency.

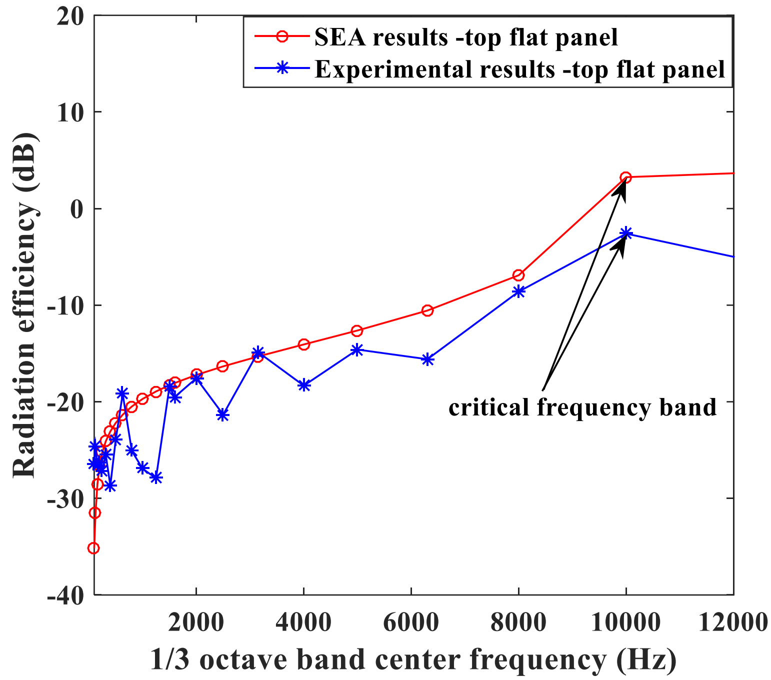

Figure 3.11 Analytical and experimental comparison of radiation efficiency of the top flat panel at the center frequency of 1/3 octave band

The amplitude of radiation efficiency of the top panel below the critical frequency is very low in the range between -10 dB and -25 dB. This implies that the flat top panel radiates inadequately except at the critical frequency with high radiation. The measured radiation efficiency of the conical shell is shown in Fig. 3.12 and compared with the analytical predictions. The results indicate that the comparison of the analytical predictions with measured results presents fairly a good agreement.

It is seen in Fig. 3.12; the radiation efficiency of the conical shell has three peaks which are well anticipated. The first and second peak appears respectively at the lower and upper ring frequencies of the conical shell, which is linked with the structural breathing mode condition of resonance. The analytical modal predicted the lower ring frequency at about 1600 Hz nearest to the result calculated by Eq. (3.15), which is 1521 Hz. The upper ring frequency is predicted at about 2000 Hz, which is close to the result computed by Eq. (3.16), which is 1992 Hz.

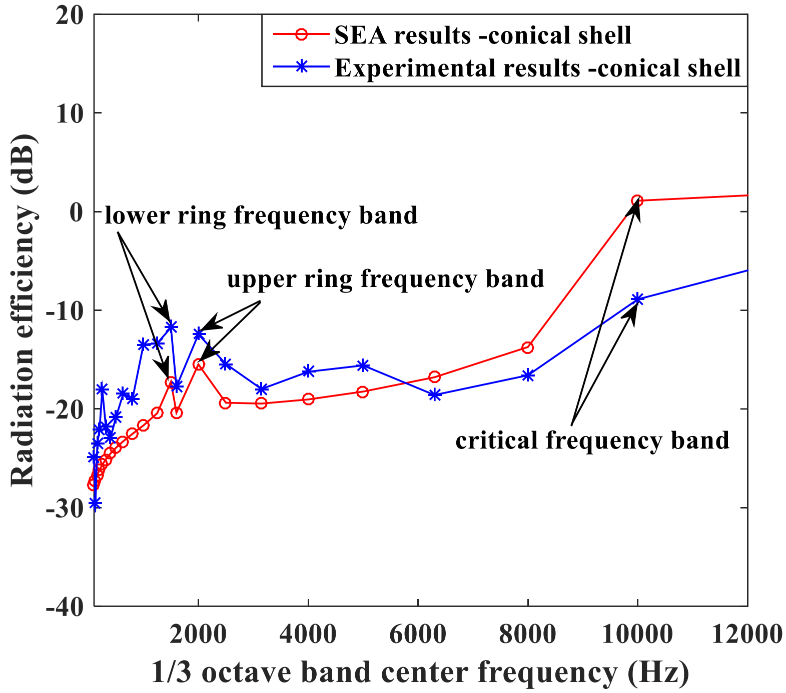

Figure 3.12 Analytical and experimental comparison of radiation efficiency of the conical shell at the center frequency of 1/3 octave band

The third peak appears at about 10000 Hz, which is the critical frequency of the conical shell nearest to the result computed by Eq. (3.17), which is 10280 Hz. In this situation, the conical shell has a high amplitude of radiation efficiency, tends to unity, and radiates in the same way to the enclosure flat top panel. This indicates that the conical shell radiates poorly except at the lower, upper, and critical frequencies with more significant sound radiation.

Based on the foregoing consideration, it is of interest to evaluate the sound power levels radiated through various sections of the enclosure surface area. The measured sound power radiated from the top flat panel is drawn in Fig. 3.13 and compared with the analytical results at the center frequency of one-third octave bands. The measured results show fairly a good agreement with the analytical results.

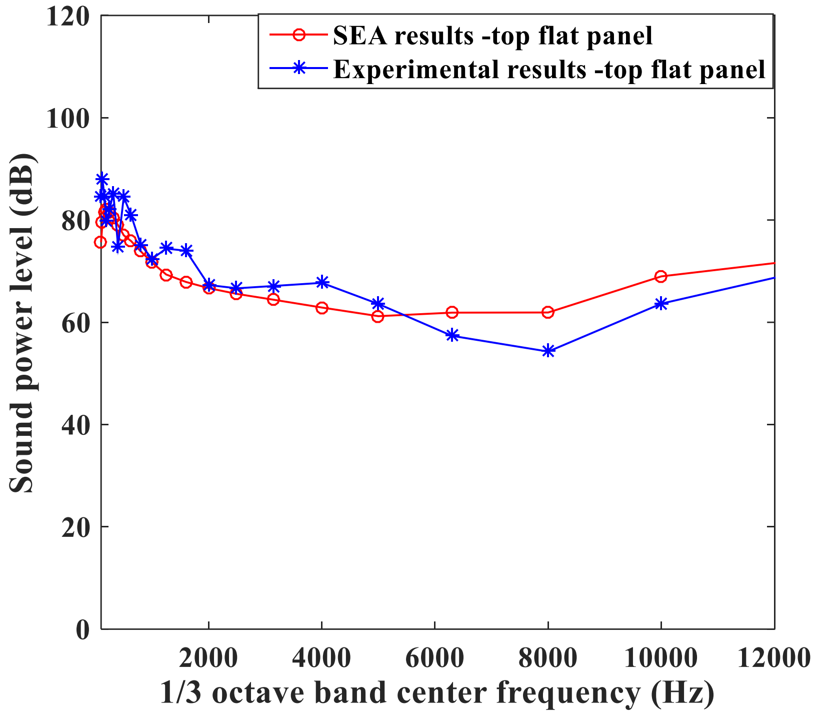

Figure 3.13 Analytical and experimental comparison of the radiated sound power level of the top flat panel at the center frequency of 1/3 octave band

It is observed that the sound power radiated through the structural top panel is increased through the lower and intermediate frequency range below the critical frequency based on mass law sound transmission and regulated by the mass per unit surface area of the structure in this region of frequency. The radiated sound power level becomes higher at the critical frequency of the top panel, which is about 10000 Hz due to the high amplitude of radiation efficiency and strong excitation of the structural top panel in the resonance condition. Fig. 3.14 compares the sound power level radiated through the conical section of the acoustic enclosure analytically and experimentally in the one-third octave frequency band. It is seen in Fig. 3.14 that the analytical predictions of the radiated sound power level are in good agreement with the measured results.

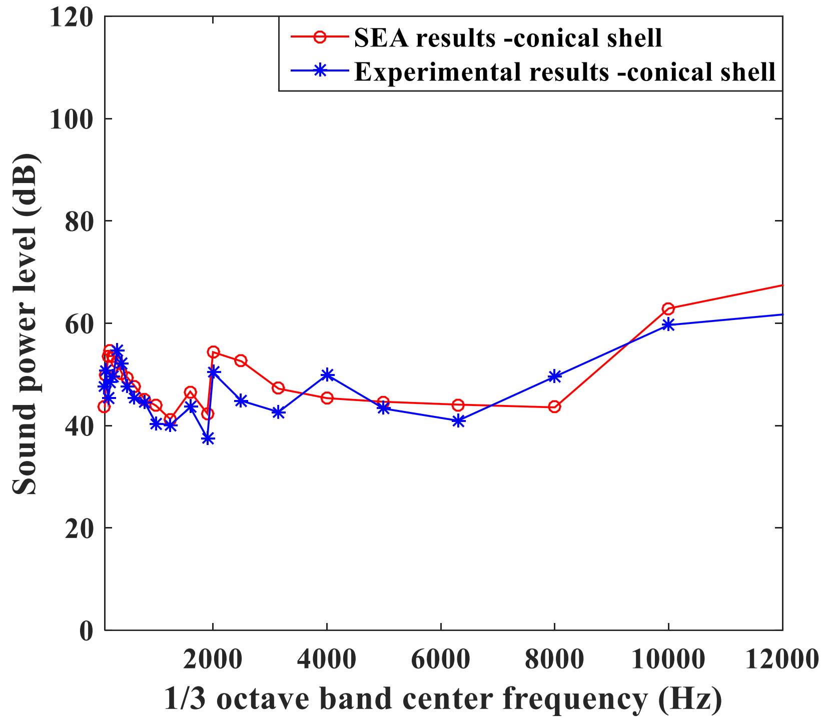

Figure 3.14 Analytical and experimental comparison of the radiated sound power level of the conical shell at the center frequency of 1/3 octave band

The sound power radiated through the conical shell is increased through the lower and intermediate frequency region below the critical frequency based on mass law sound transmission and principally governed by the mass per unit surface area of the structural panel in this range of frequency. The conical shell radiates poorly except at the lower ring frequency, upper ring frequency, and critical frequency because of the strong acoustic excitation of the conical shell in the resonance condition. It has higher radiation efficiencies at the corresponding frequencies of 1600 Hz, 2000 Hz, and 10000 Hz, respectively. Fig. 3.15 compares the results of the SEA model prediction and measured sound transmission loss of a conical acoustic enclosure using the experimental sound intensity method in the 1/3 octave frequency band.

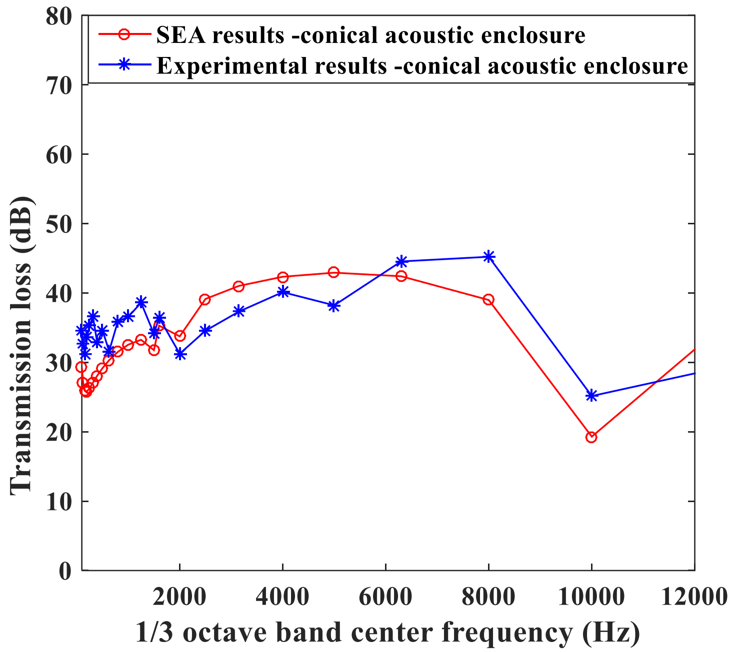

Figure 3.15 Analytical and experimental comparison of transmission loss of conical acoustic enclosure at the center frequency of 1/3 octave band

It is seen that the analytical and measured results followed a similar trend, and measured transmission loss agrees well with the analytical predictions, specifically at the lower ring frequency, upper ring frequency, and critical frequencies. The discrepancy between analytical and experimental results is due to not considering the non-resonant transmission in the modeling. It should be noted that the transmission loss prediction at the ring and critical frequencies is very important in the acoustic design of any structure. As expected, the developed analytical model and the experimental predictions estimated the three noticeable dips in the sound transmission loss curve presented in Fig. 3.15. It can be observed from the analytical and experimental predictions shown in Fig. 3.15 that sound transmission loss increases through the low-frequency range to the lower ring frequency at which a sudden drop occurs because of the structural breathing mode of conical shell resonance. Thereafter, the transmission loss continues to increase to the upper ring frequency, at which a sudden drop appears because of the structural breathing mode resonance. The transmission loss further rises to the critical frequencies of the enclosure panels above the upper ring frequency. The trend of the theoretical curve is to be anticipated, which is increased through the lower and intermediate frequency range based on mass law transmission and regulated by the mass per unit surface area of the structure in this region of frequency. As the frequency of impinging sound waves gets closer to the critical frequency, about 10000 Hz, an abrupt drop occurs due to the higher radiation efficiencies and a strong excitation of enclosure panels in a resonance condition. The transmission loss further increases beyond the critical frequency because sound transmission strongly depends on the frequency of the impinging sound waves and panel damping, which limits the sound radiation characteristics of the enclosure panels. The percentage error between predicted and computed lower ring frequencies is 5.1 % and that for the upper ring frequencies is 0.4 %. The percentage error between predicted and calculated critical frequencies is 2.7 %. The results demonstrate a good agreement between the analytical and experimental investigations. It is seen in Fig. 14 that sound transmission loss of the conical acoustic enclosure increases about 28 dB and 32 dB, respectively, in the lower and intermediate range of frequency. The transmission loss is enhanced by about 40 dB in the high-frequency region, which is a great achievement from an acoustic point of view.

3.5 Parametric studies

The analytical model formulated for the conical acoustic enclosure can be used very efficiently at the fundamental design and assessment stages of conical shape vibro-acoustic systems. In order to investigate the efficacy of various design parameters to improve the effectiveness and transmission loss performance of conical acoustic enclosure, parametric studies are conducted.

3.5.1 Influence of absorption coefficient

The absorption coefficient of the enclosure acts significantly in transmission loss performance. Fig. 3.16 depicts that the use of a larger internal absorption coefficient ($3.6\times10^{-4}\sqrt{f}$) inside the acoustic enclosure in comparison to a smaller internal absorption coefficient ($1.8\times10^{-4}\sqrt{f}$), enhances the transmission loss performance effectively. It is seen in Fig. 3.16 that sound transmission loss can be raised to 5 dB if the internal absorption coefficient is doubled.

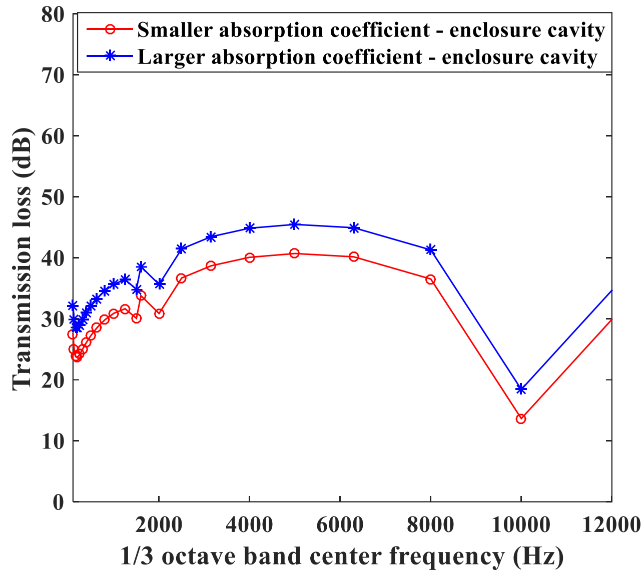

Figure 3.16 Effect of absorption coefficient on the transmission loss of the conical acoustic enclosure

3.5.2 Effect of the cone angle

In Fig. 3.17, the sound transmission loss of the conical acoustic enclosure is calculated at different one-half angles at apex, ψ = 6.94°, 10°. The cone angle enhancement slightly reduces the sound transmission loss in the lower range of frequencies up to 1371 Hz which is the upper ring frequency of the conical shell at a semi-vertex angle of 10°. The transmission loss decreases at the low frequencies with the increment of cone angle probably due to a reduction in stiffness of the conical shell. However, transmission loss increases in the intermediate frequency region with a rise in the cone angle because the conical shell has a higher modal density in this range of frequencies.

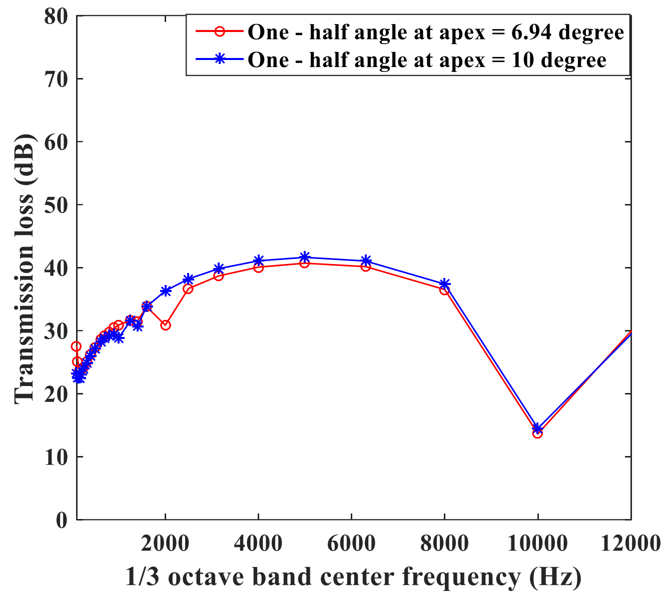

Figure 3.17 Effect of the one-half cone angles at the apex on the transmission loss of the conical acoustic enclosure

Moreover, it can be observed that increasing the cone angle provides slightly better transmission loss in the region of higher frequencies.

3.5.3 Effect of thickness

In a practical application, the enclosure panels are designed only as thick as required due to weight constraints. It is seen in Fig. 3.18 that doubling the thickness caused about 5 dB enhancement of transmission loss below the frequency band of 3150 Hz. There is no improvement of transmission loss by increasing the thickness in the frequency region between 3150 Hz to 6300 Hz. Above the frequency of 6300 Hz, the transmission loss increases greatly about 15 dB. Therefore, changing the thickness of panels has a significant influence on the transmission loss performance of the conical acoustic enclosure. If the target transmission loss is known from the noise level consideration, an appropriate thickness of the enclosure panels can be easily estimated.

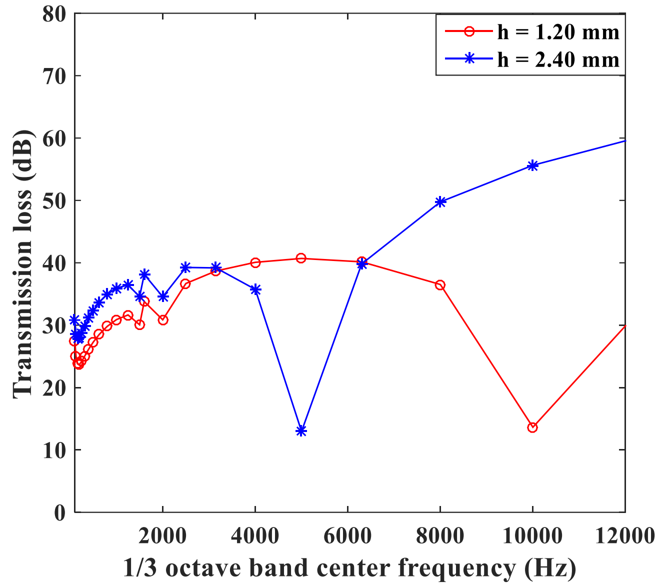

Figure 3.18 Effect of the thickness on the transmission loss of the conical acoustic enclosure

3.5.4 Effect of length-diameter ratio

Fig. 3.19 shows the influence of l/d ratio on the transmission loss of conical acoustic enclosure.

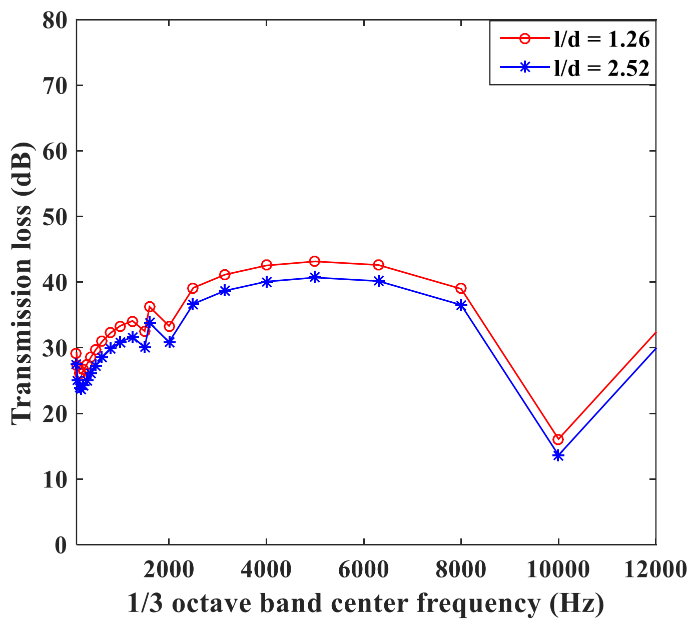

Figure 3.19 Effect of length-diameter ratio on the transmission loss of the conical acoustic enclosure

A larger l/d ratio reduces transmission loss performance of an enclosure which is mainly due to the curvature effect of the conical shell on its stiffness and larger surface area as shown in Fig. 3.19 This important parameter should be considered with more care while designing the conical acoustic enclosure.

3.5.5 Effect of different materials

Fig. 3.20 presents the influence of the panel materials on the sound transmission efficiency of the conical acoustic enclosure. The materials selected for the comparison are steel, aluminum, and brass with the properties of materials given in Table 3.2.

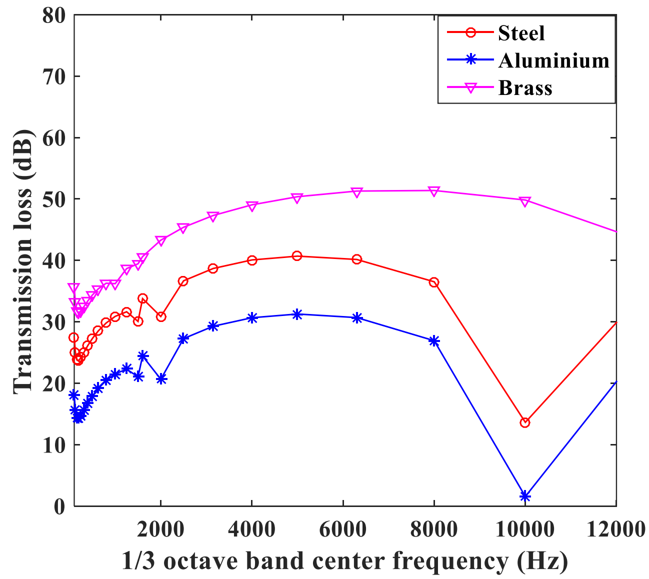

Figure 3.20 Effect of different materials on the transmission loss of the conical acoustic enclosure

Fig. 3.20 indicates that the transmission loss performance of a conical acoustic aluminum enclosure is least effective in the entire frequency regions because of the lowest mass and stiffness which is well anticipated. Fig. 3.20 shows that the conical acoustic enclosures made of steel and brass provide the superior sound transmission loss performance effectively in the broad frequency regions. These results are well anticipated because both the steel and brass have higher stiffness and mass respectively.

Table 3.2 Material properties used of a conical acoustic enclosure made of different materials

Material	Density (kg/m^3)	Elastic Young's modulus (GPa)	Poisson's ratio
Steel	7850	200	0.3
Aluminum	2710	69	0.32
Brass	8525	102	0.35

Moreover, the transmission loss performance of the conical acoustic enclosure made of brass is most effective because the brass has the largest density which enables it more efficient in the mass-controlled high-frequency region.

3.6 Conclusions

This chapter presents an analytical model based on the statistical energy analysis (SEA) technique to predict the sound transmission loss of a conical shape acoustic enclosure. One of the essential SEA parameters, the dissipation loss factor was obtained using the decay rate experimental technique for enclosure panels. Another significant acoustic parameter, the radiation efficiency was measured for enclosure panels and compared with the analytical predictions. The sound intensity experimental technique was employed for measuring the sound transmission loss. It was found that the analytical predictions demonstrated good agreement with the measured transmission loss. The percentage error between predicted and measured lower ring frequency was 5.1 % and that for the upper ring frequency was 0.4 %. The percentage error between predicted and measured critical frequency was 2.7 %. The results obtained indicate that the proposed analytical model is efficient for predicting the transmission loss of conical shape structures.

Chapter 4

Prediction of sound transmission loss of hemispherical acoustic enclosure

In this chapter, sound transmission loss of the hemispherical shape acoustic enclosure (hemispherical shell) is predicted analytically and validated experimentally. The Statistical energy analysis (SEA) technique is employed to formulate an analytical model for computing the sound transmission loss of a hemispherical shell across a wide frequency range. The sound intensity experimental method was used to verify the proposed SEA formulation. The analytical predictions and the measured transmission loss were found to be in good agreement. Based on the proposed SEA model, the influence of design variables, the absorption coefficient, thickness, radius, and material density on the transmission loss was investigated.

4.1 Introduction

Hemispherical shape acoustic enclosure (hemispherical shell) consisting of thin elastic structural panels offer various industrial applications in different fields. They are used in aircraft, tanks, undersea vehicles, machine parts, and architectural structures. Several numerical approaches were proposed based on finite elements (FE) and boundary elements (BE) techniques, in order to compute the transmission loss engineering panels [57–61]. The transmission loss prediction of structural panels using the statistical energy analysis (SEA) method has also gained notable consideration. Numerous research [38,39,48,50,56] focused on investigating the vibration response and noise control of structural panels through SEA approach.

Additionally, few numerical models are developed to study the acoustic performance of spherical and hemispherical structures [87,88]. Hasheminejad and Mehdizadeh [29] developed an analytical formulation using Biot theory along with Havriliak-Negami model to compute the noise reduction of multi-layer hemispherical enclosure. Eslaminejad et al. [80] presented the experimental and numerical modal analysis to study the modal frequencies and mode shapes of a fluid-filled aluminum hemispherical shell.

Less research is done to investigate the sound transmission behavior of hemispherical shape structure and gained little attention. With regards to model the acoustic performance and predicting the sound transmission loss of hemispherical panel, there is only a little reference in a SEA framework. The main objective of this chapter is to present an analytical formulation using SEA technique for evaluating the sound transmission loss of a hemispherical shell. The sound intensity technique is employed to measure the transmission loss to validate the proposed SEA model.

4.2 Analytical model of a hemispherical shell

In SEA method the system to be analyzed is divided into sub-systems. An external sound source causes an acoustic excitation and provides the power input to each subsystem. The input power is equivalent to the summation of dissipation power losses of the subsystems and transmitted power between them. In this study a hemispherical shape acoustic enclosure (hemispherical shell) is considered.

The schematic diagram of this hemispherical shell is displayed in Fig. 4.1. The spherical coordinate system (r, θ, ϕ) is implemented to represent the structure. Table 4.1 presents the various parameters of hemispherical shell.

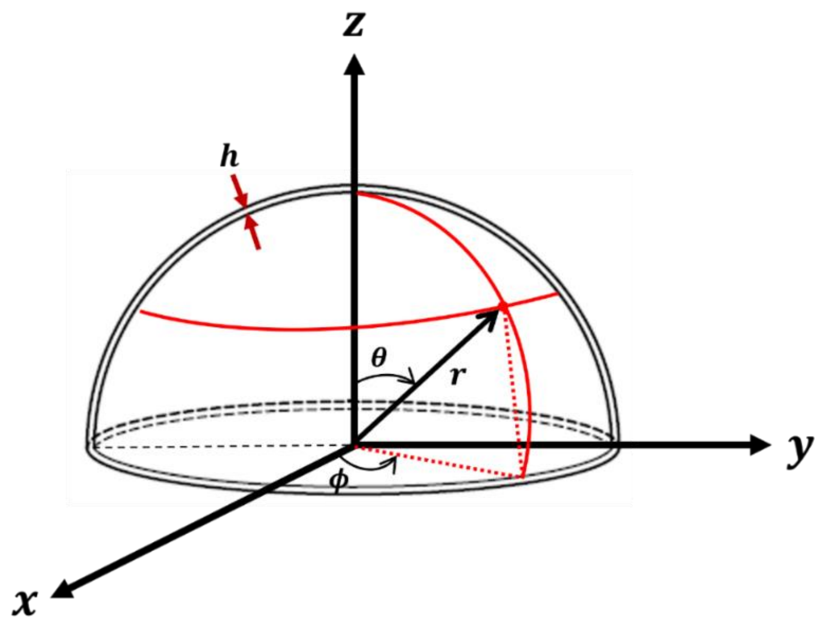

Figure 4.1 Schematic diagram of a hemispherical shell

Table 4.1 Parameters of hemispherical shell

Symbol	System variable	Value
ρ	Mass density	7850 kg/m^3
E	Elastic Young's modulus	2×10^{11} Pa
υ	Poisson's ratio	0.3
r	Hemispherical radius	0.72 m
h	Thickness	1.20 mm
ρ_o	Air density	1.21 kg/m^3
c_o	Speed of sound in air	343 m/s

It can be noted that the hemispherical shell has insufficient resonant modes below the ring frequency [117]. Therefore, to perform SEA the system must be divided into resonant and non-resonant sub systems. In the proposed SEA model, the hemispherical shell's resonant and non-resonant responses have been divided into two subsystems.

The SEA model of the hemispherical shell above the ring frequency consists of three individual systems coupled together and shown schematically in Fig. 4.2.

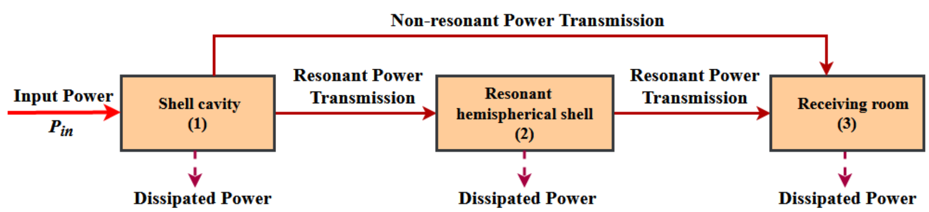

Figure 4.2 Schematic illustration of the energy flow paths of the hemispherical shell above the ring frequency

The resonant hemispherical shell is represented as subsystem 2, and subsystem 1 is regarded as the shell cavity of the hemispherical shell, which is the internal sound field of the shell, while the receiving room is considered as subsystem 3. The SEA formulation is developed through consideration of resonant power transmission between the resonant hemispherical shell and the acoustic spaces (shell cavity and receiving room). Also, there is non-resonant power transmission between two acoustic spaces. Inside the shell cavity, an acoustic sound source is placed and vibrating the shell by generating an interior sound field. As a result, sound is transmitted into space outside of the exciting shell. Since the sound source is located inside the hemispherical shell. only subsystem 1 receives an input power; thus, no power supply into the other subsystems.

A 3×3 matrix equation is essential to formulate the power supply in a three-element acoustic system, presuming that the power flow is proportional to the difference of modal energy of linked subsystems. It is assumed that the losses due to internal damping of subsystem $\boldsymbol{i}$ is greater than the coupling loss factors coupling it to other subsystems and neglecting the coupling loss factor in the total dissipation of subsystem $\boldsymbol{i}$.

The subsystem 1, subsystem 2, and subsystem 3 power flow equations are stated as follows:

$$\omega\left[n_1^d E_1 - n_{21}E_2 - n_{31}E_3\right] = P_{in} \tag{4.1}$$

$$\omega\left[n_2^d E_2 - n_{12}E_1 - n_{32}E_3\right] = 0 \tag{4.2}$$

$$\omega\left[n_3^d E_3 - n_{13}E_1 - n_{23}E_2\right] = 0 \tag{4.3}$$

where, $\omega = 2\pi f$ is the angular frequency, P_{in} is the exterior acoustic input power to subsystem 1, E_i is the subsystem ***i*** mean acoustic energy, n_i^d is the dissipation loss factors of subsystem ***i***. n_{ij} is the coupling loss factor between subsystem ***i*** and subsystem ***j***.

The reciprocity rule is adopted to calculate the coupling loss factor in opposite direction between resonant subsystems [31,34]:

$$n_{ij}n_i = n_{ji}n_j \tag{4.4}$$

where n_i and n_j are signified as modal density parameter of subsystem ***i*** and ***j***, that depends on the frequency and explains as the total modes which are resonant per unit band of frequency.

Eqs. (4.1), (4.2) and (4.3) are reorganized in the matrix equation. Therefore, the matrix equation for the SEA model of hemispherical shell above the ring frequency can be written as follows:

$$\omega\begin{bmatrix} n_1^d & -n_{21} & -n_{31} \\ -n_{12} & n_2^d & -n_{32} \\ -n_{13} & -n_{23} & n_3^d \end{bmatrix}\begin{Bmatrix} E_1 \\ E_2 \\ E_3 \end{Bmatrix} = \begin{Bmatrix} P_{in} \\ 0 \\ 0 \end{Bmatrix} \tag{4.5}$$

The mean acoustic energy of each subsystem is estimated by inverting the coefficient matrix of Eq. (4.5).

Therefore, the ratio of mean acoustic energy of the shell cavity to mean acoustic energy of the receiver room above the ring frequency can be obtained as:

$$\frac{E_1}{E_3} = \frac{n_2^d n_3^d - n_{23}n_{32}}{n_{12}n_{23} + n_2^d n_{13}} \tag{4.6}$$

The SEA model of the hemispherical shell below the ring frequency consists of three individual systems coupled together and shown schematically in Fig. 4.3. The non-resonant hemispherical shell is represented as subsystem 4, and subsystem 1 is regarded as the shell cavity of the hemispherical shell, while the receiving room is considered as subsystem 3.

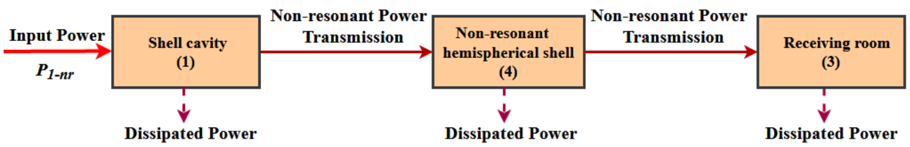

Figure 4.3 Schematic illustration of the energy flow paths of the hemispherical shell below the ring frequency

The non-resonant structural response of the hemispherical shell is directly linked to the acoustic spaces, which are not directly connected. The power flowing equations of subsystem 1, subsystem 4, and subsystem 3 are scripted in the same way as the SEA model of the hemispherical shell above the ring frequency. Thus, the SEA matrix equation for the SEA model below the ring frequency can be written as follows:

$$\omega \begin{bmatrix} n_1^d & -n_{41} & 0 \\ -n_{14} & n_4^d & -n_{34} \\ 0 & -n_{43} & n_3^d \end{bmatrix} \begin{Bmatrix} E_1 \\ E_4 \\ E_3 \end{Bmatrix} = \begin{Bmatrix} P_{1-nr} \\ 0 \\ 0 \end{Bmatrix} \tag{4.7}$$

where, P_{1-nr} is the acoustic power that induces the non-resonant wave response, which is given as:

$$P_{1-nr} = \tau P_{in} \tag{4.8}$$

where, τ is the transmission coefficient based on mass law, which can be obtained as [30,35]:

$$\tau = \frac{\ln\left[1+\left(\dfrac{\pi f \rho h}{\rho_o c_o}\right)^2\right]}{\left(\dfrac{\pi f \rho h}{\rho_o c_o}\right)^2} \tag{4.9}$$

By inverting the coefficient matrix of Eq. (4.7), each subsystem's mean acoustic energy is computed. Therefore, the ratio of the mean acoustic energy of shell cavity to the mean acoustic energy of the receiver room below the ring frequency can be obtained as:

$$\frac{E_1}{E_3} = \frac{n_3^d n_4^d - n_{34} n_{43}}{n_{14} n_{43}} \tag{4.10}$$

4.2.1 SEA parameters computation

To estimate the analytical transmission loss of a hemispherical shell, the key SEA parameters (modal density and loss factors) are imperative to estimate.

4.2.1.1 Modal density

The modal density of the hemispherical shell cavity is given by [33]:

$$n_1 = \frac{4\pi f^2 V_1}{c_o^3} \tag{4.11}$$

where, V_1 is the shell cavity volume.

The modal density of the resonant hemispherical shell is expressed by [117]:

$$n_2 = \begin{cases} 0 & f < f_r\,, \\ \dfrac{\sqrt{3}\pi^2 r^2}{hc_L}\left[\dfrac{f}{f_r\sqrt{(f/f_r)^2 - 1}}\right] & f > f_r \end{cases} \tag{4.12}$$

where, f_r is the ring frequency of the hemispherical structure, C_L is the panel longitudinal wave speed, expressed as:

$$C_L = \sqrt{\frac{E}{\rho(1-\upsilon^2)}} \tag{4.13}$$

The modal density of the reception room is expressed by [53]

$$n_3 = \frac{4\pi f^2 V_3}{c_o^3} + \frac{\pi f S_3}{2c_o^2} + \frac{P_3}{8c_o} \tag{4.14}$$

where, V_3, S_3 and P_3 respectively, are the volume, surface area, and the total edge length of the receiving room.

4.2.1.2 Dissipation loss factor

The loss factor due to dissipation for the hemispherical shell cavity is given as follows [44]:

$$n_1^d = \frac{S_1 c_o \gamma}{4\omega V_1}, \tag{4.15}$$

where, γ is the hemispherical shell's internal absorption coefficient, $\gamma = 1.8 \times 10^{-4}\sqrt{f}$ (least value) when no acoustic treatment inside the cavity is considered.

Since there is no accurate theoretical formula for determining the loss factor owing to dissipation, the hemispherical shell's dissipation loss factor was calculated through the decay rate approach.

The dissipation loss factor of receiving space is given as [34]:

$$n_3^d = \frac{2.2}{fT_{60}} \tag{4.16}$$

where, T_{60} is the reverberation time of the receiving acoustic space, which is computed using the given expression:

$$T_{60} = \frac{55.26 V_3}{c_o S_3} \tag{4.17}$$

4.2.1.3 Coupling loss factor

The coupling loss factor from resonant subsystem 2 to two acoustic spaces is given as [44]:

$$n_{21} = n_{23} = \begin{cases} \dfrac{2\rho_o c_o \sigma_2}{2\pi f \rho h} & f < f_c, \\ \dfrac{\rho_o c_o \sigma_2}{2\pi f \rho h} & f \geq f_c \end{cases} \tag{4.18}$$

where, ρ_o is the air density, σ_2 is the hemispherical shell's radiation efficiency and measured experimentally. Since there is no analytical expression available to estimate the radiation efficiency of the hemispherical shell.

The coupling loss factor between two acoustic spaces is obtained as [30,35]:

$$n_{13} = \frac{c_o S}{8\pi f V_1} \tau \tag{4.19}$$

where, S is the total surface area of the hemispherical shell.

The coupling loss factor between acoustic spaces to the non-resonant subsystem 4 is expressed as [38]:

$$n_{14} = 2\tau S c_o \left(1 + n_4^d a\right) / 8\pi f V_1 \tag{4.20}$$

$$n_{34} = 2\tau S c_o \left(1 + n_4^d a\right) / 8\pi f V_3 \tag{4.21}$$

where, $a = \dfrac{\rho h \omega}{2\rho_o c_o}$,

The loss factor due to coupling from the non-resonant subsystem 4 to the acoustic spaces is expressed by the given relation [38]:

$$n_{41} = n_{43} = \frac{\rho_o c_o}{2\pi f \rho h} \tag{4.22}$$

4.2.2 Ring and critical frequencies

The ring frequency and critical frequency significantly characterizing the acoustic behavior of a hemispherical shell. The ring frequency f_r is described as the parameter at which the longitudinal wavelength is equivalent to the hemisphere circumference and related to the structural breathing mode resonance condition.

Another significant parameter, the critical frequency (lower limiting coincidence frequency), f_c is the frequency at which the speed of panel flexural waves is equal to the speed of acoustical sound waves in the medium of air.

The ring frequency and the critical frequency are given by Refs.[2,31,117]:

$$f_r = \frac{c_L}{2\pi r}, \tag{4.23}$$

$$f_c = \frac{\sqrt{12}c_o^2}{2\pi h c_L}, \tag{4.24}$$

4.2.3 Noise reduction (*NR*)

The difference in sound pressure level between the internal and external sound fields of the structure is called noise reduction.

The average acoustic energy E_i of the acoustic space is related to the acoustic pressure p_i is given as [2,45]:

$$E_i = \frac{p_i^2 V_i}{\rho_o c_o^2} \tag{4.25}$$

where, V_i is the volume of the acoustic space.

Therefore, NR of the hemispherical shell in decibels (dB) can be obtained as follows:

$$NR = 10\log_{10}\left[\frac{E_1 V_1}{E_3 V_3}\right] \tag{4.26}$$

Hence, the noise reduction of the hemispherical shell above the ring frequency can be calculated using Eq. 4.6 and Eq. 4.26. Similarly, the noise reduction of the hemispherical shell below the ring frequency can be computed using Eq. 4.10 and Eq. 4.26.

4.2.4 Transmission loss (*TL*)

The acoustic performance of a hemispherical shell is characterized by TL, which is the significant and relevant acoustic indicator.

It is dissimilar to NR that is induced through the structural and absorbent properties of acoustic space. The sound transmission loss is influenced by the structural vibration parameters, principally the stiffness, mass, and damping.

Thus, TL is expressed in decibels (dB) and theoretically obtained as [32]:

$$TL = NR + 10\log_{10}\frac{S}{S_3} \tag{4.27}$$

Thus, the transmission loss of the hemispherical shell above the ring frequency can be calculated using Eqs. 4.6, 4.26, and 4.27. Similarly, the transmission loss of the hemispherical shell below the ring frequency can be computed using Eqs. 4.10, 4.26, and 4.27.

4.3 Experimental studies

The experimental measurements were performed in the soundproof chamber to validate the presented SEA model. The volume, total surface area, and the total edge length of the soundproof chamber are 16 m^3 and 38 $m^{2,}$ and 30 m, respectively. The experiments were conducted on a galvanized steel hemispherical shell with the same dimensions as those used in the analytical modeling.

4.3.1 Dissipation loss factor measurement

The hemispherical shell's dissipation loss factor are determined through the experimental decay rate method based on the transient response theory of resonant modes [33].

The decay rate method is employed to the measurement of the damping of a single resonant mode or the average damping of a group of modes resonating in a frequency band. The initial excitation to the structure is given by an impulsive source that is suddenly released. The initial slope of the decay after the excitation stops is proportional to the net effective loss factor of the structure.

The dissipation loss factor of a structure is related to time-averaged decay time through the following relation [33]:

$$n_i^d = 0.22 / fT_{1/2} \tag{4.28}$$

where, $T_{1/2}$ is the time-averaged decay time which is defined as the time required for the response amplitude to decay by half.

The schematic and photographic views of the test arrangement for evaluating the dissipation loss factor of the hemispherical structure are demonstrated in Figs. 4.4 and 4.5, respectively.

During the test, the hemispherical shell was hung freely by light strings and provided the excitation through the impulse hammer [Modal: Dytran 5800B4 series], which has a sensitivity of 2.25 mV/N. The LMS (Leuven Measurement Systems) data acquisition analyzer of 16-channel was connected to lightweight accelerometers (PCB356A16 series) of sensitivity of 100 mV/g, PC and the impulse hammer.

At several positions on the accelerometer, the decay characteristic of the hemispherical structure was evaluated. The test was performed repeatedly, and nine impacts were executed at several locations of the sensor to achieve accurate and consistent findings. Subsequently, mean averaging decay time was recorded.

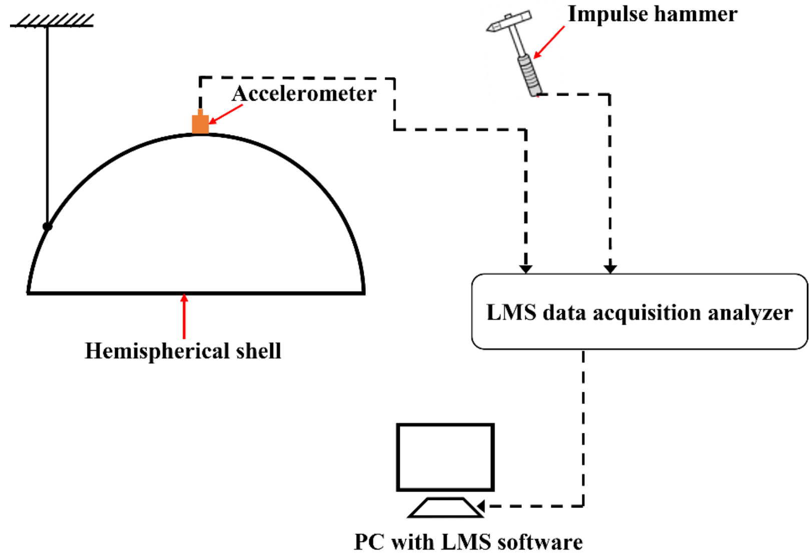

Figure 4.4 Schematic diagram of the experimental setup (decay rate technique) to measure the dissipation loss factor of hemispherical shell

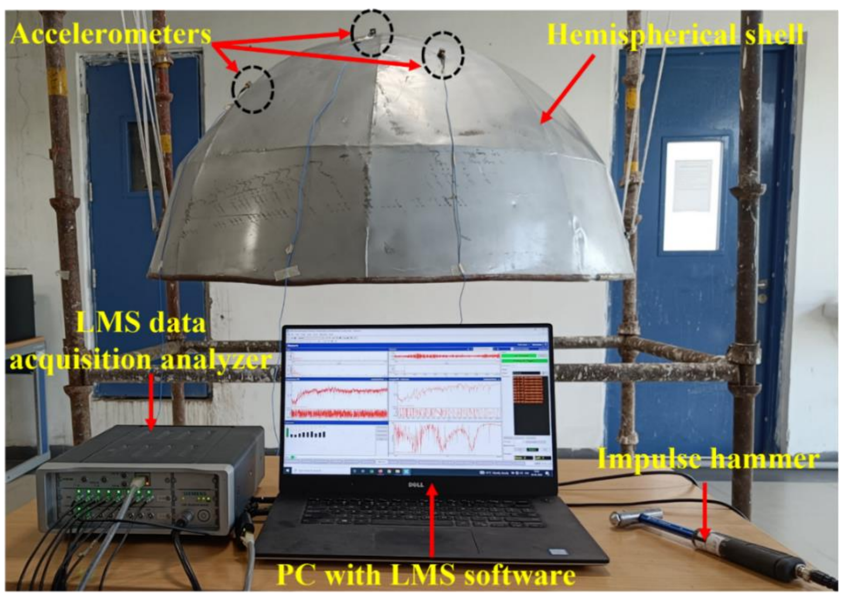

Figure 4.5 Photographic view of the experimental setup (decay rate technique) to measure dissipation loss factor of hemispherical shell

Fig. 4.6 illustrates the hemispherical shell's time-averaged dissipation loss factor at 1/3 octave bands. For more precise results, the tested dissipative loss factor was employed for the transmission loss prediction of hemispherical shell.

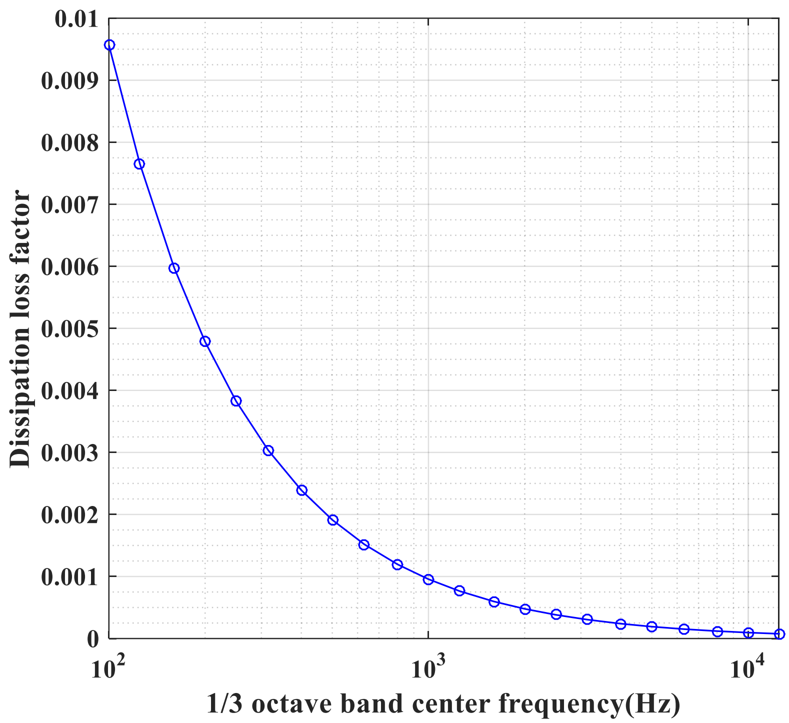

Figure 4.6 Experimental dissipation loss factor: hemispherical shell

4.3.2 Radiation efficiency measurement

The sound radiation efficiency is a significant acoustic parameter that characterizes the sound radiation properties of the panel.

The radiated sound power W_r , shell mean square velocity $\left\langle v^2 \right\rangle$, and area of radiating surface S , all have a mathematical relationship [1,120]:

$$\sigma = \frac{W_r}{\rho_o c_o S \left\langle v^2 \right\rangle}, \tag{4.29}$$

To compute the experimental radiation efficiency of the hemispherical shell, it is important to test the mean square velocity and radiating sound power from the shell. The acoustic excitation was supplied to the hemispherical shell through an omnidirectional sound source [Model: 4292-L, Brüel & Kjær system] placed inside the shell cavity. The sound power radiated from the shell was measured utilizing the pp-type sound intensity probe through the discrete point technique.

Simultaneously, the vibration responses were obtained at different positions on the shell using the PCB356A16 series lightweight accelerometers. Then, the radiation efficiency of the hemispherical shell was measured based on Eq. (4.29). The response of the measured vibration time history is shown in Fig. 4.7 for the hemispherical shell.

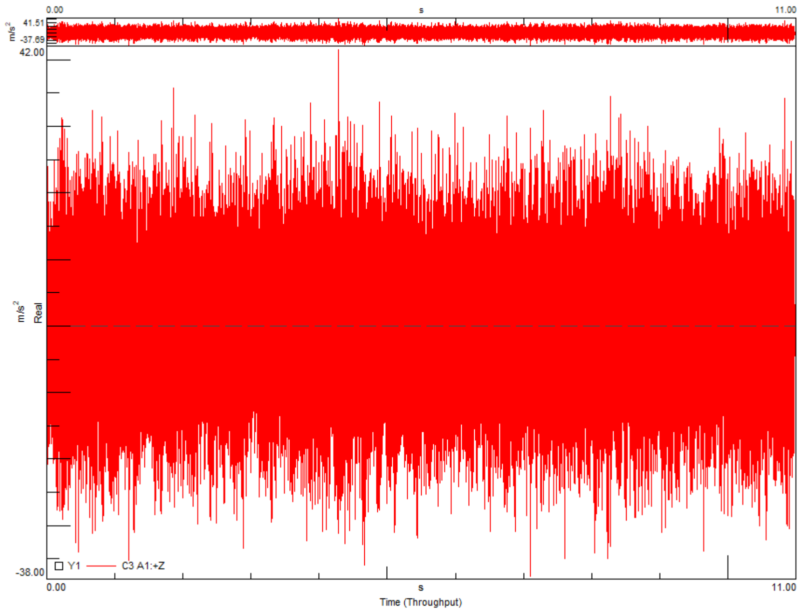

Figure 4.7 Measured vibration response of the hemispherical shell

4.3.3 Transmission loss measurement using sound intensity technique

The sound intensity method is subjected to determine the sound intensity of the internal sound source and the transmission sound intensity from the shell.

The sound transmission loss is calculated experimentally using the formula presented [53]:

$$TL = 10\log_{10}\left(\frac{I_{in}}{I_t}\right) \tag{4.30}$$

where, I_{in} and I_t are correspondingly the incident and transmission sound intensity.

It was necessary to compute the sound transmission loss of the hemispherical shell using Eq. (4.30) to examine the performance of the hemispherical shell and the accuracy of the developed formulation. The schematic sketch and the photographic views of the test setup are demonstrated in Fig. 4.8 and Fig. 4.9, respectively, where the sound is produced inside the cavity of the hemispherical shell. A sound source was employed to excite the shell cavity acoustically to evaluate the transmission loss. The sound source was situated in the centre of the shell and causing the white-noise excitations to produce the diffuse internal sound field. The tested sound transmission loss is determined by the sound intensity approach. The sound intensity approach involves measuring the spatial mean sound intensity over the hemispherical shell and determining the noise source's incidence sound intensity. The sound intensity was tested with a sound intensity probe (G.R.A.S type 50 GI-R), which was coupled to the LMS analyzer for data acquisition and a computer.

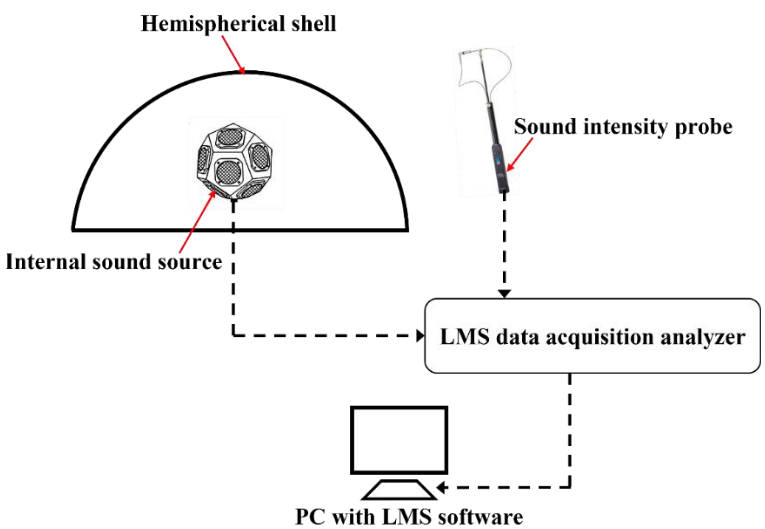

Figure 4.8 Schematic measurement setup to evaluate the transmission loss of a hemispherical shell

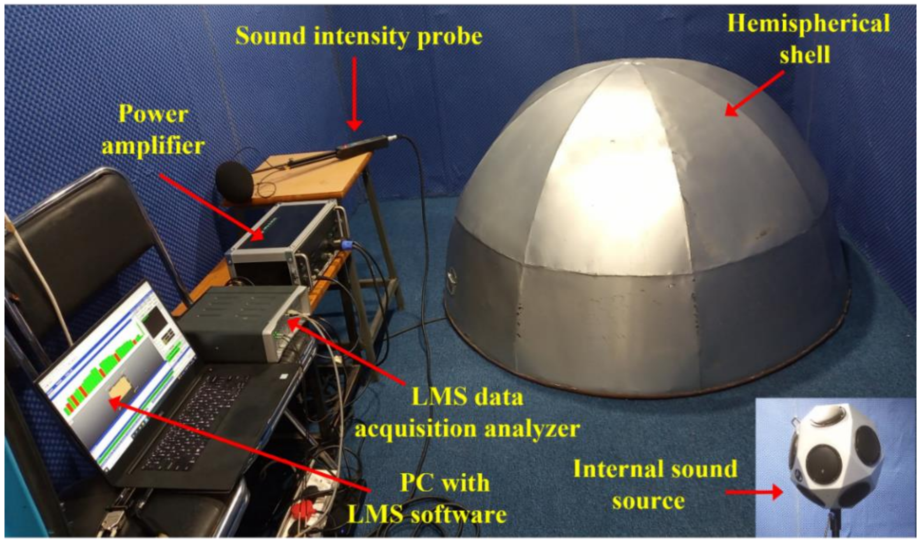

Figure 4.9 Photographic view of the measurement setup to evaluate the transmission loss of a hemispherical shell through the sound intensity experimental approach

As shown in Fig. 4.10, the probe was made up of two 1/2-inch microphones that were separated by a spacer and phase-matched. During the experiments, four different spacers were utilized to keep the microphone spacing at 12 mm, 25 mm, 50 mm, and 100 mm to cover the wide range of frequencies.

Figure 4.10 Sound intensity probe with interchangeable solid spacers

By separating the shell surface into different segments, the sound intensity was tested according to the international standard ISO 9614-1 discrete point technique [111]. To acquire more precise and consistent findings, each segment was tested two times by replacing various spacers. The sound intensity was evaluated at a distance of 0.05 m from the shell area.

Fig. 4.11 depicts the tested sound power of the hemispherical shell's interior sound field at 1/3 octave frequency bands.

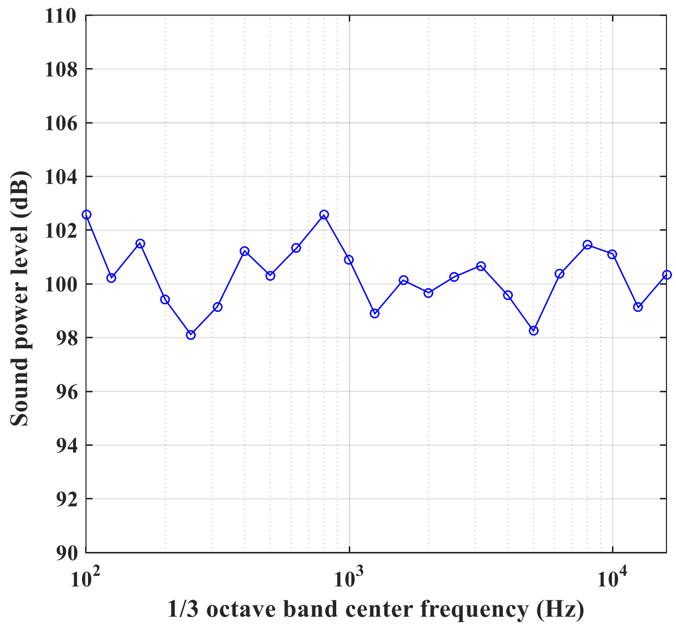

Figure 4.11 Experimental sound power of the interior sound field

4.4 Results and Discussion

The measured radiation efficiency of the hemispherical shell at the 1/3 octave band centre frequencies is depicted in Fig. 4.12. The hemispheric shell's radiation efficiency features two substantial peaks, as seen in Fig. 4.12, which are well expected. The first peak occurs at the hemispherical shell's ring frequency, that is related to the structural breathing mode resonance state. The measured ring frequency is 1250 Hz, whereas the ring frequency computed using Eq. (4.23) is 1170 Hz. The second peak appears at about 10000 Hz, the hemispherical shell's critical frequency, whereas the critical frequency computed by Eq. (4.24) is 10215 Hz. At the ring and the critical frequencies, the hemispherical shell's radiation efficiency has a large amplitude. The results show that the hemispherical shell radiates insufficiently, with the exception of the ring and critical frequencies, which have higher sound radiation.

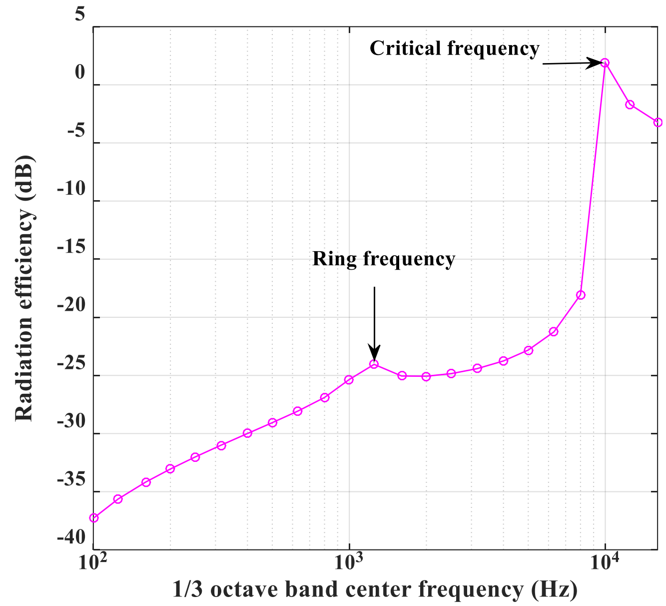

Figure 4.12 Experimental radiation efficiency of the hemispherical shell

The measured sound power radiated through the hemispherical shell is plotted in Fig. 4.13 and compared to analytical predictions at one-third octave bands' centre frequency. The experimental and analytical results are in reasonably good agreement.

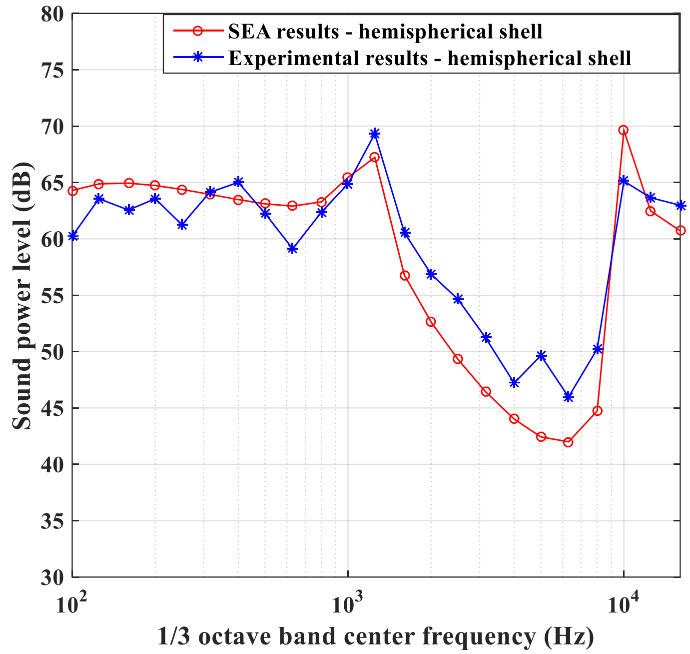

Figure 4.13 Comparison of analytical and experimental radiating sound power of the hemispherical shell

The sound power radiated from the hemispherical shell increases in the low and medium frequency ranges below the critical frequency according to mass law sound transmission. Moreover, in this frequency range, the radiated sound power is controlled through the mass per unit surface area of the shell. The hemispherical shell radiates inadequately excluding at the ring and critical frequencies due to large acoustical excitation of the hemispherical structure in the resonance mode. It exhibits a greater radiation efficiency at the respective frequencies of 1250 Hz and 10000 Hz, which are respectively the ring and critical frequency of the hemispherical shell. The difference between the experimental results and analytical predictions between 100 Hz and 10000 Hz may be presumably due to limited number of measurement points. At 1/3 octave frequency band, Fig. 4.14 compares the analytical results with the tested transmission loss of a hemispherical shell. The analytical and experimental data indicate a similar pattern, and the observed transmission loss matches the analytical results quite well.

It can be highlighted that during the design and assessment steps of such panels, sound transmission computation at the ring and critical frequencies is more influential.

The presented SEA model and the experimental results, as expected, exhibit two distinct drops in the transmission loss plot seen in Fig. 4.14.

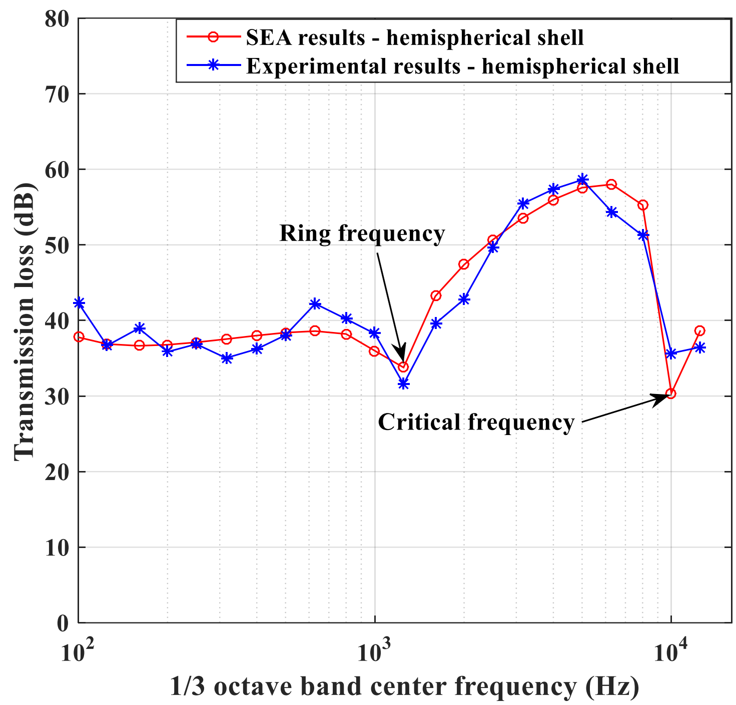

Figure 4.14 Comparison of analytical and measured results for transmission loss of the hemispherical shell

The first drop occurs at 1250 Hz, which is the hemispheric shell's ring frequency. The ring frequency is significantly linked to the structural breathing mode of hemisphere resonance closest to 1170 Hz, as determined using Eq. (4.23). The second drop occurs at 10000 Hz, corresponding to the hemispherical shell's critical frequency and nearest to the calculated result around 10215 Hz as determined using Eq. (4.24). The Sound transmission loss rises from the lower range of frequency to the ring frequency, where the structural breathing mode of hemisphere resonance causes a sudden reduction, as demonstrated in Fig. 4.14. The transmission loss then increases until it reaches the hemispheric shell's critical frequency.

The theoretical curve's tendency is to be expected, which increases across the low and medium range of frequencies according to mass law transmission and governed through structure's mass per unit surface area in these frequency range. Because of enhanced radiation efficiency and a significant shell excitation in a resonance situation, as the frequency of incident sound waves approaches the critical frequency, around 10000 Hz, a sudden dip appears. In this situation, the amplitude of shell vibration is equivalent to the amplitude of the displacement of the air particles associated with the impinging sound wave. Above the critical frequency, sound transmission is greatly controlled by the frequency of incident sound waves and structural dampening, both of which limit the structure's sound radiation characteristics. To determine the acoustic performance and sound radiation properties of the hemispherical shell, an accurate prediction of the ring frequency and critical frequency is essential. The error of percentage between predicted and computed ring frequency is 6.8 %, and that for the critical frequency is 2.1 % that, indicates that the analytical and experimental investigations are in reasonably good agreement.

4.5 Parametric study

Parametric studies are conducted to examine the usefulness of many design factors in improving the hemispherical shell's acoustic performance and transmission loss.

4.5.1 Influence of the absorption coefficient

The shell's absorption coefficient substantially impacts transmission loss efficiency. Compared to a smaller internal absorption coefficient ($1.8\times10^{-4}\sqrt{f}$), Fig. 4.15 shows that using a greater internal absorption coefficient ($3.6\times10^{-4}\sqrt{f}$) inside the shell cavity effectively increases the transmission loss. Sound transmission loss is increased to 3 dB by doubling the internal absorption coefficient, as shown in Fig. 4.15.

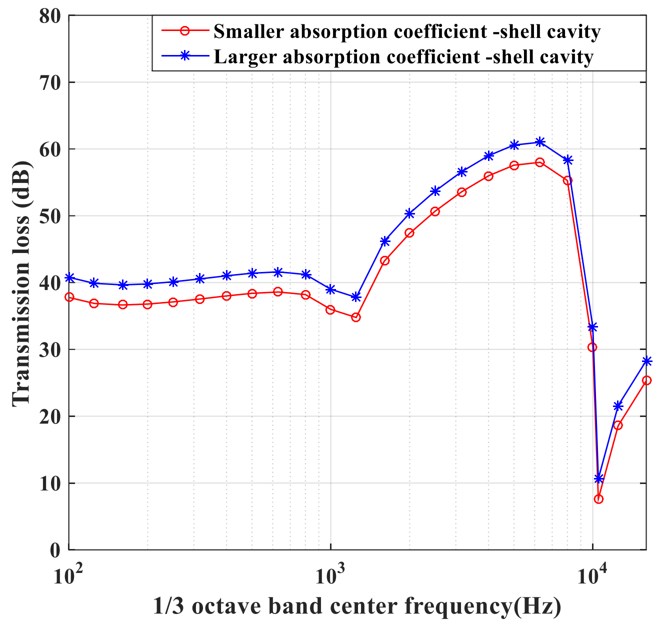

Figure 4.15 Effect of the absorption coefficient on the transmission loss of the hemispherical shell

4.5.2 Effect of thickness

It can be observed from Fig. 4.16 for the thickness, the locations of the critical frequencies significantly affect the sound transmission performance.

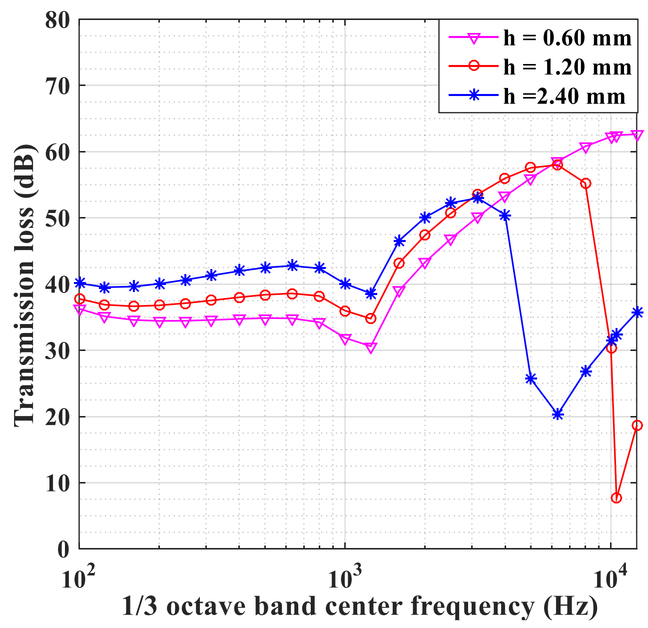

Figure 4.16 Effect of the thickness on the transmission loss of the hemispherical shell

In this regards, it can be seen that greater transmission loss can generally be achieved in the low and middle frequency region by shifting these frequencies towards left from 10000 Hz to 5000 Hz for the case of doubling the thickness. Therefore, regardless other design limitations, an enhancement in the thickness can improve the sound insulation performance of the hemispherical shell in the low and intermediate frequency range. Fig. 4.16 shows that doubling the thickness resulted in a 4 dB rise in transmission loss below the 3150 Hz frequency range. In a practical application, the shell has to be designed only a thick as required because of the design constraint in the weight, costs and construction procedure. The type of analysis, developed in this work is significantly useful in such a situation.

4.5.3 Effect of radius

As seen in Fig. 4.17, a larger radius reduces transmission loss of a hemispherical shell, mainly due to the hemisphere's curvature effect on its stiffness and greater surface area.

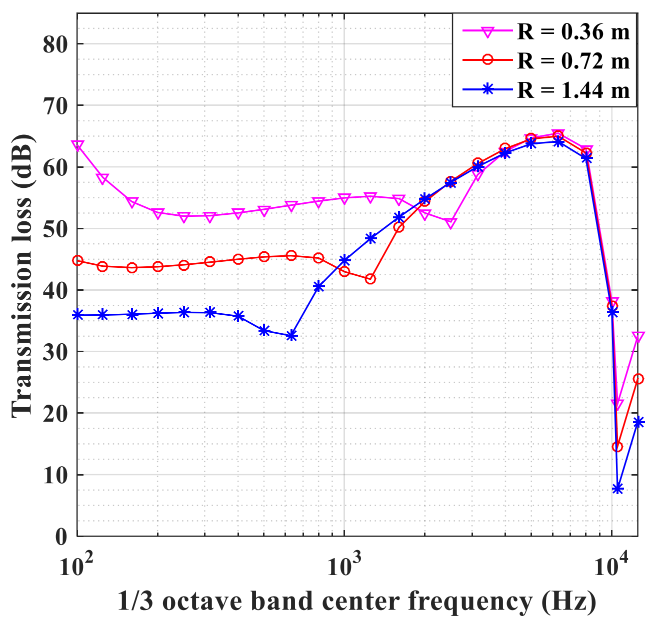

Figure 4.17 Influence of radius on the transmission loss of the hemispherical shell

A large radius of a structure will have a panel of smaller stiffness, which also act as an effective radiator because of large surface area. As a result, the hemispheric surface transmits acoustic energy more effectively. Therefore, during the hemispherical shell's design stage, this significant parameter should be given additional consideration.

4.5.4 Effect of various materials

Fig. 4.18 depicts the impact of various materials on the hemispherical shell's transmission loss. Steel, aluminum, and copper were chosen for the comparison, with material density listed in Table 4.2.

Table 4.2 Hemispherical shell material properties

Material	Density (kg/m^3)
Steel	7850
Aluminum	2710
Copper	8960

As can be observed from Fig. 4.18, that the transmission loss of an aluminum-made hemispherical shell is the least effective across the entire frequency range due to its low mass and stiffness.

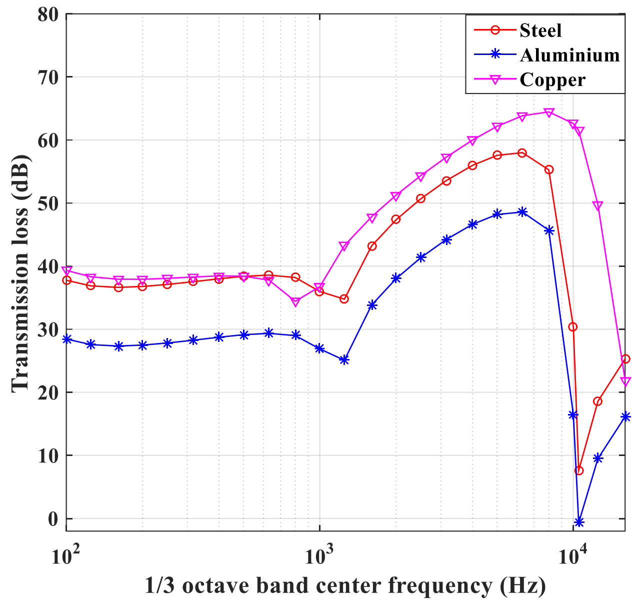

Figure 4.18 Influence of various materials on the sound transmission loss of the hemispherical shell

It is noted that low frequency region is controlled by stiffness while the higher frequency range is governed by mass law. Fig. 4.18 demonstrates that the steel and copper made hemispherical shell effectively provides the superior transmission loss in a broad frequency range because both the steel and copper have greater mass and stiffness properties. Therefore, without consideration of other design constraints, steel or copper can be chosen as the material of the shell in order to increase the sound insulation.

4.6 Conclusions

This chapter proposes an analytical model for predicting the sound transmission loss of hemispherical shells using the SEA technique. The analytical formulation models the hemispherical shell in a broad frequency region. The significant SEA parameters involved in the analytical formulation of the hemispherical shell, such as modal density and coupling loss factor, are computed. The dissipation loss factor and radiation efficiency of the hemispherical shell are measured experimentally. The sound transmission loss of the hemispheric shell is measured using the sound intensity experimental approach.

The analytical results agree with the experimental results and accurately evaluate the hemispherical shell's ring and critical frequency. The percentage error between predicted and computed ring frequency is 6.8 %, and that for the critical frequency is 2.1 %. Based on the proposed SEA technique, parametric studies were conducted. The influence of design parameters such as the internal absorption coefficient, thickness, radius, and different panel materials on the transmission loss was investigated. It was found that the greater transmission loss of hemispherical shell can be achieved using a higher absorption coefficient inside the shell cavity. Further, it was shown that the sound insulation performance of the hemispherical shell increases with the increases of shell thickness in the low and intermediate frequency range. Moreover, it was demonstrated that the larger radius reduces transmission loss of a hemispherical shell. It was found that the steel and copper made high density hemispherical shell effectively provides the superior transmission loss in a wide frequency range compared to that of low-density material.

Chapter 5

Experimental study of sound transmission loss of different shapes acoustic enclosures

In this chapter, an experimental study is performed to study the impact of different shapes of enclosure on sound transmission loss using sound intensity technique. There is a need to determine the acoustic performance of enclosures due to the commercial demand for quieter systems of limited space. Four different shapes of enclosures (rectangular, cylindrical, conical, and hemispherical) are chosen for investigating transmission loss. The results obtained show that the acoustic enclosure of the hemispherical shape is efficient in improving the acoustic performance of the enclosure and provides a maximum transmission loss of about 41.85 dB. The presented experimental results can also be utilized as reference data for more analytical and numerical investigation.

5.1 Introduction

Assessment of sound transmission behavior is usually needed during the development and assessment phases of acoustic enclosures. Ensuring adequate transmission loss with enclosed noise sources is a significant factor in determining enclosures' acoustic efficiency. Many numerical and experimental studies are performed to investigate effectiveness of the acoustic enclosures [43,62–64,72,89,121,122]. However, they fail to study the influence of the shapes of enclosures on the sound transmission. Several approaches and computer simulations concern the analysis of internal sound field of different shapes of enclosures, but they are complex and difficult to implement by designers. Due to the intensive demand of the various industrial applications for quieter systems and suppressing the noise source in a limited space, there is a need to determine the acoustic performance of enclosures. Moreover, less research has been done to investigate the influence of different shapes of enclosures of the same volume on the transmission loss and received little consideration.

The objective of this paper to investigate the sound transmission performance of different shape enclosure of same volume employing the sound intensity method. In order to study the impact of shape on the sound transmission loss, four different shapes of enclosure are chosen (rectangular, cylindrical, conical, and hemispherical). The present study will help to select an optimal shape of the enclosure and curb the noise problem of the acoustic enclosure when there is a space constraint.

5.2 Experimental studies

In order to explore the transmission loss of different shapes of acoustic enclosures of the same volume, the experiments were performed in the soundproof chamber. The soundproof chamber's volume and total surface area are 16 m^3 and 38 m^{2,} respectively.

Sound transmission loss is calculated experimentally using the formula presented [2,53]:

$$TL = 10\log_{10}\left(\frac{I_{in}}{I_t}\right) \tag{5.1}$$

where, I_{in} and I_t are correspondingly the incident and transmission sound intensity.

A schematic sketch of different shapes of acoustic enclosure is displayed in Fig. 5.1. Table 5.1 presents the parameters employed for the acoustic problem of different shapes of acoustic enclosure. To study the enclosure's acoustic performance, the transmission loss was determined adopting the sound intensity experimental approach based on Eq (1).

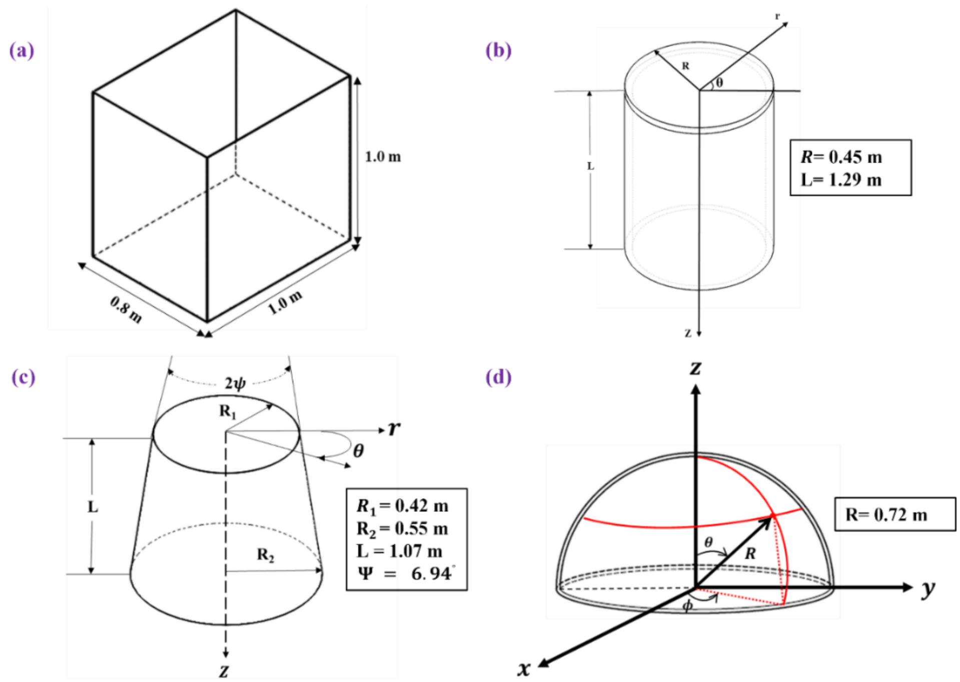

Figure 5.1 A schematic sketch of the acoustic enclosure: (a) Rectangular enclosure (b) Cylindrical enclosure (c) Conical enclosure (d) Hemispherical enclosure

Table 5.1 Dimensions and material properties utilized for the acoustic problem of different shapes of enclosure

Material property	**Acoustic enclosure shape**			
	Rectangular	**Cylindrical**	**Conical**	**Hemispherical**
Mass density	7850 kg/m^3			
Young's modulus	2×10^{11} Pa			
Poisson's ratio	0.3			
Thickness	1.20 mm			
Volume	0.8 m^3			

The photographic view of the experimental arrangement for evaluating the transmission loss of rectangular shape acoustic is demonstrated in Fig. 5.2.

In order to measure the transmission loss of cylindrical, conical and hemispherical shapes of acoustic enclosure, similar experimental setup was employed as depicted in Fig. 5.2. To determine the transmission loss, the enclosure's internal volume was excited acoustically through an internal noise source. Inside the enclosure cavity, an acoustic sound source produces an interior sound field which excites the enclosure panel. The exciting panel thus transmits sound into externally to the enclosure, that is reception room. To produce the acoustic sound power, the omnidirectional sound source was located in the centre of the enclosure and supplied through white-noise excitations.

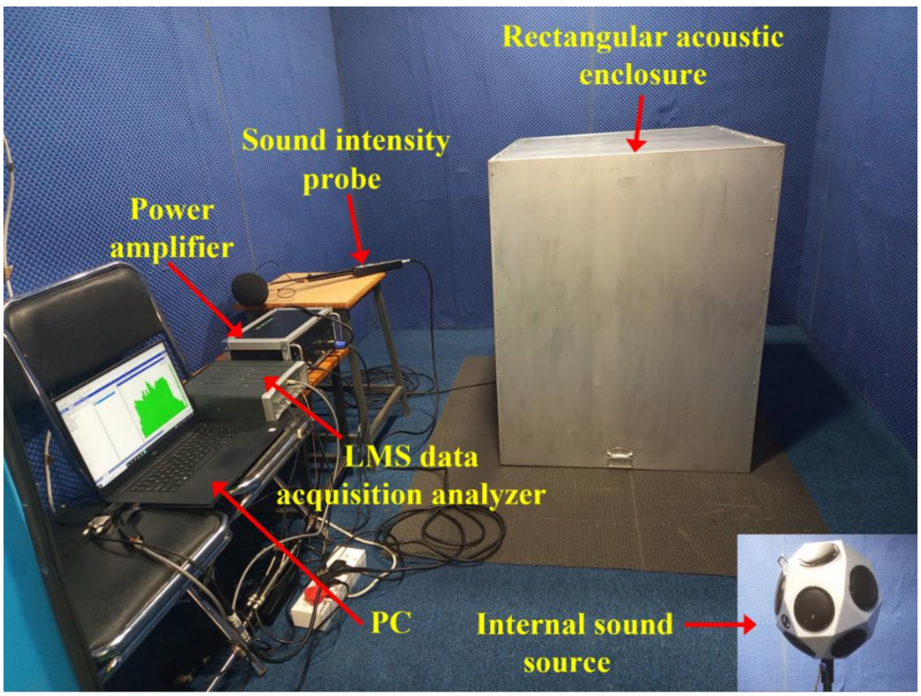

Figure 5.2 Experimental setup to evaluate the transmission loss of rectangular acoustic enclosure

The incident sound intensity evaluation of the sound source as well as the transmission sound intensity was tested using the sound intensity approach. Thereafter, sound transmission loss is determined. The sound intensity was tested with a sound intensity probe (G.R.A.S model 50 GI-R), which was coupled to the LMS analyzer for data acquisition and a computer.

The probe was made up of two 1/2-inch microphones that were separated by a spacer and phase-matched. During the experiments, four different spacers were utilized to keep the microphone spacing at 12 mm, 25 mm, 50 mm, and 100 mm to cover the wide range of frequencies. By separating the enclosure surface into different segments, the sound intensity was tested according to the international standard ISO 9614-1 discrete point technique [111]. To acquire more precise and consistent findings, each segment was tested two times by replacing various spacers. The sound intensity was evaluated for a distance of 0.05 m from the surface area.

5.3 Results and Discussion

The experimental results of the measurements performed on different shape acoustic enclosures utilizing the sound intensity approach are presented in this section. The curve drawn in Fig. 5.3 depicts the overall values of sound power level radiated from different shapes of acoustic enclosures.

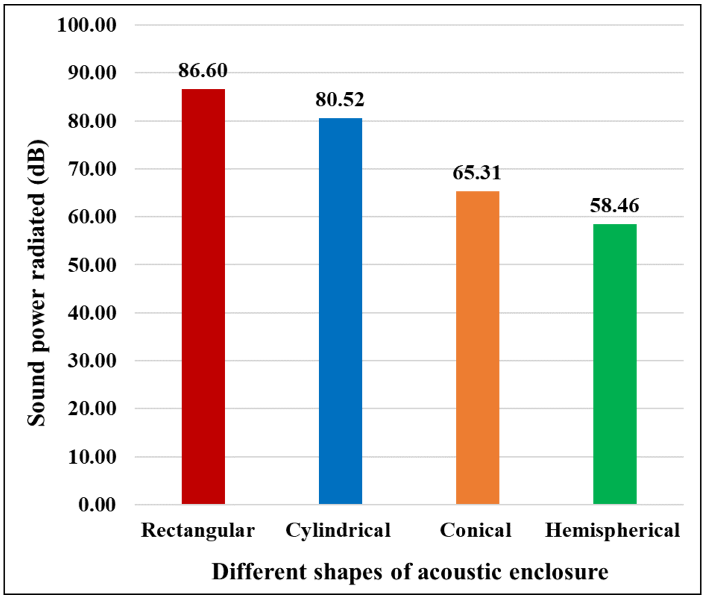

Figure 5.3 Radiated sound power level comparison of different shapes of acoustic enclosures

The overall value of sound power level radiated from the rectangular shape enclosure is 86.60 dB which is maximum. Compared to the rectangular, cylindrical, and conical shape enclosure, the lowest overall sound power level emitted is observed for the case of hemispherical shape enclosure, which is 58.46 dB.

Fig. 5.4 shows the overall value of transmission loss of various shapes enclosures.

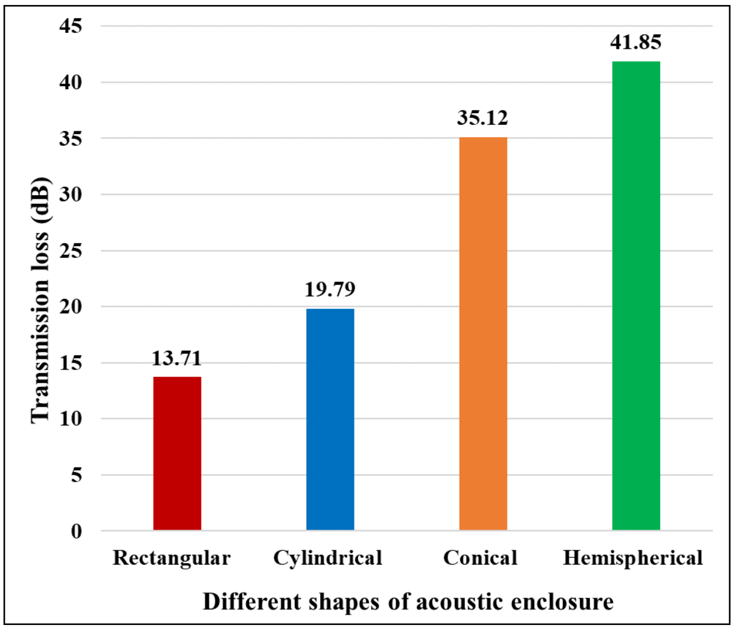

Figure 5.4 Comparison of the sound transmission loss of different shapes of acoustic enclosures

It can be seen that the hemispherical shape enclosure demonstrates efficient acoustic performance and causes a higher transmission loss of 41.85 dB. It is seen directly from Fig. 5.4 that the rectangular shape acoustic enclosure has the least effective transmission loss compared to the enclosure built up of curved panels. The rectangular shape enclosure produces a transmission loss of 13.71 dB, whereas cylindrical and conical shape enclosures cause transmission loss of 19.79 dB and 35.12 dB, respectively. It can be noted that a cylindrical shape enclosure results in 6.08 dB transmission loss compared to a rectangular shape enclosure.

The conical shape enclosure produces a transmission loss of 21.41 dB in comparison to the rectangular shape enclosure. It can be observed that the hemispherical shape enclosure yields 28.14 dB greater transmission loss than the rectangular shape enclosure. Fig. 5.4 depicts that hemispherical shape enclosure has a more significant transmission loss of 22.06 dB and 6.73 dB, respectively in comparison to cylindrical and conical shape enclosures. The enclosure shape has a direct influence on the transmission loss of the enclosure and demonstrated in Fig. 5.4. With an increase in the frequencies of the standing wave resonance, the enclosure cavity shapes effects not only the acoustic resonance of the enclosure's internal sound field, but also the standing wave magnitude.

The 1/3 octave study is conducted to investigate the influence of shapes of acoustic enclosure in the different frequency bands, as displayed in Fig. 5.5.

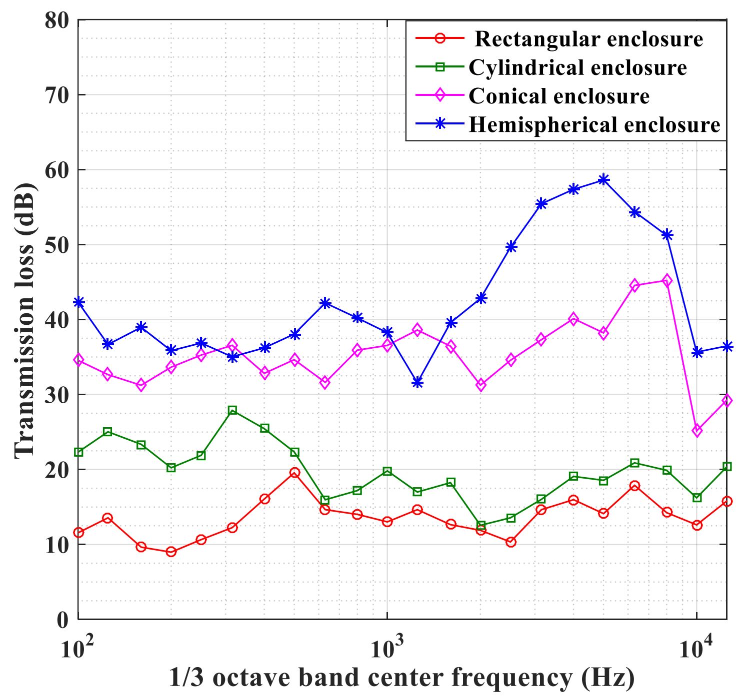

Figure 5.5 Transmission loss comparison of the different shapes of acoustic enclosures at 1/3 octave bands

The cylindrical shape enclosure has a more significant transmission loss at the low-frequency ranges between 100 Hz to 400 Hz compared to the rectangular shape enclosure.

Compared to the conical shape enclosure, it can be demonstrated in Fig. 5.5 that the hemispherical shape enclosure has a higher transmission loss in the low-frequency range between 100 Hz to 1250 Hz and increases significantly for the high-frequency region through 1600 Hz to 12500 Hz. The hemispherical shape of acoustic enclosure has superior acoustic performance in comparison to cylindrical, conical, and rectangular shape enclosures in the entire frequency bands as indicated in Fig. 5.5.

It is clear from the experimental evaluation of transmission loss of enclosure of constant volume that the hemispherical shape acoustic enclosure is efficient to improve the noise reduction of the enclosure.

5.4 Conclusions

This chapter presents an experimental study to investigate the transmission loss of four different shape enclosures viz. rectangular, cylindrical, conical and hemispherical. The volume of all the shapes has been kept the same. The sound intensity approach is adopted to determine the transmission loss of enclosures in wide frequency range. The experimental study shows that the acoustic enclosure of hemispherical shape provides maximum transmission loss as compared to rectangular, cylindrical, and conical shape enclosures of the same volume.

Chapter 6

Experimental study of sound-absorbing material of different surface shapes on noise reduction performance of an acoustic enclosure

In this chapter, an experimental work is presented for investigating the influence of sound-absorbing material of different surface shapes on the noise reduction of an acoustic enclosure. The polyurethane foam (PU) is considered as a sound-absorbing material in the present study. The commercially available acoustic material of three surface shapes, i.e., plane, wedge, and pyramid surface are chosen for the analysis. The presented experimental results can also be utilized as reference data for more analytical and numerical investigation.

6.1 Introduction

Noise pollution of the factory and the industrial workspace is a serious concern. The environment of intense noise plays a major role in a worker's performance. The high exposure to noise not only impacts the adverse effects on psychological health but also cause hearing damage, poor voice communication, and impaired efficiency [123] . The noise generated from cutting tools during machining is one of the main sources of noise in the factory workspace such as portable saw, spindle, drilling machine [124–126]. The acoustic enclosure is one of the most important engineering designed structures for modifying the sound transmission path and suppressing the airborne noise effectively by adding sound-absorbing materials [28,51,127]. Cole et al. [35] and many other researchers [36,37,43,44,128] demonstrated theoretically and experimentally the effectiveness of acoustic absorbing materials on the noise reduction characteristics for the acoustic enclosure made of different materials. Cao et al. [129] and several other researchers [11,76,130] predicted analytically and experimentally the noise reduction capability of engineering structures by incorporating the acoustic absorbing materials in the studies.

It is shown that the implementation of sound-absorbing materials has a significant role in the noise control of an enclosure and other complex structures. Airborne noise transmission can be diminished by adding the sound-absorbing material which is directly linked with the energy of the acoustic waves. The noise reduction performance of acoustic enclosure depends on many factors such as material, geometry, panel thickness, location of the source, the thickness of sound-absorbing material.

In the present chapter, an experimental work is presented for investigating the influence of sound-absorbing material of different surface shapes on the noise reduction of an acoustic enclosure. The polyurethane foam (PU) is considered as a sound-absorbing material in the present study. The commercially available acoustic material of three surface shapes, i.e., plane, wedge, and pyramid surface are chosen for the analysis.

6.2 Experimental study

The acoustic performance of an acoustic enclosure is defined in terms of noise reduction which is defined as the difference of sound pressure level of unenclosed noise source and the enclosed noise source [2,89]. The various commercially acoustic materials used in the experimental work are shown in Fig. 6.1. The thickness of the polyurethane foam employed for the study is 50 mm. The initial noise level of the noise sources was measured without an enclosure to have a reference value for comparison purposes. Thereafter all the iterations have been implemented according to Table 6.1. The noise measurement was conducted in the Noise and Vibration Control laboratory at IIT Indore.

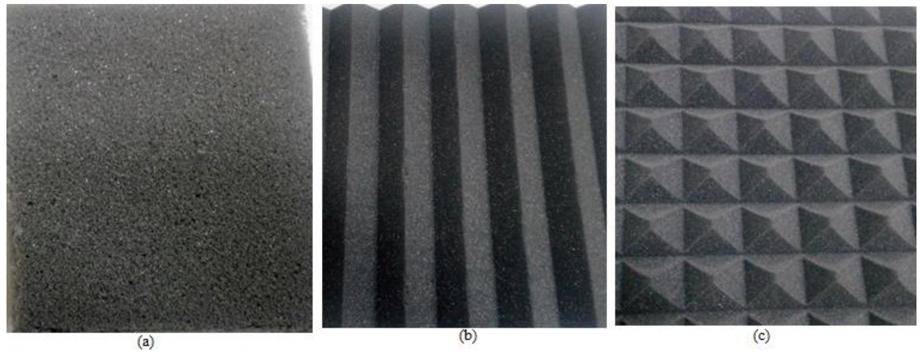

Figure 6.1 Polyurethane sound-absorbing material of various shapes (a) Plane (b) Wedge (c) Pyramid

Table 6.1 Different conditions of noise measurement

Condition	Measurement detail of acoustic enclosure
Case -1	Enclosed source
Case -2	Enclosed source with plane shape PU foam
Case -3	Enclosed source with wedge shape PU foam
Case -4	Enclosed source with pyramid shape PU foam

A rectangular acoustic enclosure made of steel material was employed in the experimental work. The enclosure has dimensions of 1 m × 0.8 m × 1 m and the thickness of each panel was 1.20 mm. The polyurethane foam of different shapes was used in the study. Four piezotronics microphones (PCB made) were employed around the enclosure. The sound pressure level (SPL) measurement is taken at a distance of 1 meter for each surface of the enclosure. The spatial mean average value of the sound pressure level was taken. The measurement data was acquired using the 16 channel LMS data acquisition system in the range of frequency between 63 Hz to 8000 Hz of 1/3 octave band. Noise radiated by the cutting tools is the prime cause of noise pollution in the factory environment. In the present study, therefore hand-held circular saw of model GKS 7000 with a rated power input of 1100 watt is considered as a noise source for the experimental work which is shown in Fig. 6.2. The measurement set-up and photographic views for the implementation of PU foam are shown in Fig. 6.3. and Fig. 6.4. respectively.

Figure 6.2 Noise source: Handheld circular saw

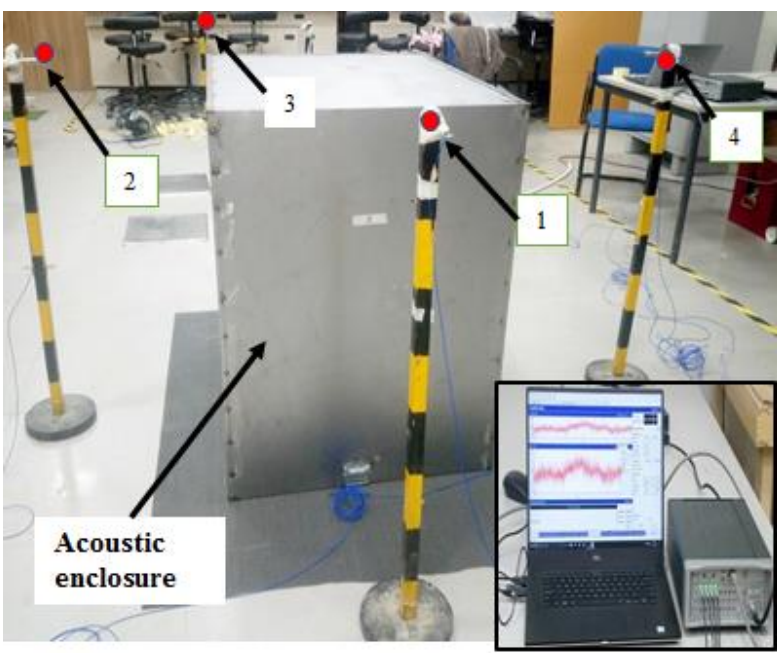

Figure 6.3 Insertion loss measurement setup using microphones (1-4) with LMS data acquisition system and noise source inside the enclosure

(a) (b) (c)

Figure 6.4 The photographic views for the implementation of PU foam: (a) Enclosed source with plane shape PU foam, (b) Enclosed source with wedge shape PU foam, (c) Enclosed source with pyramid shape PU foam

Fig. 6.5 shows the sound power level (SWL) spectrum of the handheld circular saw.

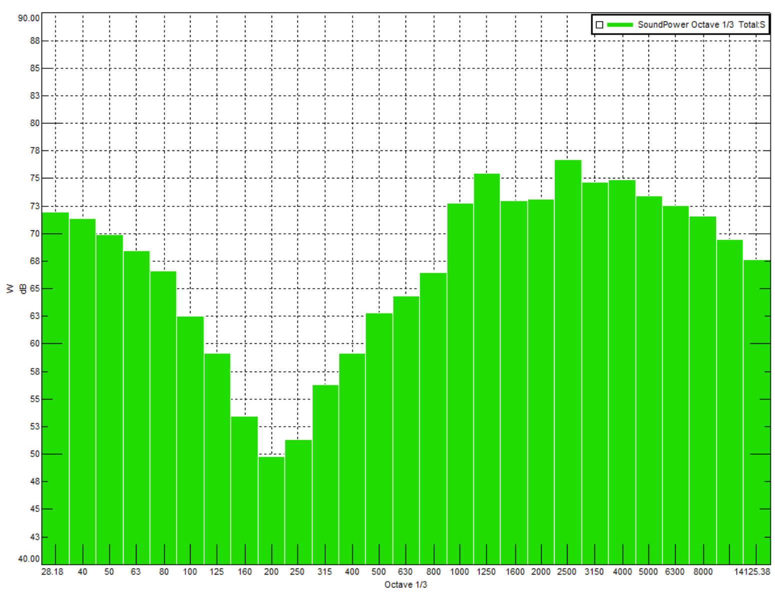

Figure 6.5 SWL spectrum of the handheld circular saw

Fig. 6.6 shows the sound pressure level (SPL) spectrum of the handheld circular saw.

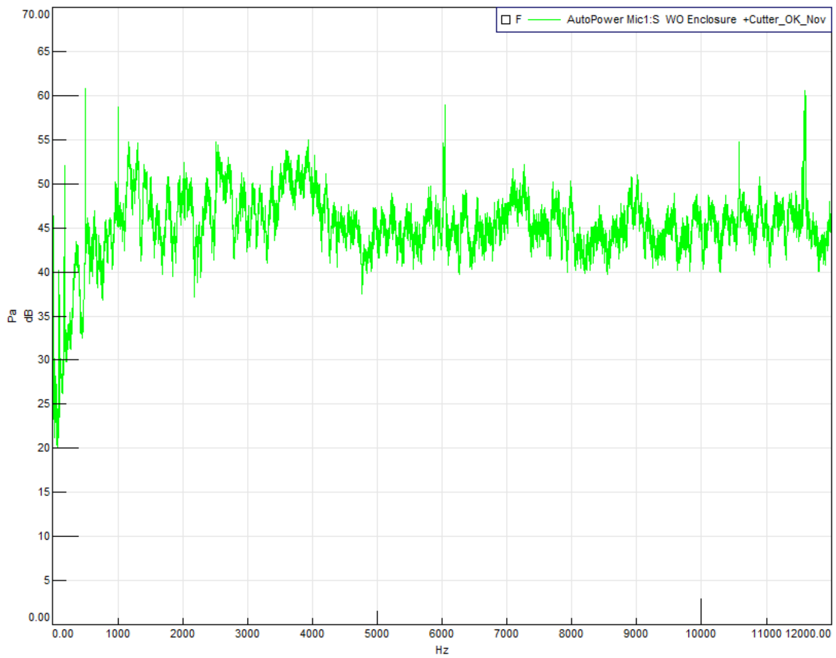

Figure 6.6 SPL spectrum of the handheld circular saw

The sound pressure level value of the noise source is measured was 88.75 dB(A). The background noise was measured to be 45 dB(A) which is far lesser than the sound pressure level of the noise source. Therefore, background noise has a negligible influence on the noise measurement of the source. All the measurements were repeated for ensuring the reliability of measurement.

6.3 Results and Discussion

The overall SPL values in various cases of the measurement are shown in Fig. 6.7. It is observed from the Fig. 6.7 that adding the sound-absorbing PU foam inside the enclosure reduces the noise level efficiently. The acoustic materials not only suppress the acoustic resonance inside the enclosure but also demises the magnitude of standing waves with an increment of the frequencies of the resonance of the standing wave. It can be seen that surface shapes of the acoustic material inside the enclosure directly influence the acoustical performance of the enclosure. The overall value of SPL for the noise source was observed is 88.75 dB(A) which is maximum. The minimum SPL is achieved in the case of using pyramid shape PU foam which is 65 dB(A).

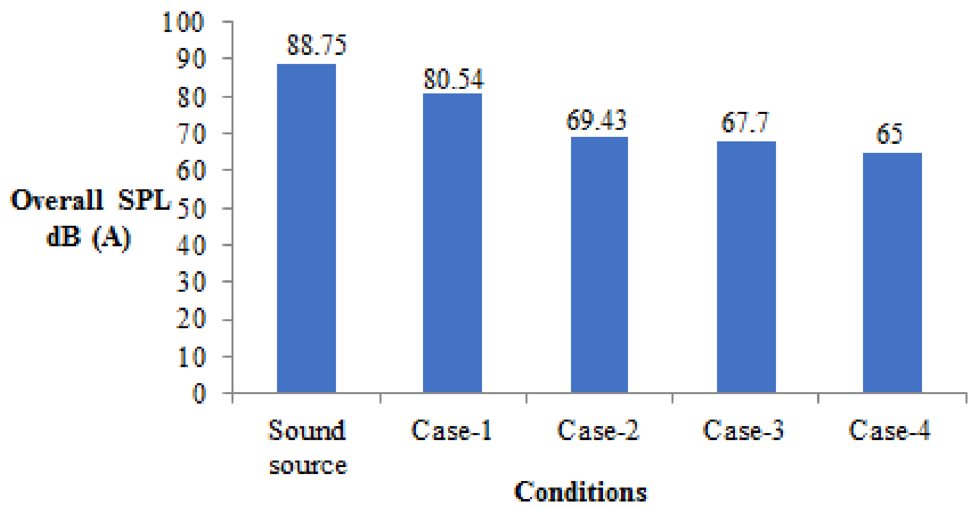

Figure 6.7 Overall sound pressure level values of various measurement conditions

The noise reduction for various conditions is shown in Fig. 6.8. It is found that adding a pyramid shape PU foam inside the acoustic enclosure, causes a larger noise attenuation of 23.75 dB(A).

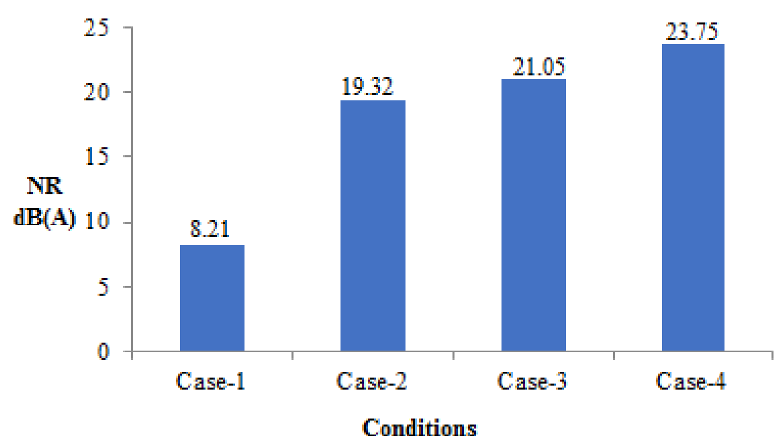

Figure 6.8 Noise reduction values of various measurement conditions

It can be observed directly from Fig. 6.8 that the plane shape and wedge shape PU foam causes a noise reduction of 19.32 dB(A) and 21.05 dB(A) respectively.

The 1/3 octave analysis is carried out as shown in Fig. 6.9 to study the effect of various shapes of acoustic material in the different frequency bands.

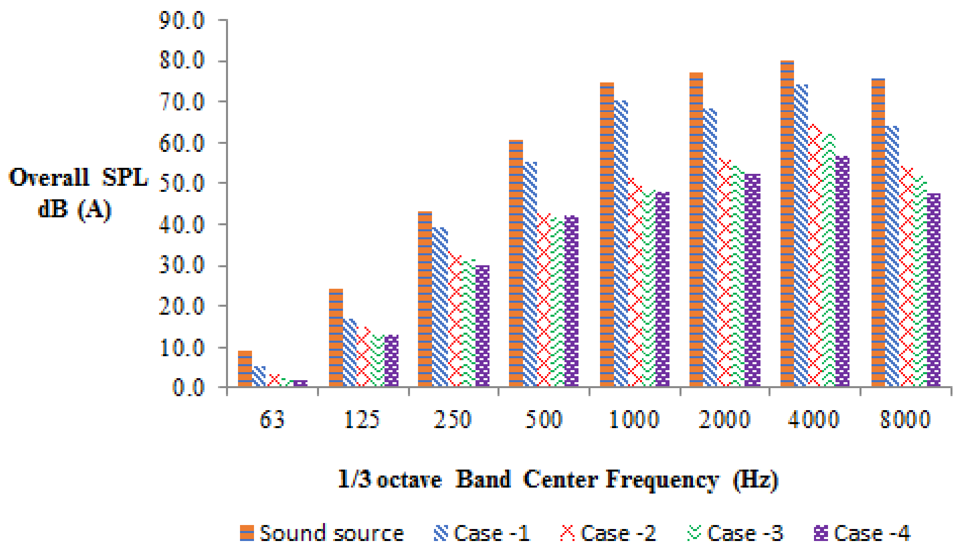

Figure 6.9 Overall sound pressure level values at the center frequency of 1/3 Octave band

The 1/3 octave analysis shows that wedge shape and pyramid shape acoustic material have an overall better effect in comparison to plane PU foam in the entire frequency region as shown in Fig. 6.9. 1/3 octave band analysis shows that the wedge and pyramid shape PU foam has a similar effect in the frequency range between 500 to 2000 Hz. The pyramid shape PU foam is very efficient in the high-frequency region between 2000 to 8000 Hz.

In general, when an incident sound-wave hits on the panel plain surface, some of the sound wave is reflected off, some is absorbed, and some transmitted through the panel. To minimize the amount of sound transmitted through the wall, pyramid shape surface is designed in order to suppress sound effectively.

Pyramid shape surface provides best absorption and following are the reasons:

- Since arranging an air gap or even a vacuum gap in the wall can do a lot to cut down on the transmission of sound. A vacuum is a perfect sound break because it eliminates the transfer of sound pressure waves.
- Covering the plain surface with pyramids, sound-waves emerge at different angles, refracted up and down and sideways, scattering the sound like frosted glass scatters light. Some of the sound energy will hit an adjacent pyramid and absorbed.
- A sound wave hitting the shallow angle of a pyramid will bounce into the neighbouring pyramid at a shallow angle, and from there back to the first, losing energy with each bounce, finally dissipating completely.
- A right-angle between pyramids is acts as a like a reflector, in that a given sound-wave will bounce off one wall, into the next, and then right back at the emitter which causes a reduced sound transmission. It is clear from the experimental results that the pyramid shape PU foam is efficient for improving the acoustic performance of the enclosure.

6.4 Conclusion

In the present chapter, an experimental study in the laboratory was carried out for investigating the effect of various shape acoustic materials on the noise reduction performance of an acoustic enclosure The noise source was considered as a handheld saw. The various conditions have been considered for the measurement by using the different shapes of sound-absorbing polyurethane foam. Therefore, commercially available acoustic material of three surface shapes, i.e., plane, wedge, and pyramid surface are chosen for the analysis. It is found from the experimental results that surface shapes of the acoustic material influence the acoustical performance of the enclosure greatly. The experimental result shows that a larger noise reduction of about

23.75 dB(A) is achieved for the case of using pyramid shape PU foam. The 1/3 octave analysis is also carried out to study the effect of various shapes of acoustic material in the different frequency bands. The 1/3 octave analysis shows that wedge shape and pyramid shape acoustic material have a better effect on the acoustic performance of enclosure in comparison to plane PU foam in the entire frequency region. The pyramid shape PU foam is very efficient in the high-frequency region between 2000 to 8000 Hz. Therefore it can be concluded from the experimental results that the pyramid shape PU foam is very effective for improving the acoustic performance of the enclosure. The present experimental study demonstrates that the implementation of sound-absorbing material of different surface shapes would be an appropriate method for improving the acoustical performance of the enclosure.

Chapter 7

Conclusions and future scope

This chapter presents the conclusions and the significant contributions of this thesis toward the evaluation of sound transmission methodologies for the different shapes of acoustic enclosures It also enlists the possible extension and the future scope of this work.

7.1 Conclusions

In this chapter, the conclusions of the sound transmission loss evaluation methodologies based on SEA method and experimental technique are discussed. The analytical and experimental methods are employed for the study of sound transmission through different shapes of acoustic enclosures namely, cylindrical enclosure, conical enclosure and hemispherical enclosure. The experimental set-ups for individual shape of enclosure are fabricated and the volume is kept same for all the enclosures for the transmission loss study. The conclusions are as follows:

- The analytical model is presented based upon the SEA method for predicting the transmission loss of cylindrical shape acoustic enclosures in a broad frequency region. It is found that the analytical predictions show fairly a good agreement with the measured transmission loss using sound intensity technique and predict well the ring and critical frequencies of enclosure panels.

  The percentage error between analytical and measured ring frequencies is 5.32 %, and that for the critical frequency of enclosure panels is 3.89 %. It is found that resonant responses and non-resonant responses are very much significant at frequencies around the critical frequencies of panels. It is demonstrated that, below the critical frequency, transmission loss of cylindrical enclosure is principally regulated by the non-resonant wave modes only.

- An analytical formulation is proposed using SEA method for evaluating the transmission loss of conical shape acoustic enclosures in a broad frequency region. The sound intensity experimental technique was employed for measuring the sound transmission loss. It is found that the analytical predictions demonstrated good agreement with the measured transmission loss.

  The percentage error between predicted and measured lower ring frequency was 5.1 % and that for the upper ring frequency was 0.4 %. The percentage error between predicted and measured critical frequency was 2.7 %. The results obtained indicate that the proposed analytical model is efficient for predicting the transmission loss of conical shape structures.
- A SEA model is presented for predicting the transmission loss of hemispherical shape acoustic enclosure. The analytical formulation models the hemispherical enclosure in a broad frequency region. The sound transmission loss of the hemispheric enclosure is measured using the sound intensity experimental approach. The analytical model agrees well with the experimental results and accurately evaluate the hemispherical enclosure ring and critical frequency. The percentage error between predicted and computed ring frequency is 6.8 %, and that for the critical frequency is 2.1 %.
- The parametric study is performed using SEA method to study the influence of design parameters such as the internal absorption coefficient, thickness, radius, and different panel materials on the transmission loss of different shapes of acoustic enclosures. It is found that the greater transmission loss of acoustic enclosure can be achieved using a higher absorption coefficient inside the cavity. Further, it is shown that the sound insulation performance of the acoustic enclosure increases with the increases of shell thickness.

Moreover, it is demonstrated that the larger radius reduces transmission loss of acoustic enclosure. It is found that the enclosure made of high-density material effectively provides the superior transmission loss in a wide frequency range compared to enclosure made of low-density material.

- The experimental study is performed to investigate the transmission loss of four different shape enclosures viz. rectangular, cylindrical, conical and hemispherical. The volume of all the shapes has been kept the same. The sound intensity approach is adopted to determine the transmission loss of enclosures in wide frequency range. The experimental study shows that the acoustic enclosure of hemispherical shape provides maximum transmission loss as compared to rectangular, cylindrical, and conical shape enclosures of the same volume.
- An experimental study is conducted for investigating the influence of various shape sound absorbing material on the noise reduction performance of an acoustic enclosure. The commercially available sound absorbing material (polyurethane foam) of three surface different shapes are chosen for the analysis viz. plane, wedge, and pyramid. It is found from the experimental results that the use of sound absorbing material improves the acoustic performance of the acoustic enclosure effectively. It is also shown that the surface shapes of the acoustic material influence the noise reduction capability of the acoustic enclosure greatly. The experimental result shows that the pyramid shape sound absorbing material is very efficient compared to plane and wedge shape sound absorbing material for noise reduction of acoustic enclosure. The experimental study demonstrates that the implementation of sound-absorbing material of different surface shapes would be an appropriate method for improving the acoustical performance of the enclosure.

7.2 Scope for future work

- Development of the analytical model based on SEA for the transmission loss evaluation of different shapes of acoustic enclosures lined with different surface shape sound absorbing material. In this case, an optimization study using SEA method is required to maximize the sound transmission loss with the weight and volume constraints.
- The proposed SEA model can be used to predict the transmission loss of acoustic enclosures with a consideration of the external mean flow and air gap flow of the sound absorbing material in future.
- The effect of damping with a combination of sound absorbing material on the transmission loss and sound radiation efficiency of acoustic enclosure was not studied in this thesis. An investigation of these effects can also be helpful in the development of SEA model in future.
- The proposed analytical model based on SEA can be explored for predicting the sound transmission loss of perforated panels.
- Combination of the SEA method and numerical method for the sound transmission analysis of the acoustic enclosures.

Appendix A

SEA parameters for the subsystems used in the sound transmission loss problem of the cylindrical acoustic enclosure

Modal density

The modal density of the subsystem 1 is expressed by [33]:

$$n_1 = \frac{4\pi f^2 V_1}{c_o^3} \tag{A.1}$$

where, V_1 is the volume of the internal sound field .

The modal density of the resonant subsystem 2 is given as follows [117]:

$$n_2 = \begin{cases} \dfrac{9\sqrt{3}L\left(\dfrac{f}{f_r}\right)^{1/2}}{8\pi R h f_r} & f < f_r, \\ \dfrac{\sqrt{3}\mathrm{L}}{2hf_r} & f > f_r \end{cases} \tag{A.2}$$

where, R , L and h are the radius and length and thickness of the cylindrical shell respectively, f_r is the ring frequency of cylindrical shell which is given as :

$$f_r = \frac{C_L}{2\pi R} \tag{A.3}$$

where, C_L is the longitudinal wave speed in the panel and obtained from [30]:

$$\mathrm{C}_L = \sqrt{\frac{E}{\rho(1-\upsilon^2)}} \tag{A.4}$$

where, E and υ are the Young's modulus and Poisson's of the material.

The modal density of the subsystem 3 is given as follows [117]:

$$n_3 = \frac{8\sqrt{3}}{\pi^2 h C_L} \tag{A.5}$$

Dissipation loss factor

The dissipation loss factor of the subsystem 1 is expressed by [44]:

$$n_1^d = \frac{S_1 c_o \gamma}{4\omega V_1}, \tag{A.6}$$

where, γ is the internal absorption coefficient of the enclosure, $\gamma = 1.8 \times 10^{-4}\sqrt{f}$ (minimum value) for the ambient condition when no absorbing material was used for the enclosure.

The dissipation loss factors of the enclosure panels were measured experimentally using the decay rate technique since there is no exact analytical expression available for computing the loss factor due to dissipation.

Coupling loss factor

The loss factor due to coupling between resonant subsystem 2 to subsystem 1 is given as [44]:

$$n_{21} = \begin{cases} \dfrac{2\rho_o c_o \sigma_2}{2\pi f \rho h} & f < f_c, \\ \dfrac{\rho_o c_o \sigma_2}{2\pi f \rho h} & f \geq f_c \end{cases} \tag{A.7}$$

where, σ_2 is the radiation efficiency for the resonant cylindrical shell [31].

The loss factor due to coupling between resonant subsystem 3 to subsystem 1 is given as [44]:

$$n_{31} = \begin{cases} \dfrac{2\rho_o c_o \sigma_3}{2\pi f \rho h} & f < f_c, \\ \dfrac{\rho_o c_o \sigma_3}{2\pi f \rho h} & f \geq f_c \end{cases} \tag{A.8}$$

where, σ_3 is the radiation efficiency for the resonant flat panel [30].

The coupling loss factor between resonant cylindrical shell/plate subsystems is given by [131]:

$$n_{23} = \left[1 \big/ \omega \pi \eta_2 \right] \sum_{m=0}^{M} \tau_{cpm} \tag{A.9}$$

where, n= circumferential mode number, M = total number of modes, τ_{cpn} is the transmission efficiency of coupled cylindrical shell/plate junction for the nth mode which is computed from Tso and Hansen [132].

It should be noted that the coupling loss factor between resonant subsystems in opposite direction is estimated using the reciprocity rule [30]:

$$n_{12} n_1 = n_{21} n_2 \tag{A.10}$$

$$n_{13} n_1 = n_{31} n_3 \tag{A.11}$$

$$n_{23} n_2 = n_{32} n_3 \tag{A.12}$$

The coupling loss factor between the subsystem 1 and non-resonant structural subsystem 4 is given by [38]:

$$n_{14} = 2\tau_4 S_4 C_o \left(1 + n_4^d a\right) / 8\pi f V_1 \tag{A.13}$$

where, $a = \dfrac{\omega\rho h}{2\rho_o c_o}$,

The coupling loss factor between the subsystem 1 and non-resonant structural subsystem 5 is given by [38]:

$$n_{15} = 2\tau_5 S_5 C_o \left(1 + n_5^d a\right) / 8\pi f V_1 \tag{A.14}$$

The coupling loss factor between non-resonant subsystem 4 and subsystem 1 and loss factor due to coupling between non-resonant subsystem 5 and the subsystem 1 is given by the following expression [38]:

$$n_{41} = n_{51} = \rho_o c_o / \omega\rho h \tag{A.15}$$

Table A.1 : Table of resonating modes computed using numerical method through ANSYS software.

S.No	Enclosure Shapes			
	Rectangular enclosure Mode frequency ((Hz)	Cylindrical enclosure Mode frequency (Hz)	Conical enclosure Mode frequency (Hz)	Hemispherical enclosure Mode frequency (Hz)
1	24.61	42.17	74.14	36.72
2	51.22	122.93	74.23	100.29
3	79.94	124.79	163.73	106.29
4	103.36	164.56	197.18	190.68
5	117.34	250.41	321.7	201.89
6	142.97	253.41	323.25	307.59
7	153.59	344.52	358.71	315
8	186.6	346.3	359.52	440.86
9	202.44	353.28	476.65	449.68
10	233.66	361.48	497.54	595.43

REFERENCES

[1] Cremer L, Heckl M, Petersson BAT. Structure-borne sound: Structural vibrations and sound radiation at audio frequencies. 3rd ed. Springer; 2005.

[2] Ver IL, Beranek LL. Noise and vibration control engineering, principles and applications. 2006.

[3] Trochidis A, Kalaroutis A. Sound transmission through double partitions with cavity absorption. J Sound Vib 1986;107:321–7.

[4] Chonan S, Kugo Y. Acoustic characteristics and the design of two-layered soundproof plates. J Sound Vib 1989;129:501–11.

[5] Osipov A, Mees P, Vermeir G. Low-frequency airborne sound transmission through single partitions in buildings. Appl Acoust 1997;52:273–88.

[6] Pellicier A, Trompette N. A review of analytical methods, based on the wave approach, to compute partitions transmission loss. Appl Acoust 2007;68:1192–212.

[7] Cherif R, Wareing A, Atalla N. Evaluation of a hybrid TMM-SEA method for prediction of sound transmission loss through mechanically coupled aircraft double-walls. Appl Acoust 2017;117:132–40.

[8] Rhazi D, Atalla N. Transfer matrix modeling of the vibroacoustic response of multi-materials structures under mechanical excitation. J Sound Vib 2010;329:2532–46.

[9] Vigran TE. Sound transmission in multilayered structures - Introducing finite structural connections in the transfer matrix

method. Appl Acoust 2010;71:39–44.

[10] Li Z, Chen S, Wu Z, Yang L. An improved approach for normal-incidence sound transmission loss measurement using a four-microphone impedance tube. JVC/Journal Vib Control 2021;27:332–42.

[11] Campolina B, Dauchez N, Atalla N, Doutres O. Effect of porous material compression on the sound transmission of a covered single leaf panel. Appl Acoust 2012;73:791–7.

[12] Zhou J, Bhaskar A, Zhang X. Optimization for sound transmission through a double-wall panel. Appl Acoust 2013;74:1422–8.

[13] Koval LR. On sound transmision into a thin cylindrical shell under “flight conditions.” J Sound Vib 1976;48:265–75.

[14] Koval LR. Effects of cavity resonances on sound transmission into a thin cylindrical shell. J Sound Vib 1978;59:23–33.

[15] Koval LR. Sound transmission into a laminated composite cylindrical shell. J Sound Vib 1980;71:523–30.

[16] Blaise A, Lesueur C, Gotteland M, Introduction I. On sound transmission into an orthotropic infinite shell: comparison with Koval’s results and understanding of phenomena. J Sound Vib 1991;150:233–43.

[17] Lee JH, Kim J. Analysis and measurement of sound transmission through a double-walled cylindrical shell. J Sound Vib 2002;251:631–49.

[18] Lee JH, Kim J. Sound transmission through periodically stiffened cylindrical shells. J Sound Vib 2002;251:431–56.

[19] Lee J, Kim J. Study on sound transmission characteristics of a

cylindrical shell using analytical and experimental models. Appl Acoust 2003;64:611–32.

[20] Zhou J, Bhaskar A, Zhang X. The effect of external mean flow on sound transmission through double-walled cylindrical shells lined with poroelastic material. J Sound Vib 2014;333:1972–90.

[21] Soedel W. Vibrations of shells and plates. 2005.

[22] Zhou J, Bhaskar A, Zhang X. The effect of external mean flow on sound transmission through double-walled cylindrical shells lined with poroelastic material. J Sound Vib 2014;333:1972–90. https://doi.org/10.1016/j.jsv.2013.11.038.

[23] Farshidianfar A, Farshidianfar MH, Crocker MJ, Smith WO. Vibration analysis of long cylindrical shells using acoustical excitation. J Sound Vib 2011;330:3381–99.

[24] Liu Y, He C. Diffuse field sound transmission through sandwich composite cylindrical shells with poroelastic core and external mean flow. Compos Struct 2016;135:383–96.

[25] Oliazadeh P, Farshidianfar A. Analysis of different techniques to improve sound transmission loss in cylindrical shells. J Sound Vib 2017;389:276–91.

[26] Marco A. Nonlinear vibrations and stability of shells and plates. 2008th ed. Cambridge university press; 2008.

[27] Golzari M, Jafari AA. Sound transmission through truncated conical shells. Appl Acoust 2019;156:186–207.

[28] Golzari M, Jafari AA. Effect of poroelastic material on vibroacoustic behavior of truncated conical shells. Aerosp Sci Technol 2021;118:106982.

[29] Hasheminejad SM, Mehdizadeh S. Acoustic performance of a multi-layer close-fitting hemispherical enclosure. Noise Control Eng J 2006;54:86.

[30] Oliazadeh P, Farshidianfar A, Crocker MJ. Study of sound transmission through single- and double-walled plates with absorbing material: Experimental and analytical investigation. Appl Acoust 2019;145:7–24.

[31] Oliazadeh P, Farshidianfar A, Crocker MJ. Experimental and analytical investigation on sound transmission loss of cylindrical shells with absorbing material. J Sound Vib 2018;434:28–43.

[32] Maidanik G. Response of ribbed panels to reverberant acoustic fields. J Acoust Soc Am 1962;34:809–26.

[33] Lyon RH. Statistical energy analysis of dynamical systems: theory and applications. 1975.

[34] Crocker MJ, Price AJ. Sound transmission using statistical energy analysis. J Sound Vib 1969;9:469–86.

[35] Cole V, Crocker MJ, Raju PK. Theoretical and experimental studies of the noise reduction of an idealized cabin enclosure. Noise Control Eng J 1983;20:122–32.

[36] Oldham D J, Hillarby SN. The acoustical performance of small close fitting enclosures,part 1: Theoritical models. J Sound Vib 1991;150:261–81.

[37] Oldham D J, Hillarby SN. The acoustical performance of small close fitting enclosures, part 2 : Experimental investigation. J Sound Vib 1991;150:283–300.

[38] Renji K, Nair PS, Narayanan S. Non-resonant response using statistical energy analysis 2001;241:253–70.

[39] Renji K, Nair PS, Narayanan S. Response of a plate to diffuse acoustic field using statistical energy analysis. J Sound Vib 2002;254:523–39.

[40] Craik RJM. Non-resonant sound transmission through double walls using statistical energy analysis. Appl Acoust 2003;64:325–41.

[41] Bernblit M V. Application of statistical energy analysis for vibration and sound radiation prediction of multi-sectional cylindrical shells. J Acoust Soc Am 1994;95:2970–1. https://doi.org/10.1121/1.409008.

[42] Trompette N, Barbry J-L, Sgard F, Nelisse H. Sound transmission loss of rectangular and slit-shaped apertures: Experimental results and correlation with a modal model. J Acoust Soc Am 2009;125:31–41.

[43] Sgard F, Nelisse H, Atalla N, Amedin CK, Oddo R. Prediction of the acoustical performance of enclosures using a hybrid statistical energy analysis: Image source model. J Acoust Soc Am 2010;127:784–95.

[44] Ming R, Pan J. Insertion loss of an acoustic enclosure. J Acoust Soc Am 2004;116:3453–9.

[45] Lei Y, Pan J, Sheng MP. Investigation of structural response and noise reduction of an acoustical enclosure using SEA method. Appl Acoust 2012;73:348–55.

[46] Zhang J, Xiao X, Sheng X, Zhang C, Wang R, Jin X. SEA and contribution analysis for interior noise of a high speed train. Appl Acoust 2016;112:158–70.

[47] Culla A, D'Ambrogio W, Fregolent A, Milana S. Vibroacoustic optimization using a statistical energy analysis model. J Sound Vib 2016;375:102–14.

[48] Christen JL, Ichchou M, Troclet B, Bareille O, Ouisse M. Global

sensitivity analysis and uncertainties in SEA models of vibroacoustic systems. Mech Syst Signal Process 2017;90:365–77.

[49] Petrone G, Melillo G, Laudiero A, De Rosa S. A Statistical Energy Analysis (SEA) model of a fuselage section for the prediction of the internal Sound Pressure Level (SPL) at cruise flight conditions. Aerosp Sci Technol 2019;88:340–9.

[50] Lee HR, Kim HY, Jeon JH, Kang YJ. Application of global sensitivity analysis to statistical energy analysis: Vehicle model development and transmission path contribution. Appl Acoust 2019;146:368–89.

[51] Liu Z, Fard M, Davy JL. Prediction of the acoustic effect of an interior trim porous material inside a rigid-walled car air cavity model. Appl Acoust 2020;165:107325.

[52] Zhou R, Crocker MJ. Sound transmission loss of foam-filled honeycomb sandwich panels using statistical energy analysis and theoretical and measured dynamic properties. J Sound Vib 2010;329:673–86.

[53] Oliazadeh P, Farshidianfar A, Crocker MJ. Experimental study and analytical modeling of sound transmission through honeycomb sandwich panels using SEA method. Compos Struct 2021;280:114927.

[54] Chronopoulos D, Troclet B, Ichchou M, Lainé JP. A unified approach for the broadband vibroacoustic response of composite shells. Compos Part B Eng 2012;43:1837–46.

[55] Xie SL, Zhang YH, Xie Q, Chen CH, Zhang XN. Identification of high frequency loads using statistical energy analysis method. Mech Syst Signal Process 2013;35:291–306.

[56] Chronopoulos D, Ichchou M, Troclet B, Bareille O. Predicting the broadband response of a layered cone-cylinder-cone shell. Compos Struct 2014;107:149–59.

[57] Denli H, Sun JQ. Structural-acoustic optimization of sandwich cylindrical shells for minimum interior sound transmission. J Sound Vib 2008;316:32–49.

[58] Marinova P, Lippert S, von Estorff O. On the numerical investigation of sound transmission through double-walled structures with membrane-type acoustic metamaterials. J Acoust Soc Am 2017;142:2400–6.

[59] Yang Y, Mace BR, Kingan MJ. Prediction of sound transmission through, and radiation from, panels using a wave and finite element method. J Acoust Soc Am 2017;141:2452–60.

[60] Kingan MJ, Yang Y, Mace BR. Sound transmission through cylindrical structures using a wave and finite element method. Wave Motion 2019;87:58–74.

[61] Deng J, Guasch O, Maxit L, Zheng L. Annular acoustic black holes to reduce sound radiation from cylindrical shells. Mech Syst Signal Process 2021;158:107722.

[62] Shi D, Liu G, Zhang H, Ren W, Wang Q. A three-dimensional modeling method for the trapezoidal cavity and multi-coupled cavity with various impedance boundary conditions. Appl Acoust 2019;154:213–25.

[63] Zhou L, Carter AE, Herrin DW, Shi J, Copley DC. Airborne path attenuation of partial enclosures: Simulation and sensitivity study. Appl Acoust 2011;72:380–6.

[64] Cui H, Hu R, Chen N. Modelling and analysis of acoustic field in a

rectangular enclosure bounded by elastic plates under the excitation of different point force. J Low Freq Noise, Vib Act Control 2017;36:43–55.

[65] Lin TR, Pan J. Sound radiation characteristics of a box-type structure. J Sound Vib 2009;325:835–51.

[66] Chen Y, Jin G, Zhu M, Liu Z, Du J, Li WL. Vibration behaviors of a box-type structure built up by plates and energy transmission through the structure. J Sound Vib 2012;331:849–67.

[67] Al-Bassyiouni M, Balachandran B. Sound transmission through a flexible panel into an enclosure: Structural-acoustics model. J Sound Vib 2005;284:467–86.

[68] Liu ZS, Lee HP, Lu C. Passive and active interior noise control of box structures using the structural intensity method. Appl Acoust 2006;67:112–34.

[69] Haitao W, Xiangyang Z, Ling C. Calculation of sound fields in small enclosures using a meshless model. Appl Acoust 2013;74:459–66.

[70] Remillieux MC, Pasareanu SM, Svensson UP. Numerical modeling of the exterior-to-interior transmission of impulsive sound through three-dimensional, thin-walled elastic structures. J Sound Vib 2013;332:6725–42.

[71] Xie X, Yang H, Zheng H, Wang H, Zeng X, Chen L, et al. Calculation of sound fields in small enclosures using a meshless model. J Sound Vib 2013;74:175–86.

[72] Cheng L, Nicolas J. Radiation of sound into a cylindrical enclosure from a point-driven end plate with general boundary conditions. J Acoust Soc Am 1992;91:1504–13.

[73] Estève SJ, Johnson ME. Reduction of sound transmission into a

circular cylindrical shell using distributed vibration absorbers and Helmholtz resonators. J Acoust Soc Am 2002;112:2840–8.

[74] Da Rocha J, Suleman A, Lau F. Flow-induced noise and vibration in aircraft cylindrical cabins: Closed-form analytical model validation. J Vib Acoust Trans ASME 2011;133:1–9.

[75] Xie K, Chen M. Wave based method for vibration analysis of double-walled cylindrical shells. Appl Acoust 2018;139:293–306.

[76] Errico F, Tufano G, Robin O, Guenfoud N, Ichchou M, Atalla N. Simulating the sound transmission loss of complex curved panels with attached noise control materials using periodic cell wavemodes. Appl Acoust 2019;156:21–8.

[77] Errico F, Ichchou M, Franco F, Rosa S De, Bareille O, Droz C. Schemes for the sound transmission of flat , curved and axisymmetric structures excited by aerodynamic and acoustic sources. J Sound Vib 2019;456:221–38.

[78] Vipperman JS, Li D, Avdeev I, Lane SA. Investigation of the sound transmission into an advanced grid-stiffened structure. J Vib Acoust Trans ASME 2003;125:257–66.

[79] Wang X, Wu W, Yao X. Structural and acoustic response of a finite stiffened conical shell. Acta Mech Solida Sin 2015;28:200–9.

[80] Eslaminejad A, Ziejewski M, Karami G. An experimental–numerical modal analysis for the study of shell-fluid interactions in a clamped hemispherical shell. Appl Acoust 2019;152:110–7.

[81] Parrinello A, Ghiringhelli GL. Transfer matrix representation for periodic planar media. J Sound Vib 2016;371:196–209.

[82] Parrinello A, Ghiringhelli GL, Atalla N. Generalized Transfer Matrix Method for periodic planar media. J Sound Vib 2020;464:114993.

[83] Magliacano D, Petrone G, Franco F, De Rosa S. Numerical investigations about the sound transmission loss of a fuselage panel section with embedded periodic foams. Appl Acoust 2021;182:108265.

[84] Ghinet S, Atalla N, Osman H. The transmission loss of curved laminates and sandwich composite panels. J Acoust Soc Am 2005;118:774–90.

[85] Parrinello A, Kesour K, Ghiringhelli GL, Atalla N. Diffuse field transmission through multilayered cylinders using a Transfer Matrix Method. Mech Syst Signal Process 2020;136:106514.

[86] Tebyanian A, Ghazavi MR. Vibro-acoustic and sound transmission loss analysis of truncated conical shell subjected to incident sound wave. JVC/Journal Vib Control 2019;25:435–44.

[87] Zou MS, Liu SX. A mixed analytical-numerical method for the acoustic radiation of a double elastic spherical shell in finite-depth water. Eng Anal Bound Elem 2020;119:140–50.

[88] Zang Y, Lin W, Zheng Y, Su C, Wu P, Chang Q. Acoustic radiation torque of a Bessel vortex wave on a viscoelastic spherical shell nearby an impedance boundary. J Sound Vib 2021;509:116261.

[89] Kim HS, Kim JS, Lee SH, Seo YH. A simple formula for insertion loss prediction of large acoustical enclosures using statistical energy analysis method. Int J Nav Archit Ocean Eng 2014;6:894–903.

[90] Wang YS, Crocker, Malcolm J, Raju PK. Theoretical and Experimental Evaluation of Transmission Loss of Cylinders 1983;21:186–92.

[91] Lai JCS, Burgess M. Application of the sound intensity technique to measurement of field sound transmission loss. Appl Acoust

1991;34:77–87.

[92] Chen YH, Chen KT, Chaing YH. Plate-damping measurements in a single reverberation room. Appl Acoust 1996;47:251–61.

[93] Mace BR. Statistical energy analysis: Coupling loss factors, indirect coupling and system modes. J Sound Vib 2005;279:141–70.

[94] Wester ECN, Mace BR. A Statistical analysis of acoustical energy flow in two coupled rectangular rooms. Acta Acust United with Acust 1998;84:114–21.

[95] Maxit L, Guyader JL. Extension of SEA model to subsystems with non-uniform modal energy distribution. J Sound Vib 2003;265:337–58.

[96] Seçgin A. Numerical determination of statistical energy analysis parameters of directly coupled composite plates using a modal-based approach. J Sound Vib 2013;332:361–77.

[97] Seçgin A, Kara M, Ozankan A. A modal impedance technique for mid and high frequency analysis of an uncertain stiffened composite plate. J Sound Vib 2016;366:396–406.

[98] Kara M, Seçgin A, Baygün T. Discrete Singular Convolution Method for Acoustic Transmission Lines. Acoust Aust 2020;48:271–85.

[99] Seçgin A, Kara M, Güler S. Mid and high frequency vibration analysis of line connected uncertain composite structures by using modal impedance based statistical energy analysis procedure. J Fac Eng Archit Gazi Univ 2019;34:727–38.

[100] Totaro N, Dodard C, Guyader JL. SEA coupling loss factors of complex vibro-acoustic systems. J Vib Acoust Trans ASME 2009;131:0410091–8.

[101] Zarate R, Lopez M, Ortega M. Estimation of coupling loss factors employed in the statistical energy analysis of kitchen appliances. Proc Meet Acoust 2017;30.

[102] Bies DA, Hamid S. In situ determination of loss and coupling loss factors by the power injection method. J Sound Vib 1980;70:187–204.

[103] De Langhe K, Sas P. Statistical analysis of the power injection method. J Acoust Soc Am 1996;100:294–303.

[104] Bloss BC, Rao MD. Estimation of frequency-averaged loss factors by the power injection and the impulse response decay methods. J Acoust Soc Am 2005;117:240–9.

[105] Seçgin A, Güler S, Kara M. Determinations of in-situ energy loss factors of point-connected composite plates. Compos Part B Eng 2016;87:27–32.

[106] Fahy FJ, Gardonio P. Sound and structural vibration: radiation, transmission and response. vol. I,. 2007.

[107] Reynolds DD. Engineering principles of acoustics, noise and vibration control. 1981.

[108] Szechenyi E. Sound transmission through cylinder walls using statistical considerations. J Sound Vib 1971;19:83–94.

[109] Davy JL. Predicting the sound insulation of single leaf walls: Extension of Cremer's model. J Acoust Soc Am 2009;126:1871.

[110] Crocker MJ, Kessler FM. Noise and noise control. vol. 2. 2018.

[111] ISO 9614-1:1993 : Determination of sound power levels of noise sources using sound intensity — Part 1: Measurement at discrete points. 1993.

[112] Lyon RH. Random noise and vibration in space vehicles. 1967.

[113] Pope LD. On the transmission of sound through finite closed shells: Statistical Energy Analysis, modal coupling, and nonresonant transmission. J Acoust Soc Am 1971;50:1004–18.

[114] Manning JE. Comment on “Sound Transmission through a Finite, Closed, Cylindrical Shell” [P. H. White, J. Acoust. Soc. Am. 40, 1192–1193 (L) (1966)]. J Acoust Soc Am 1968;43:886–7.

[115] Lyon RH. Noise Reduction of Rectangular Enclosures with One Flexible Wall. J Acoust Soc Am 1963;35:1791–7.

[116] Eichler E. Thermal Circuit Approach to Vibrations in Coupled Systems and the Noise Reduction of a Rectangular Box. J Acoust Soc Am 1965;37:995–1007.

[117] Hart FD, Shah KC. Compendium of modal densities for structures, NASA contractor report, CR-1773. 1971.

[118] Norton MP, Nelson FC. Fundamentals of noise and vibration analysis for engineers. vol. 88. 1990.

[119] Ellington FH, Hart FD. Acoustic radiation efficiency of truncated conical shells, contractor report (CR), Document ID:19710006391 ,NASA. NASA; 1969.

[120] Putra A, Thompson DJ. Sound radiation from rectangular baffled and unbaffled plates. Appl Acoust 2010;71:1113–25.

[121] Lee YY. Insertion loss of a cavity-backed semi-cylindrical enclosure panel. J Sound Vib 2003;259:625–36.

[122] Alberto G, Santos DO, Oliveira E, Weinschutz R, Luiz Á, Henrique P, et al. Evaluation of tube-shaped bus shelters as a noise mitigation solution for passengers. Appl Acoust 2020;164:107245.

[123] Lazarus H, Sehrndt GA, Jacques J. European standards for occupational and machinery noise control. Saf Sci 1992;15:375–86.

[124] A. R. Barbosa A, R. Bertoli S. Noise generated by portable saw in different construction materials. Am J Civ Eng Archit 2017;5:17–24.

[125] Cao H, Kang T, Chen X. Noise analysis and sources identification in machine tool spindles. CIRP J Manuf Sci Technol 2019;25:26–35.

[126] Licow R, Chuchala D, Deja M, Orlowski KA, Taube P. Effect of pine impregnation and feed speed on sound level and cutting power in wood sawing. J Clean Prod 2020;272:122833.

[127] Tandon N, Nakra BC, Ubhe DR, Killa NK. Noise Control of Engine Driven Portable Generator Set. Appl Acoust 1998;55:307–28.

[128] Kim H, Kim J, Lee S, Seo Y. A simple formula for insertion loss prediction of large acoustical enclosures using statistical energy analysis method. Noval Archit Ocean Eng 2014;6:894–903.

[129] Cao L, Fu Q, Si Y, Ding B, Yu J. Porous materials for sound absorption. Compos Commun 2018;10:25–35.

[130] Bolton JS, Shiau NM, Kang YJ. Sound transmission through multi-panel structures lined with elastic porous materials. J Sound Vib 1996;191:317–47.

[131] Tso YK, Hansen CH. An investigation of the coupling loss factor for a cylinder/plate structure. J Sound Vib 1997;199:629–43.

[132] Tso YK, Hansen CH. Wave propagation through cylinder/plate junctions 1995;186:447–61.

LIST OF PUBLICATIONS

International Journal papers

1. Gupta P, Parey A, Prediction of sound transmission loss of cylindrical acoustic enclosure using statistical energy analysis and its experimental validation. J Acoust Soc Am 2022;151:544–60. https://doi.org/10.1121/10.0009358

2. Gupta P, Parey A, Prediction of sound transmission loss of conical acoustic enclosure using statistical energy analysis and its experimental validation. JVC/Journal Vib Control 2022:1–13. DOI: 10.1177/10775463221076665

3. Gupta P, Parey A. Prediction of sound transmission loss of hemispherical shell using statistical energy analysis and its experimental validation. Measurement 2022;204:1-12. https://doi.org/10.1016/j.measurement.2022.112089.

International Conference papers

1. Gupta P, Parey A, Experimental investigation of sound-absorbing material of different surface shapes on noise reduction performance of an acoustic enclosure. In: Jha K., Gulati P., Tripathi U.K. (eds) Recent Advances in Sustainable Technologies 2021; Lecture Notes in Mechanical Engineering, Singapore. https://doi.org/10.1007/978-981-16-0976-3_21

List of Publications (Outside PhD)

International Conference papers

1. Gupta P, Parey A, (2021) To investigate the influence of sound-absorbing materials on the transmission loss of double-wall panel. In: "Materials today proceedings 2021; 44:1500-1503. https://doi.org/10.1016/j.matpr.2020.11.691.